

Microglia in the embryonic brain and spinal cord during the development of neuronal networks

Nina Swinnen

Promotors: Prof. dr. J.-M. Rigo (Universiteit Hasselt)
Dr. P. Legendre (Université Pierre et Marie Curie)

Copromotor: Prof. dr. B. Brône (Universiteit Hasselt)

Members of the jury

Prof. dr. I. Lambrichts, Universiteit Hasselt, Diepenbeek, Belgium, *chairman*

Prof. dr. J.-M. Rigo, Universiteit Hasselt, Diepenbeek, Belgium, *promotor*

Dr. P. Legendre, Université Pierre et Marie Curie, Paris, France, *promotor*

Prof. dr. B. Brône, Universiteit Hasselt, Diepenbeek, Belgium, *copromotor*

Prof. dr. M. Ameloot, Universiteit Hasselt, Diepenbeek, Belgium

Dr. E. Audinat, Université Paris Descartes, Paris, France

Dr. I. Dusart, Université Pierre et Marie Curie, Paris, France

Prof. dr. E. Hermans, Université catholique de Louvain, Brussel, Belgium

Prof. dr. R. Lambert, Université Pierre et Marie Curie, Paris, France

Table of Contents

Table of Contents	I
List of Figures	IV
List of Tables.....	VI
List of Abbreviations.....	VII
1 General introduction and aims	1
1.1 Microglia in the adult central nervous system	2
1.1.1 Discovery of microglial cells and their definition.....	2
1.1.2 Microglial cell markers.....	5
1.1.3 Electrophysiological properties of microglia	6
1.2 Microglia in the developing central nervous system	12
1.2.1 Origin of embryonic microglial cells.....	12
1.2.2 Microglial entry and dispersion in the developing central nervous system	13
1.2.3 Microglial functions in CNS development.....	15
1.3 Neuropsychiatric disorders and maternal inflammation	18
1.4 Aims of the study.....	22
2 Complex invasion pattern of the cerebral cortex by microglial cells during development of the mouse embryo	25
2.1 Abstract.....	26
2.2 Introduction	27
2.3 Materials and methods	29
2.3.1 Animals	29
2.3.2 Tissue Preparation and Immunostaining	29
2.3.3 Microscopy and Analysis of Immunostainings	31
2.3.4 Time-lapse imaging.....	32
2.4 Results	33
2.4.1 Invasion of the embryonic cortex and ganglionic eminences by microglia between E10.5 and E17.5.....	33
2.4.2 Microglia accumulate in the region of the choroid plexus primordium and associate with dying cells.....	40
2.4.3 Migration behavior of microglial cells in the embryonic cortex.....	44
2.5 Discussion	49

2.5.1 Initial invasion of the embryonic cortex occurs in different phases ..	49
2.5.2 Microglial cells accumulate in a region where developmental cell death occurs	50
2.5.3 Embryonic microglial cells are highly dynamic cells that scan their local environment during their migration process	51
3 Microglia proliferation is controlled by P2X7 receptors in a Pannexin-1-independent manner during early embryonic spinal cord invasion	53
3.1 Abstract.....	54
3.2 Introduction	55
3.3 Materials & Methods.....	57
3.3.1 Animals	57
3.3.2 Whole-cell recordings and analysis.....	59
3.3.3 Drug application and pharmacological agents	61
3.3.4 Immunohistochemistry and confocal microscopy	62
3.3.5 Microglia isolation	65
3.3.6 RNA isolation, reverse transcription-PCR and qPCR	65
3.3.7 Statistics	66
3.4 Results	67
3.4.1 P2X1R, P2X4R and P2X7R expression in embryonic microglia	67
3.4.2 ATP evokes biphasic membrane currents in embryonic microglia that result from P2X7R activation	70
3.4.3 P2X7R activation does not need Panx1 expression to generate a biphasic current.	78
3.4.4 Embryonic microglia proliferation requires the expression of P2X7R but not of Panx1.	81
3.5 Discussion	85
3.5.1 Functional P2XRs expressed by embryonic microglia in situ.....	85
3.5.2 P2X7R is not coupled to Panx1 in embryonic microglia	86
3.5.3 P2X7Rs control microglia proliferation independently of microglia activation.....	87
4 Electrophysiological characterization of microglia in the embryonic cortex and choroid plexus.....	89
4.1 Abstract.....	90
4.2 Introduction	91

4.3 Materials & Methods	93
4.3.1 Animals	93
4.3.2 Whole-cell recordings and analysis.....	93
4.3.3 Statistics	95
4.4 Results	96
4.4.1 The expression of K^+ currents is linked to the microglial activation state	96
4.4.2 Stretch-sensitive ion channels	98
4.4.3 Embryonic microglia express few ligand-gated ion channels	103
4.5 Discussion	106
4.5.1. The expression of IK_{IR} correlates with microglial activation level ..	106
4.5.2 Microglia in the embryonic brain express a small stretch-sensitive current	107
4.5.3 Besides P2X receptors, embryonic microglia express few ligand-gated receptors	107
5 Maternal immune activation and neuropsychiatric disorders - a role for microglia? - A preliminary study	109
5.1 Abstract.....	110
5.2 Introduction	111
5.3 Materials & Methods.....	113
5.3.1 Animals	113
5.3.2 Maternal immune activation and IL-6 determination.....	113
5.3.3 Immunohistochemistry	113
5.3.4 Statistics	115
5.4 Results	116
5.5 Discussion	121
6 Summary and general discussion	117
7 Nederlandse samenvatting	127
8 Résumé français	127
Reference list	129
Curriculum Vitae.....	147
Dankwoord	151

List of Figures

Figure 1.1. Examples of a ramified and an amoeboid microglial cell morphology.

Figure 1.2. Microglial activation pathway.

Figure 1.3. Microglial activation in facial nerve axotomy is paralleled by changes in membrane currents.

Figure 1.4. Hypothetical scheme of microglial invasion of the developing CNS.

Figure 1.5. Migration modes of microglial cells in CNS regions with a layered architecture.

Figure 1.6. Schematic presentation of the different functions that have been ascribed to microglial cells in the developing CNS.

Figure 2.1. Invasion and distribution of microglial cells in the developing cortex.

Figure 2.2. Quantification of microglial cell invasion.

Figure 2.3. Proliferation in the developing mouse embryonic cortex and pia.

Figure 2.4. Activated microglia accumulate in the choroid plexus region during developmental cellular death.

Figure 2.5. Proliferation in the developing mouse embryonic choroid plexus primordium.

Figure 2.6. Microglial distribution in the embryonic cortical wall.

Figure 2.7. Microglial migration in the embryonic cortical wall.

Figure 2.8. Time-lapse confocal imaging demonstration of microglial cell behavior at E14.5.

Figure 3.1. P2X1R, P2X4R, P2X7R, Panx1 and Panx2 expression in microglia.

Figure 3.2. Voltage-activated current profile in microglia of the developing SC.

Figure 3.3. ATP evokes inward currents in embryonic microglia.

Figure 3.4. Whole-cell currents evoked by ATP and P2XR agonists in embryonic microglia *in situ*.

Figure 3.5. Effects of TNP-ATP, PPADS, suramin, copper, zinc, BBG, A438079 and A740003 on ATP-evoked currents in SC microglia.

Figure 3.6. ATP-evoked biphasic currents were not observed in SC microglia of P2X7R^{-/-} mouse embryos.

Figure 3.7. Panx1 immunostaining was not observed in the SC of Panx1^{-/-} mouse embryos.

Figure 3.8. ATP-evoked biphasic currents did not result from Panx1 activation.
Figure 3.9. Microglia proliferation was dramatically reduced in the SC of P2X7R^{-/-} mouse embryos but was unchanged in the SC of Panx1^{-/-} mouse embryos.
Figure 3.10. Microglia activation and motoneuron developmental cell death were not altered in the SC of E13.5 P2X7R^{-/-} mouse embryos.

Figure 4.1. Inward and outward currents expressed by microglia in the embryonic brain.

Figure 4.2. Inward rectifying K⁺ currents expressed by microglia in the embryonic brain.

Figure 4.3. Run up development in E13.5 cortical microglia after application of 2 mmHg via the patch pipette.

Figure 4.4. Mean peak current density at 100 mV at different time point during development of the run up.

Figure 4.5. Effect of low extracellular Cl⁻ concentration on the outward current.

Figure 4.6. Effect of TEA and 4-AP on the outward current.

Figure 4.7. Embryonic microglia expression of ligand-gated ion channels.

Figure 4.8. ATP (3 mM) induced a biphasic current in cortical microglia.

Figure 5.1. Indication of the analyzed areas in the embryonic cortex and hippocampus.

Figure 5.2. IL-6 concentration in the maternal serum 5 hours after injection at E11.5 and E15.5 with saline or poly (I:C).

Figure 5.3. IL-6 concentration in the embryonic brain 5 hours after injection at E11.5 and E15.5 with saline or poly (I:C).

Figure 5.4. Examples of the activation marker staining on the acute slices treated with LPS.

Figure 5.5. Microglial expression of activation markers in acute brain slices.

Figure 6.1. Schematic representation of the microglial characteristics in the developing CNS.

List of Tables

Table 1.1. Overview of the different purinergic receptors with their agonists.

Table 2.1. Overview of the primary antibodies

Table 3.1. Primers used for PCR analysis for genotyping P2X7 and Panx1 KO mice

Table 3.2. Primary antibodies

Table 3.3. Primers used for real time PCR analysis

Table 5.1. Overview of the primary antibodies

Table 5.2. Microglial cell density in the cortex and hippocampal area of embryos derived from the control group and the group that was subjected to maternal inflammation at E11.5 and E15.5.

List of Abbreviations

2-MeSATP	2-methylthio-adenosine triphosphate
2-MeSADP	2-methylthio-adenosine diphosphate
4-AP	4-aminopyridine
A438079	3-[[5-(2,3-Dichlorophenyl)-1 <i>H</i> -tetrazol-1-yl]methyl]pyridine hydrochloride
A740003	<i>N</i> -[1-[[[(Cyanoamino)(5-quinolinylamino)methylene]amino]-2,2-dimethylpropyl]-3,4-dimethoxybenzeneacetamide
α,β -Me-ATP	α,β -methylene ATP
ACSF	artificial cerebrospinal fluid
ADP	adenosine diphosphate
AMPA	α -amino-3-hydroxy-5-methylisoxazole-4-propionic acid
Ap4A	Diadenosine tetraphosphate
ATP	adenosine triphosphate
BBG	Brilliant Blue G
BMP	bone morphogenic protein
bzATP	2'(3')-O-(4-Benzoylbenzoyl) adenosine 5'-triphosphate triethylammonium salt
Ca ²⁺	calcium
CBX	carbenoxolone
CCPA	2-chloro-N(6)-cyclo-pentyladenosine
CD	cluster of differentiation
Cl ⁻	chloride
CNS	central nervous system
CSF-1R	colony stimulating factor-1 receptor
Ct	cycle threshold
Cu ²⁺	copper
CZS	centraal zenuwstelsel
DAPI	4,6-diamidino-2-phenylindole
DIDS	4,4'-Diisothiocyanatostilbene-2,2'-disulfonic acid disodium salt hydrate
E	embryonic day
eGFP	enhanced green fluorescent protein
FACS	fluorescence-activated cell-sorting

GABA	γ -aminobutyric acid
GAD67	glutamate decarboxylase 67
HCO ₃ ⁻	bicarbonate
Iba-1	ionized calcium binding adaptor molecule-1
<i>IK_{IR}</i>	inward rectifying K ⁺ current
<i>IK_{DR}</i>	delayed (outward) rectifying K ⁺ current
iNOS	inducible nitric oxide synthase
IrC	inward rectifying current
K ⁺	potassium
KO	knockout
KOMP	knockout mouse project
LGE	lateral ganglionic eminences
LPS	lipopolysaccharide
MGE	medial ganglionic eminences
MHC class II	major histocompatibility complex class II
MIA	maternal immune activation
MN	motoneuron
NA	numerical aperture
Na ₂ ATP	adenosine triphosphate disodium salt
NMDA	N-methyl-D-aspartate
OrC	outward rectifying current
P	postnatal
Panx	pannexin
PBS	phosphate-buffered saline
Poly (I:C)	polyinosinic:polycytidylic acid
PPADS	pyridoxalphosphate-6-azophenyl-2',4'-disulfonic acid
qPCR	quantitative PCR
qRT-PCR	quantitative real-time PCR
RT-PCR	reverse-transcription PCR
SC	spinal cord
SNC	système nerveux central
TEA	tetraethylammonium chloride
TLR	toll-like receptor
TNF α	tumor necrosis factor α

TNP-ATP	2',3'- <i>O</i> -(2,4,6-Trinitrophenyl)adenosine-5'-triphosphate tetra (triethylammonium)
UDP	uridine diphosphate
UTP	uridine triphosphate
VEGF	vascular endothelial growth factor
Zn ²⁺	zinc

1 General introduction and aims

1.1 Microglia in the adult central nervous system

1.1.1 Discovery of microglial cells and their definition

The concept of microglia was first introduced by Pio del Rio-Hortega in the early 20th century. The findings of del Rio-Hortega provided the basis for our current view on microglia. He claimed that these cells enter the brain in an early stage of development, they can transform from a ramified into an amoeboid morphology (Fig. 1.1) and vice versa, and are able to migrate, proliferate and phagocytose [1-4], findings that are still valid in our modern-day research. The observations of del Rio-Hortega initiated new research, however it was not until the second part of the 20th century that the study of microglial cells bloomed and our knowledge on these cells increased drastically. Being the resident immune cells of the central nervous system (CNS), most of this research focused on the role of microglial cells in pathologies of the adult CNS.

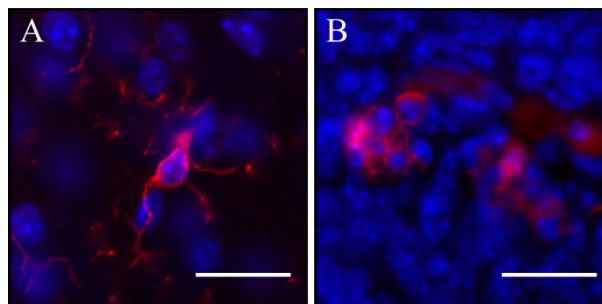


Figure 1.1. Examples of a ramified and an amoeboid microglial cell morphology. A) A ramified microglial cell with a small cell soma and long thin processes. **B)** An amoeboid microglial cell, the cell volume is increased and processes are retracted. Microglial cells were stained for Iba-1 (red), nuclei were visualized with DAPI (blue). Scale bars = 20 μm .

Microglia are the intrinsic macrophages of the CNS. In the healthy, adult CNS they have a ramified morphology with a small cell soma and long thin processes. The cell body remains stable and fixed on its location but the branches of the ramified processes are highly dynamic, continuously extending and retracting processes which enables them to scan their environment [5, 6]. These ramified microglia have a very slow turn-over and a down-regulated expression of cell surface markers.

The microglial cells are distributed over the CNS; however their distribution and morphology are influenced by the local cytoarchitecture. More microglial cells can be found in the gray matter than in the white, in particular in the hippocampus, substantia nigra, basal ganglia and olfactory telencephalon. The morphology and direction of the microglial branches is also influenced by the location in the CNS. At regions that lack a blood-brain barrier the microglia have a few short "limbs", and while white matter microglia processes are oriented along fibers, those present in the grey matter are mostly radially orientated [7]. Also the expression of certain immunoregulatory markers and neurotrophins by microglia is subject to their location in the CNS and thus the local environment [8-11].

The scanning property of microglial cell processes enables them to rapidly detect and react to a disturbance in the CNS homeostasis. Upon the appearance of signs indicating such a disturbance, microglial cells can transform into an activated state. The microglia will retract their processes and acquire a more rounded cell body with more perinuclear cytoplasm resulting in an amoeboid morphology. Besides this morphological transformation, the microglial cells will acquire the ability of directed migration towards the disturbed site. Additionally, they will increase the expression of surface markers, cytokines and other inflammatory mediators. Finally, when the microglial cells are fully activated they adopt a phagocytic phenotype [6, 12-15]. Microglial activation is not a linear process (Fig. 1.2). The reactive phenotype in which a microglia will transform depends on the type and duration of the activating signal, the interpretation and context of these signals, and the feedback of their microenvironment. Finally, the cells can emigrate, die, or transform back into a resting phenotype [16].

Once activated, microglial cells can have beneficial effects, via phagocytosis of cell debris, presentation of antigen, or the release of trophic or anti-inflammatory molecules. However they can also be detrimental via the production of reactive oxygen species or inflammatory cytokines [17, 18]. In addition, there is increasing evidence that, besides their protective role,

microglial cells can also fulfill other functions such as regulating synaptic functions, glial cell progenitor development and neurogenesis [18-26].

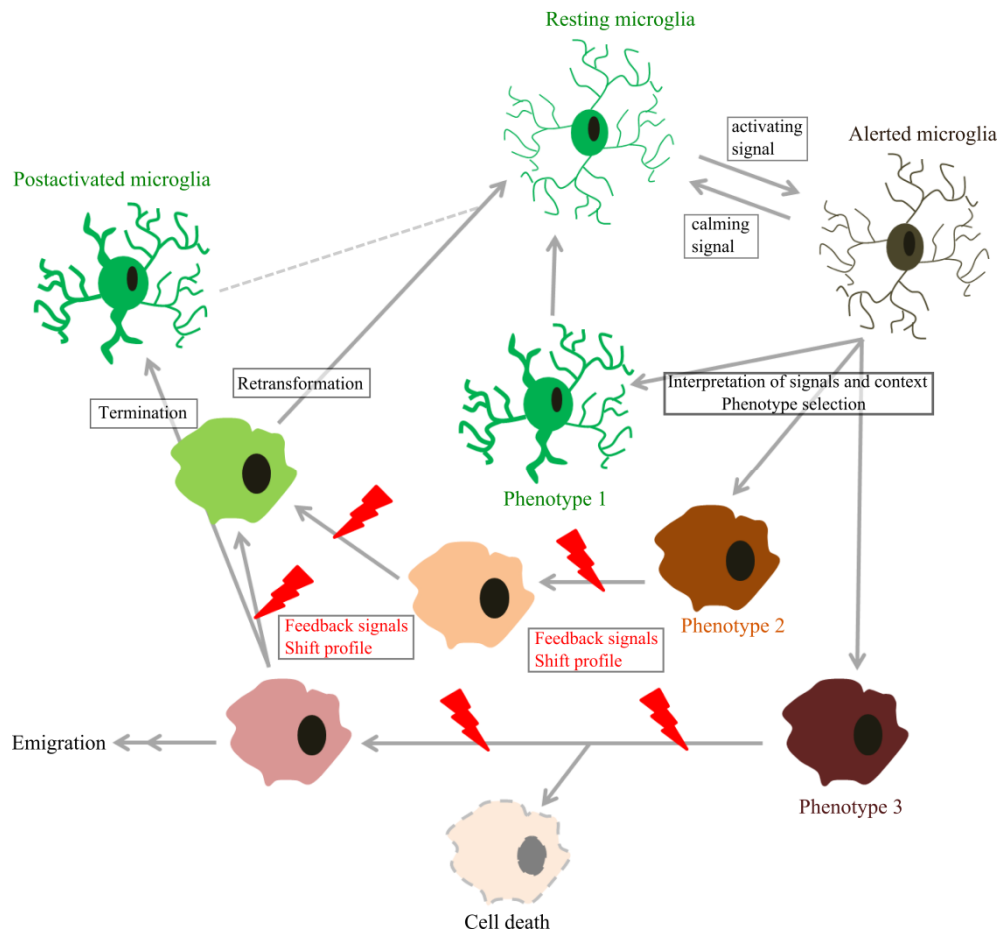


Figure 1.2. Microglial activation pathway. Resting microglia continuously scan their environment for signals of a disturbed homeostasis indicated by the loss of calming inputs or the appearance of activating inputs. Upon encountering such an input the microglia will become alerted. These alerted microglial cells can subsequently transform into a specific phenotype by interpreting the different signals and their context. Feedback signals from CNS cells or infiltrated immune cells will shift the profile of the cells which results in emigration or cell death or a return to the resting state. (Based on Hanisch and Kettenmann [16].)

1.1.2 Microglial cell markers

Over the years much progress has been made in identifying microglial cells and determining their activation state by using immunohistochemical markers. A recent paper showed that there is a lot of diversity in gene-expression profiles between different populations of macrophages. Microglia differed considerably in the expression of several mRNA transcripts that were expressed in other macrophage populations [27]. There are many intra- and extracellular proteins expressed by microglia that can be used as cell marker; the focus in this work is on the most commonly used ones.

Identification

One of the early markers used to identify microglia are lectins, sugar-binding proteins. Different types of lectins can be used to stain microglial cells, some examples are tomato lectin, simplicifolia B4 isolectin and Ricinus communis agglutinin-120. Their advantage is that they stain both amoeboid as ramified microglial cells. However they are not restricted to microglia, they can also stain other cell types and structures such as endothelial cells and the blood vessels [28-32]. Another general marker that has been used in several studies to identify microglial cells is F4/80 [7, 33]. This antibody recognizes a membrane protein that is expressed by monocytes and macrophages [34-36]. A more recent microglial cell marker is ionized calcium binding adaptor molecule-1 (Iba-1). Iba-1 is a small protein of 17-kDa that contains two EF-hand motifs. It is suggested to function as an adaptor molecule that mediates calcium signals in cells of the monocytic lineage and in microglia, and to be involved in membrane ruffling and phagocytosis [37-40]. Hirasawa et al. have developed a transgenic Iba-1-eGFP mouse line; this permits the study of microglia without the need for antibodies and allows the study microglia *in vivo* [38]. Jung et al. created another transgenic mouse line that expresses enhanced green fluorescent protein (eGFP) under the promoter of the fractalkine receptor (CX3CR1) [41]. In this transgenic mouse, CX3CR1 is expressed by subsets of natural killer cells and dendritic cells, microglia and in less extent by monocytes. The natural ligand of this receptor, fractalkine (CX3CL1), is widespread throughout the CNS [41, 42]. The CX3CL1/CX3CR1 signaling is thought to act as an "off" signal, keeping microglial cells in a quiescent state. Research of Cardona et al. has showed that

signaling via the CX3CR1 indeed regulates microglial neurotoxic activity [43, 44]. The murine homologue of cluster of differentiation (CD)68, macrophage mannose receptor, can also be used as a microglial cell marker. CD68 is a transmembrane glycoprotein which is mainly expressed intracellularly, in lysosomes and endosomes of monocytes, macrophages and microglia [40, 45-47]. Finally, microglia can also be identified by CD11b, a protein that is expressed at the surface of the cell and involved in adhesion, activation and phagocytosis. Besides being used as a marker, this protein also gives an indication of microglial activation since its expression is increased in activated microglia [15, 48, 49].

Functional orientation

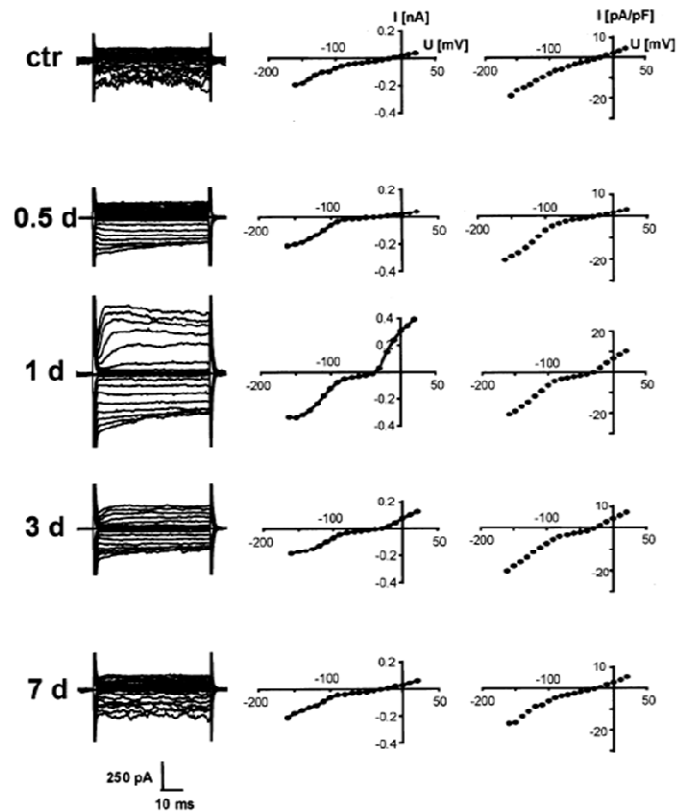
Besides CD11b there are more proteins that indicate microglial activation state. Two commonly used markers are Mac-2 and major histocompatibility complex (MHC) class II. Mac-2, also known as Galectin-3, is a member of the galectin family of β -galactoside binding lectins. Expression of Mac-2 is upregulated by activated microglia and is dependent on the type of injury or damage that has triggered microglial activation since its expression depends on the occurrence of an inflammatory process and the breakdown of the blood-brain barrier [50-55]. The second activation marker, MHC class II, is upregulated on microglia in CNS pathologies in order that they can present antigens to T-cells and induce an appropriate immune response. MHC class II expression by microglia is often seen as an indication of the highest level of microglial activation [56, 57]. In addition, microglia activation will also result in the production of cytokines, such as tumor necrosis factor α (TNF α), interleukin (IL)-1 β and nitric oxide, which will allow them to eliminate cells [58-60].

1.1.3 Electrophysiological properties of microglia

Microglia are non-excitabile cells, however their electrophysiology has gained a lot of interest over the last decade. Much research has studied microglial electrophysiology by making use of primary cell cultures. However as a consequence of the isolation procedure and removal of these cells from their environment microglia cultures cannot represent the *in vivo* situation. For this reason some groups have used acute brain slices to study the electrophysiological properties of microglia. They found that in the healthy adult

CNS, microglia have a small cell body with ramified processes. These resting microglia have a high input resistance, a low membrane potential and display a small inward rectifying K^+ current (IK_{IR}) upon hyperpolarization [61, 62]. This IK_{IR} is also present in microglia from postnatal acute brain slices [63, 64]. In pathological conditions of the CNS, microglial cells can get activated. They retract their processes; acquire an amoeboid morphology and upregulate the expression of inflammatory modulators. Research on the effect of CNS insults has made use of several models: facial nerve axotomy, ischemia and status epilepticus. They all found that with activation, microglia will also alter their electrophysiological properties; the membrane capacitance will increase, within 12 hours the amplitude of the IK_{IR} rises and at the peak of activation (approximately after 1 day) the microglia express additionally a delayed (outward) rectifying K^+ current (IK_{DR}). After 3 days the amplitudes of both currents start to decrease and after 1 week the currents had returned to control levels [64-66]. An example of how this activation cascade is presented after facial nerve axotomy is depicted in figure 1.3.

Figure 1.3 (Next page). Microglial activation after facial nerve axotomy is paralleled by changes in membrane currents. In response to a CNS insult like facial nerve axotomy, ischemia or status epilepticus, microglia will increase the inward rectifying current amplitude (0.5 d) and subsequently express a delayed rectifier (1 d). Currents returned at the control level after 7 days. Representative membrane currents in response to voltage steps correspond to the first column. The second column shows the corresponding I/U-curves for an individual cell. In the third column the mean normalized I/U-curve are displayed. d, days; I, current; U, voltage (From Boucsein et al. [61]).



K^+ channels are implicated in regulating membrane potential, cell volume and intracellular ions. K^+ currents have the ability to influence Ca^{2+} signaling since they can control membrane potential and in this way influence Ca^{2+} driving force. For example, an increased expression of K_{IR} correlates with a more negative membrane potential and this will increase the driving force for Ca^{2+} to enter the cell [3, 67]. The K_{DR} channels have been shown to be involved in microglial proliferation and respiratory burst [3, 68-71]. These K_{DR} channels are part of the Kv channel family and especially Kv1.3 and Kv1.5 are thought to be critical for the IK_{DR} [72, 73].

In addition to the K^+ channels, microglia also express many other ion channels, such as calcium channels, anion channels, proton channels, aquaporins and others [74-78]. However, most of the data are obtained from experiments that

were performed on cell cultures. *In vivo* experiments indicate that microglia express volume-regulated Cl⁻ channels [79] and Ca²⁺ dependent K⁺ channels [80]. Upon activation, by lipopolysaccharide, damage or in epilepsy, microglia can express aquaporins [81] and connexins [82] and increase their expression of Ca²⁺ dependent K⁺ channels [83].

Many studies have furthermore indicated that microglia also express receptors for different neurotransmitters. Much of the research was performed on cultured microglia but some used acute brain or spinal cord slices, a model that comes closer to the *in vivo* situation. From these experiments we know that microglia express γ -aminobutyric acid (GABA), dopamine, adrenergic and glutamate receptors, and purinoceptors [3]. Application of GABA_B agonists to acute brain slices activated an outward rectifying K⁺ conductance in the microglial cells. Kuhn et al. showed that activation of these GABA_B receptors modulated the immune response [84]. Another study on microglia of acute brain slices focused on the amoeboid cells that were present at the surface. These cells expressed functional dopaminergic and adrenergic receptors. Application of D₁ and D₂-like dopamine receptor agonists induced in about 30% of the cells an outward current. When a β -adrenergic agonist was applied to the slice, an outward current response was observed in about 25% of the microglial cells [85].

Liu et al. found that glutamate released from a micropipette had a chemotactic effect on microglia in spinal cord slices from postnatal mice. This effect was induced via α -amino-3-hydroxy-5-methylisoxazole-4-propionic acid (AMPA) and metabotropic glutamate receptors [86].

Many groups focused on the presence of purinoceptors on microglia since adenosine triphosphate (ATP) and its derivatives act as primary transmitters and co-transmitters in the CNS [87]. ATP can be released upon damage and act as a cell-cell mediator. Microglia express different types of P2X and P2Y receptors, both in their resting state and after activation (see table 1.1). Microglia in the developing CNS express P2X₁, P2X₄ and P2X₇ [88]. Boucsein et al. saw that application of de- and hyperpolarizing voltage steps upon ATP administration induced an outward rectifying K⁺ conductance and a cationic conductance resulting from respectively P2Y and P2X receptor activation. They found the presence of P2X₇ and several P2Y receptors (P2Y₁, P2Y_{2/4} and P2Y₆) on the microglial cells. ATP application was able to induce microglial nitric oxide release

and influence cell activation in a complex way [62]. Ulmann et al. showed that upon nerve injury, P2X4 receptors get expressed by activated spinal cord microglia. Stimulation of these P2X4 receptors led to BDNF release which in turn can contribute to the development of chronic pain [89, 90]. Davalos et al. found that administration of ATP via a micropipette induces movement of the microglial processes towards the point of application. This effect was blocked by inhibitors of P2Y receptors [6]. The importance of P2Y receptors, especially P2Y12, in microglial motility and chemotaxis was also demonstrated by Haynes et al. and Ohsawa et al. [91, 92]. Avignone et al. have shown that microglia increase the expression of several P2Y receptors after induction of status epilepticus and that this results in increased motility of the processes [66]. In a study of Koizumi et al. it was shown that activation of P2Y6 receptor on microglia mediated phagocytosis [93]. Many groups reported that stimulation of purinergic receptors induced chemotaxis and the release of several factors [94, 95]. Besides P2 receptors, microglial cells also express P1 receptors. Studies have proven that adenosine A1 receptors on microglia in the adult brain can influence their proliferation and migration [96-98], and A2A and A3 receptors are involved in morphology changes upon microglial cell activation [98, 99].

Table 1.1. Overview of the different purinergic receptors with their agonists. The receptors that can be expressed by microglia are put in bold.

P2XR	Agonists	P2YR	Agonists	P1R	Agonists
P2X1	ATP (EC ₅₀ 1 μM) α,β-Me-ATP 2-MeSATP bz-ATP	P2Y1	2-MeSATP 2-Cl-ATP ATP	A1	Adenosine 2-Cl-adenosine CCPA
P2X2	ATP (EC ₅₀ 10 μM) 2-MeSATP bz-ATP	P2Y2	UTP ATP Ap4A	A2a	Adenosine 2-Cl-adenosine CGS-21680
P2X3	ATP (EC ₅₀ 1 μM) 2-MeSATP α,β-Me-ATP bz-ATP	P2Y4	UTP ATP	A2b	Adenosine
P2X4	ATP (EC ₅₀ 10 μM)	P2Y6	UDP UTP ADP 2-MeSATP	A3	Adenosine Cl-IB-MECA 2-Cl-adenosine
P2X5	ATP (EC ₅₀ 10 μM) 2-MeSATP	P2Y11	2-MeSATP bz-ATP		
P2X6	ATP (EC ₅₀ 10 μM) α,β-Me-ATP 2-MeSATP	P2Y12	2-MeSADP ADP		
P2X7	ATP (EC ₅₀ > 100 μM) bz-ATP 2-MeSATP	P2Y13	ADP 2-MeSATP ATP		
		P2Y14	UDP-glucose		

Data taken from: [3, 87, 98, 100-104]

1.2 Microglia in the developing central nervous system

1.2.1 Origin of embryonic microglial cells

The findings of del Rio-Hortega about microglial morphology and function in the CNS have stood the test of time. However the origin of these cells has been a point of discussion with two opposing sides, with on one hand supporters of a mesenchymal origin and on the other hand supporters of the neuroectodermal derivation [105, 106]. Microglial cells can be detected early in the developing CNS (embryonic day (E) 9.5 in embryonic mice) [107]. The early invasion of the CNS by microglial cell was also observed in human, rabbit, rat and quail embryos [31, 108-113]. Recently, it was shown that microglial cells derive from primitive myeloid progenitors that arise before E8 in the yolk sac of embryonic mice, the birthplace of hematopoietic progenitors in mammals [107, 114].

This notion that the yolk sac is the source of microglial (progenitor) cells was supported by the results of some recent studies. In the embryonic zebrafish, early macrophages develop in the yolk sac and subsequently spread throughout the cephalic mesenchyme [115]. Another observation that supports the notion that microglia derive from yolk sac progenitors is focused on the colony stimulating factor-1 receptor (CSF-1R). The CSF-1R is very important in adult macrophage colonies [116]. The yolk sac macrophages and microglia in embryonic mice express the CSF-1R. Absence of this receptor reduced the development of the yolk sac macrophages and microglia, as well as microglial differentiation and resulted in an almost complete lack of microglial cells in the CSF-1R deficient mice [107, 117]. The same observations were made in PU.1 deficient mice. Since the transcription factor PU.1 is expressed by microglia and PU.1 is important in the expression of the CSF receptor, its elimination also results in absence of microglial cells [25, 118-120]. Finally, research showed that CX3CR1 and Iba-1 expressing cells were present in the yolk sac of in the embryonic mouse (E9.5 - E11.5). Later in development, these cells were seen to invade the developing neuroepithelium and form the microglial population in the CNS parenchyma [38, 114].

1.2.2 Microglial entry and dispersion in the developing central nervous system

After the microglial progenitor cells have emerged from the yolk sac they migrate towards the neuroepithelium of the developing CNS. In the mouse embryo, microglia reach the spinal cord via the peripheral vasculature [121]. Microglial cells are believed to have several routes of entry into the developing CNS [122]: the meninges, the ventricles, the choroid plexus and the blood vessels (Fig. 1.4).

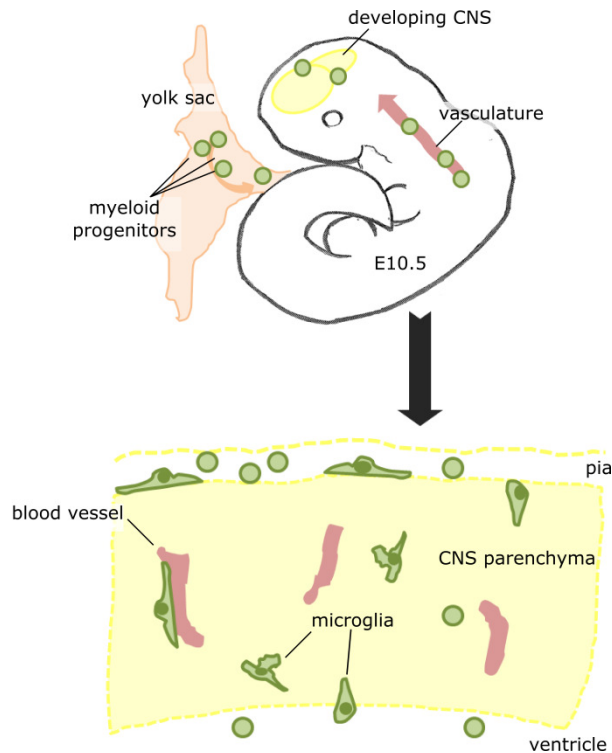


Figure 1.4. Hypothetical scheme of microglial invasion of the developing CNS. Microglial cells derive from myeloid progenitors that arise in the yolk sac and reach the developing CNS via the developing circulation. Subsequently they can enter the CNS parenchyma via several routes by crossing the pial surface and ventricle, or later in development via the blood vessels. The fourth possible entry route, the choroid plexus, is not shown in this scheme. After they have entered they will proliferate and migrate throughout the tissue to reach their final position and differentiate into a ramified morphology.

Early in development microglial cells are present in the meninges along the pial surface. A first possibility is that microglial cells enter the CNS by crossing the pial surface. This was already suggested by del Rio-Hortega, who observed an

accumulation of these cells at the pial surface [2]. Indeed, several studies also noticed the presence of microglial cells at the meninges and some showed precursors that cross the pial surface to gain access to the developing parenchyma [28, 121-127]. Another suggested route of entry is the ventricle. Microglia can be observed as free-floating cells in the ventricular lumen or attached to the ventricular wall [124]. Also in the central canal of the developing spinal cord microglial cells are observed [121]. In addition, microglial cells have been observed to cross the ventricular surface [126-128]. The third possible route is the choroid plexus. A few studies report about the presence of an accumulation of microglial cells in the choroid plexus [124, 129], suggesting that microglia can also gain access to the developing parenchyma via this structure. The last invasion route is the vasculature. In the developing CNS, passage from the blood vessels is easier than in the adult since the blood-brain barrier is not mature. Microglial cells can be observed in close proximity of the developing blood vessels [30, 115, 121, 124, 126]. However, microglia can already be detected in the developing CNS before vascularization has occurred [115, 121, 130], suggesting that this is not the principal route of entry and most probably a route that is used later in development.

After entering the developing CNS the microglial cells migrate throughout the parenchyma to their final location. Studies have reported two different modes of microglial migration through CNS regions with a layered cytoarchitecture, like the retina, being tangential and radial migration (Fig. 1.5). Tangential migration involves migration of the cell parallel to the CNS surface and allows movement over the full extent of a single layer in that region. Radial migration occurs perpendicular on the CNS surface/layer where the tangential migration occurs in and allows for the cells to access different layers in the parenchyma [112, 113]. Most of what we know today has been obtained from research on the retina. These studies showed that in the embryonic quail retina microglia make use of Müller cell endfeet and fibers as a substratum to migrate respectively tangentially and radially [112, 113, 123]. In the spinal cord of human and mouse embryos, microglia were also seen in close contact with radial cell fibers [31, 121] and in the developing quail cerebellum microglia seem to use axon bundles and radial glia as scaffold. An additional migration substratum could be

the developing vasculature, since microglial cells are also observed in close proximity of the parenchymal blood vessels [121, 124, 125].

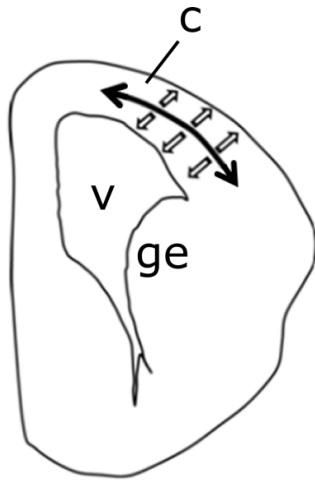


Figure 1.5. Migration modes of microglial cells in CNS regions with a layered architecture. Microglial can migrate tangentially (closed arrow), parallel to the CNS surface throughout one layer, or radially (open arrows), perpendicular to the CNS surface. c, cortex; v, ventricle; ge, ganglionic eminence (Based on Cuadros and Navascués [123]).

Besides entry and migration from the periphery, microglial cells can also increase their cell number and density by proliferating. Research has shown that the embryonic microglia are highly proliferative cells [107, 108, 125, 127]. A recent paper on the embryonic spinal cord showed that microglial cell proliferation occurs at the periphery at the onset of their colonization process [121].

With increasing development, microglial cells slowly reach their final location upon which they gradually obtain a ramified morphology until they are fully ramified, adult microglia [121, 125, 127, 131].

1.2.3 Microglial functions in CNS development

Microglial cells start to invade the embryonic CNS early in development, before the end of neurogenesis and before the onset of gliogenesis. This suggests that they play a role in (some of) the processes that are necessary for the normal development of the CNS. Indeed, various research groups have uncovered that embryonic microglia have the potential to influence several processes that take place during development of the CNS. A schematic presentation of the different

functions microglial cells are suggested to fulfill in the developing CNS is shown in figure 1.6.

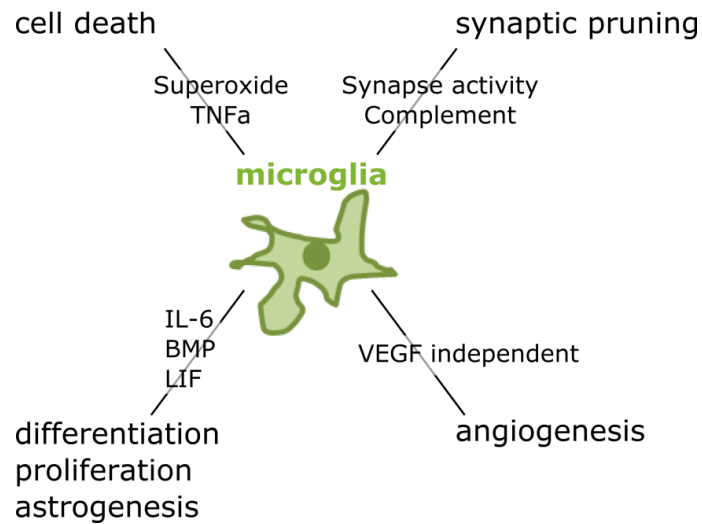


Figure 1.6. Schematic presentation of the different functions that have been ascribed to microglial cells in the developing CNS. Microglial cells have been shown to be responsible for inducing cell death. They eliminate the excessive formed synapses in the process of synaptic pruning. Microglia can influence progenitor differentiation, proliferation and astrogenesis via the secretion of several factors and they are involved in the development of vascular network. BMP, bone morphogenic protein; IL-6, interleukin 6; LIF, leukaemia inhibitory factor; TNFa, tumor necrosis factor alpha.

Microglial cells have been shown to be responsible for clearing cell debris and promote apoptosis in the developing CNS. In the developing postnatal mouse cerebellum, apoptotic Purkinje cells were always seen in close contact with microglial cells. Elimination of the microglia via the macrophages suicide technique rescued the Purkinje cells from death. Further research revealed that the microglial cells promoted Purkinje cell apoptosis by producing superoxide ions [32]. Another study showed that in the postnatal mouse hippocampus microglia also promoted the death of neurons by the production of superoxide ions. The apoptotic neurons contacted microglia positive for CD11b and DAP12. Two molecules involved in the pathway that controls the production of superoxide ions by microglia and thus in inducing neuronal death [49]. Also in the embryonic spinal cord the microglia accumulate near apoptotic cells [121]

where they seem to be involved in the programmed motoneuron cell death. Sedel et al. performed explants experiments with rat embryonic spinal cords and observed that, before the onset of programmed cell death, motoneurons become committed to cell death between E12 and E13. Microglial elimination from the explants abolished the pro-death effect. Blocking antibodies identified TNF α produced by the microglia as a diffusible activator for the early commitment of motoneurons to cell death [132]. Microglial cells are also involved in synaptic pruning, a developmental process of synapse maturation in which microglial cells monitor the synaptic activity. Based on the neural activity and expression of specific signals, such as complement components, they eliminate synapses by engulfing them [133, 134].

Besides eliminating (dead) cells, microglia can also influence the development and differentiation of neural cells. Research by Aarum et al. showed that microglia-conditioned media influenced embryonic precursor migration and differentiation in primary cultures, which increased the proportion of neurons derived from the progenitor cells [135]. Another group was able to demonstrate that microglia-conditioned medium can influence cholinergic differentiation in primary cultures from undifferentiated precursors derived from the embryonic basal forebrain. Some of the factors that were present in the medium and were, in some part, responsible for the observed effects were interleukin (IL)-6 and bone morphogenic proteins [136]. Recently, it was also shown that microglia can regulate cortical precursor proliferation and astrogenesis [25, 137]. Nakanishi et al. showed that microglia-derived IL-6 and leukaemia inhibitory factor (LIF) can induce astrocytic differentiation in primary neural stem/progenitor cell cultures derived from the embryonic rat brain via activation of the JAK/STAT and MAPK pathway [137]. Primary culture experiments by Antony et al. on embryonic precursor cultures showed that microglial cells are important for precursor proliferation and astrogenesis. In cultures depleted of microglia and cultures from PU.1 knock out embryos proliferation and astrogenesis were decreased. Addition of microglia to these cultures restored both processes and an abnormal increase in microglial cell numbers resulted in increased astrogenesis. The factors responsible for this effect are not identified yet, however it is suggested that microglia can produce and secrete a variety of growth factors such as BDNF and LIF [25]. A recently published study indicates that microglia can influence

the number of neural precursor cells. Cunningham et al. showed that deactivation of embryonic microglia with tetracyclines or elimination via the macrophages suicide technique led to an increase in neural precursor cells, while microglial activation with lipopolysaccharide (LPS) had the opposite effect [127]. Two recent papers show that, besides their effects on neural cells, microglia can influence angiogenesis since they interact with endothelial tip cells and support tip cell fusion. In the study of Rymo et al., microglial cells were seen in close association with vessel sprout anastomoses in the developing mouse retina. The results of their study suggest that direct contact between microglia and endothelial cells is most likely not necessary and that the microglia produce soluble factors, other than vascular endothelial growth factor, that stimulate vessel sprouting [138]. Fantin et al. described the same close contact of microglia with endothelial tip cells in the embryonic mouse brain and also found that the brain angiogenesis was promoted independently of vascular endothelial growth factor.[139].

All these results suggest that microglial cells are able to secrete a cocktail of soluble factors such as growth factors and cytokines that can influence several processes in the course of CNS development.

1.3 Neuropsychiatric disorders and maternal inflammation

Autism and schizophrenia are neuropsychological disorders with both a prevalence of approximately 0.5% [140-143]. Autism is characterized by repetitive behaviors and deficits in social interaction and communication skills. People with schizophrenia show disturbances in mental and emotional functions and behavior. Studies have shown that brain abnormalities and deviations in immunity can be observed in patients of both neuropsychiatric disorders [140, 141, 144-150]. A study of Vargas et al. on the brain and cerebrospinal fluid (CSF) of autistic patients, showed that there was an active neuroinflammatory process present in the brain with marked microglial and astroglial activation. Additionally, a proinflammatory cytokine profile was present in the brain and CSF, presented as an increased expression of tumor growth factor- β 1, macrophage chemoattractant protein-1 and several other cytokines and growth factors. Additionally, there was a significant loss of Purkinje cells in autistic cerebella [148]. A DNA microarray and real-time qPCR on brain samples of

schizophrenia patients revealed deficits in the GABA-related transcriptome. There was a decreased expression level of GAD67, somatostatin, neuropeptide Y and GABA_A receptor subunits [150]. Another DNA microarray showed an upregulation of several genes with immune and chaperone functions in the brain of schizophrenia patients compared to their respective controls, which the authors suggest, following the neuroimmune hypothesis, could be a consequence of early brain activation by proinflammatory cytokines [149]. Family and twin studies on the etiology of both diseases show that genetics play an important role but that there are also environmental factors involved in the development of these neuropsychiatric disorders [151, 152].

Epidemiological studies have indicated associations of schizophrenia and autism with maternal stress, diet, microbial pathogens, toxins or the season of birth. Some cohort studies focused on maternal inflammation during pregnancy and found that there was an increased risk of autism and schizophrenia in the offspring of mothers that had a viral infection, like influenza, during the first half of pregnancy. It was suggested that the acute infection can induce changes in maternal cytokine levels, like TNF α and IL-4, -5 and -8, which can be transmitted to the placental and fetal environment. In turn, this can affect the fetal brain and result in the development of autism or schizophrenia in the offspring [141, 144, 146, 147].

In order to study the mechanisms behind this correlation several animal models have been developed where pregnant female rodents were infected with the influenza virus, polyinosinic:polycytidylic acid (poly (I:C)), LPS or another agent. As observed in persons with schizophrenia and autism, behavioral analysis of the offspring subjected to this maternal immune activation (MIA) revealed deficits in prepulse inhibition in the acoustic startle response, deficits in their exploratory behavior and in social interaction [153-157]. There were also neuropathological changes present in their brains such as an increased density of pyramidal cells and increased brain size and decreased ventricle size at adulthood [158]. Studies by Meyer et al. showed a decrease in postnatal neurogenesis in the dentate gyrus, a reduction in Reelin positive cells and increase in apoptosis in the hippocampus after poly (I:C) challenge [154]. In addition, changes in neurotransmitter systems could be observed postnatally. There was a decrease in dopamine D1 receptors, and Reelin and Parvalbumin positive cells in the

cortex. In the hippocampus there was a decrease in the NMDA receptor subunit N1 and an altered distribution of the GABA_A receptor $\alpha 2$ subunit at axon initial segments [155]. Prenatal administration of LPS resulted in an increase in postsynaptic excitability and decreased short-term plasticity in the CA1 region of the hippocampus [159]. A recent study showed that maternal immune activation led to changes in brain cytokine levels in the offspring in a region- and age-specific manner: in the cortex pro- and anti-inflammatory cytokines are increased early postnatal, decreased in early adolescence and few again increased in adulthood when compared to the controls. In the hippocampal area, decreases and increases in cytokine levels occurred at early postnatal and adolescent stages [160].

As already stated, being the resident immune cells of the CNS, microglial cells can rapidly respond to a change in their local environment by the production of cytokines [14, 16]. There is the hypothesis that MIA results in a maternal "cytokine storm" that can be transferred to the fetus. The fetal microglia could be a possible target for this "cytokine storm" which results in an altered production of a variety of cytokines and growth factors that in turn could affect normal fetal brain development [18, 19, 21, 25, 32, 49, 154, 161, 162]. The results of Meyer et al. support in a part this hypothesis; they saw that several cytokine levels were increased after maternal immune challenge and that some of them were also altered in the fetal brain [154].

The role of microglia in neuropsychiatric disorders remains controversial; however there are some indications for these cells to be of importance. Some studies found indications of an active neuroinflammatory process, with microglial cell activation, in the brain of autism patients [148, 163]. Others have observed changes in microglial cell activation in the brain of schizophrenia patients [164, 165]. Recent studies also indicated an augmented microglial cell density in different brain regions of adult MIA offspring (poly (I:C) model) [166, 167] and one study saw an increased percentage of activated microglia after maternal injection with LPS [127].

These results all support the growing believe that microglial cells could be involved in neuropsychiatric disorders that are triggered by risk factors activating the immune system during embryonic development. However, until now only one study has investigated the effect of a MIA with LPS on the fetal

microglia. Studies looking at the effect of poly (I:C) on these cells are missing and important to help better understand how influenza infection during the pregnancy can lead to the increased risk on neuropsychiatric disorders. As population studies have indicated that there is an association [144, 146]

1.4 Aims of the study

The function and properties of microglial cells in the adult CNS are widely studied. This is in contrast with embryonic microglial cells, which remained for years poorly studied. Recently, fetal microglia gained attention since it is now becoming clear that these cells can already exert certain functions in the developing CNS [168, 169]. Recent studies have identified primitive myeloid progenitors from the yolk sac as being the source of microglia [107]. It is established that invasion of the embryonic CNS by microglial cells starts early in fetal development. However, their pattern of invasion and their phenotype during early brain development remain poorly understood. Therefore we investigated the properties of microglial cells present in the embryonic murine cortex, and whether microglia are involved or affected by maternal inflammation. Based on these results, microglial function in early development can be further elucidated. For the experiments in this thesis we made use of the CX3CR1eGFP mouse model created by Jung [41], to envision all microglial cells (eGFP positive cells).

The invasion pattern and phenotype of microglial cells in the embryonic cortex of the mouse

Early in development microglia have an amoeboid morphology which gradually changes into a more ramified form as the CNS matures. In the adult CNS, an amoeboid morphology represents an activated microglial phenotype which is accompanied by an increase in the expression of certain cell surface markers such as Mac-2 and MHC class II. The invasion pattern of the cortex by embryonic microglia with respect to the developmental stages of this structure is poorly documented and information about their early cellular interactions and immunohistochemical and electrophysiological phenotype are scarce. Therefore, in **chapter 2**, we investigated the colonization processes of the embryonic cortex by microglia *in vivo* and *ex vivo*, with respect to the well-known developmental pattern of the embryonic cortex by means of immunohistochemical stainings and time-lapse imaging of acute brain slices. In addition, the expression of activation markers and their proliferation potential were analyzed. In **chapter 4**, the functional expression of IK_{IR} and IK_{DR} , also indicators of activation level, and other types of ion channels and

neurotransmitter receptors was studied via patch-clamp recordings in acute embryonic brain slices.

The influence of P2X7 and Pannexin-1 on microglial cell proliferation in the embryonic spinal cord

Microglia invade the spinal cord at an early embryonic stage, which is partially associated with their ability to proliferate at the onset of motoneuron developmental cell death and of synaptogenesis in the mouse embryo (E13.5) [121]. *In vitro* studies have shown that the proliferation and activation of adult microglia can be influenced by the purinergic ionotropic receptor P2X7 via a coupling with Pannexin-1. We studied in **chapter 3** the presence of P2X receptors by performing qRT-PCR on sorted embryonic microglia and patch-clamp recordings *in situ* on an embryonic spinal cord preparation. In addition, patch-clamp recordings and immunostaining of wild-type and specific knockout embryos were used for further determination of the properties and effects of the ATP-evoked current.

The effect of maternal inflammation during pregnancy on the fetal microglial cells

Maternal immune activation during pregnancy is considered a risk factor for schizophrenia and autism in the offspring [144]. Several animal models that mimic this relation and result in similar behavioral deficits in the offspring have already been developed. The change in maternal IL-6 levels after immune challenge has been proven to be critical in the development of these changes observed in the offspring [156]. Some studies showed that the maternal cytokine response evoked after immune challenge can in some part be transferred to the fetal environment [154, 170]. Since microglia are already present in the fetal CNS we studied the effect of maternal immune activation on embryonic microglia in **chapter 5**. Maternal inflammation was induced with a synthetic analog of dsRNA. With this work we aim at better understanding the effect of maternal immune activation on microglial cell density and activation.

2 Complex invasion pattern of the cerebral cortex by microglial cells during development of the mouse embryo

This chapter is based on:

Complex invasion pattern of the cerebral cortex by microglial cells during development of the mouse embryo

Swinnen N, Smolders S, Avila A, Notelaers K, Paesen R, Ameloot M, Brône B, Legendre P, Rigo JM.

Glia. 2013 Feb;61(2):150-63. doi: 10.1002/glia.22421. Epub 2012 Sep 21.

2.1 Abstract

Microglia are the immune cells of the central nervous system. They are suspected to play important roles in adult synaptogenesis and in the development of the neuronal network. Microglial cells originate from progenitors in the yolk sac. Although it was suggested that they invade the cortex at early developmental stages in the embryo, their invasion pattern remains largely unknown. To address this issue we analyzed the pattern of cortical invasion by microglial cells in mouse embryos at the onset of neuronal cell migration using *in vivo* immunohistochemistry and *ex vivo* time-lapse analysis of microglial cells. Microglial cells begin to invade the cortex at 11.5 days of embryonic age (E11.5). They first accumulate at the pial surface and within the lateral ventricles, after which they spread throughout the cortical wall, avoiding the cortical plate region in later embryonic ages. The invasion of the cortical parenchyma occurs in different phases. First, there is a gradual increase of microglial cells between E10.5 and E14.5. From E14.5 to E15.5 there is a rapid phase with a massive increase in microglia, followed by a slow phase again from E15.5 until E17.5. At early stages, many peripheral microglia are actively proliferating before entering the parenchyma. Remarkably, activated microglia accumulate in the choroid plexus primordium, where they are in the proximity of dying cells. Time-lapse analysis shows that embryonic microglia are highly dynamic cells.

2.2 Introduction

Microglia are the resident immune cells of the central nervous system (CNS). In the healthy adult CNS, microglial cells have a ramified morphology, with a small cell soma and long, thin processes that constantly scan their environment [5, 6]. Microglia can play a beneficial role, through phagocytosis of cellular debris, trophic and anti-inflammatory factor release, but they can also have detrimental effects through reactive oxygen species production and inflammatory cytokine production [17, 18]. In addition, there is increasing evidence that they can also participate in the regulation of neuronal network and cell assembly in the adult [18, 21, 25, 32, 171-173].

Microglia derive from primitive myeloid progenitor cells that arise in the mouse before E8 in the yolk sac and can be detected in the brain at early developmental stages, by day E9.5 in mice embryos [107, 119]. This is also the case in human, rabbit, rat and quail embryos [31, 108-113]. In the mouse embryonic spinal cord, microglial cells begin to invade the parenchyma at the end of neuronal migration (E11.5), during which local neuronal networks become functional [121]. Remarkably, microglia begin to invade the brain [107] and spinal cord [121] at similar ages in mouse embryos, but at this stage the cortex is less mature than the spinal cord and is characterized by the beginning of cortical neurogenesis [174-177]. It is therefore unclear whether the embryonic microglia, although of similar origin, will have similar functions in both embryonic structures according to their developmental stages. This remains an open question, as the invasion pattern of the cortex by embryonic microglia with respect to the developmental stages of this structure is poorly documented and their functions during early brain development remain poorly understood. To address this issue, we investigated the colonization processes of the embryonic cortex by microglia *in vivo* and *ex vivo*, with respect to the already known developmental pattern of the embryonic cortex.

Using the transgenic CX3CR1-eGFP mouse, immunohistochemical methods and time-lapse imaging, we show that the invasion process of the embryonic cortex occurs in three phases, an initial phase from E10.5 until E14.5, a second one occurring between E14.5 and E15.5, and a third one after E15.5. During this process, microglia are showing a highly dynamic behavior. In the same period,

microglial cells accumulate within the choroid plexus primordium, close to dying cells.

2.3 Materials and methods

2.3.1 Animals

Transgenic CX3CR1-eGFP knock-in mice [41] were used in order to visualize microglia in the embryonic cortex *in vivo*. In these animals, eGFP is expressed under the promoter of CX3CR1, also known as the fractalkine receptor, rendering all monocyte-derived cells, including microglia, green fluorescent [41]. All experiments were conducted in accordance with the European Community guiding principles on the care and use of animals and with the approval of the Ethical Committee on Animal Research of the Hasselt University. Mice were maintained in the animal facility of the Hasselt University in accordance with the guidelines of the Belgian Law and the European Council Directive. The heterozygous CX3CR1-eGFP +/- embryos that were used in this study were obtained by crossing homozygous CX3CR1-eGFP +/+ mice (mice were obtained from the European Mouse Mutant Archive – EMMA with the approval of Stephen Jung [41]) with wild type C57BL/6 mice. Females were checked for vaginal plugs each morning, the day of conception was designated as embryonic day 0.5 (E0.5). Pregnant mice were sacrificed by means of cervical dislocation at the desired embryonic day and the embryos were removed.

2.3.2 Tissue Preparation and Immunostaining

The heads of E10.5 – E15.5 embryos were fixed in 4% paraformaldehyde for 3h at 4°C, 5h for E16.5 and E17.5 embryos. After fixation, the embryonic heads were cryoprotected overnight in phosphate-buffered saline (PBS) + 30% sucrose, frozen in optimal cutting temperature compound (Tissue-Tek) and stored at -80°C until sectioned. Ten and fifty-micrometer-thick coronal tissue sections were cut on a Leica CM1900 uv cryostat, mounted on Superfrost Plus glasses and stored at -20°C until staining.

Embryonic sections were washed three times in PBS, blocked with serum and permeabilized with Triton X-100 (Sigma-Aldrich). Subsequently they were incubated with the primary antibody (Table 2.1), this was performed overnight at 4°C, except for Ki-67 for which slices were incubated for 2h at room temperature. After washing, the sections were incubated with alexa-labeled secondary antibodies for 1h at room temperature and mounted with Vectashield (Vector laboratories) containing 4,6-diamidino-2-phenylindole (DAPI) to reveal

cellular nuclei. All primary antibodies and working solutions are listed in Table 2.1. Staining controls for the secondary antibodies were performed by omitting the primary antibodies.

To determine if the CX3CR1 eGFP cells observed in the embryonic cortex were effectively microglial cells we used antibodies directed against ionized calcium binding adaptor molecule 1 (Iba-1) and cluster of differentiation (CD)68. Iba-1 is a marker for microglial cells, it is a small protein suggested to function as an adaptor molecule that mediates calcium signals in cells of the monocytic lineage, including microglia [37]. CD68, the murine homologue for macrosialin, is a transmembrane glycoprotein which is expressed in lysosomes and endosomes of monocytes, macrophages and microglia [47, 178].

In order to determine the activation state of the microglia present in the embryonic cortex, we used an antibody against Mac-2 (ATCC; Clone M3/38.1.2.8 HL.2). Mac-2, also known as galectin-3, is a member of the galectin family of β -galactoside binding lectins. It can be expressed by many cell types and is implicated in several processes. Expression of Mac-2 is a hallmark of microglial activation [15, 50-53, 66].

A Ki-67 antibody was used to identify active proliferating microglial cells. The antigen is expressed during all active phases (the G1, S, G2 and M phases) of the cell cycle and cannot be detected in resting cells (G0 phase) [179].

Apoptotic cells were visualized using a cleaved caspase-3 antibody (Cell signaling; Asp175). This antibody detects endogenous levels of the large fragment (17/19 kDa) of activated caspase-3 and does not recognize the full length caspase-3 or other cleaved caspases [180].

Table 2.1. Overview of the primary antibodies

Primary Antibody	Company	Reference	Dilution
Anti-Iba-1	WAKO	019-19741	1:500
Anti-CD68	AbD Serotec	MCA1957GA	1:400
Anti-Mac-2	ATCC	TIB-166 Clone M3/38.1.2.8 HL.2	1:250
Anti-Ki-67	Abcam	ab15580	1:40 – 1:55
Anti-Cl. caspase-3	Cell Signaling	9661	1:500

2.3.3 Microscopy and Analysis of Immunostainings

Quantitative analysis of microglial cells was performed on images of 10- μ m-thick coronal embryonic brain sections, except when quantifying microglial morphology then 50- μ m-thick sections were used. Images were taken with a Nikon Eclipse 80i microscope and a Nikon digital sight camera DS-2MBWc. The objectives used were from Nikon; a 10x Nikon plan objective (numerical aperture (NA) of 0.25), a 20x Plan Fluor objective (NA of 0.5) and a 40x Plan Fluor objective (NA of 0.75). Ki-67 stainings were examined with an inverted Zeiss Axiovert 200M microscope attached to a Zeiss LSM 510 Meta Confocal laser scanning system. The different fluorophores were sequentially imaged through a 20x Plan-Apochromat objective (NA of 0.75). Images (1600 x 1200 or 512 x 512 pixels) were analyzed with ImageJ 1.45e software (NIH, USA; <http://rsb.info.nih.gov/ij/>). Only eGFP-positive cell bodies were taken into account for the measurements. Quantifications were made per cortical slice (supplemental table 1). Afterwards, an average of the quantifications of all the slices per embryo was made, so only one value for each embryo was included in the statistical analysis (number of embryos = n). For the quantification of cell morphology 50 μ m sections were used, all protrusions with a length equal or more than 1/2 of the cell soma were considered as a ramification.

All values are expressed as mean \pm S.E.M. Statistical significance was assessed by nonparametric Kruskal-Wallis test, p-values smaller than 0.05 were considered significant.

In order to determine the location of a microglial cell in the cortex, pictures were loaded in the home-made analysis program "Angle", developed in the Matlab environment. The straight distance between the ventricular lining and the middle of the cell soma was measured together with the straight distance between the ventricular lining and the pia, running through the microglial soma in question and corresponding to the thickness of the cortex. The microglial location was expressed as the percentage of distance from the entire neocortex (measurements were performed on 3 embryos per age, E12.5 until E17.5, number of cells = n). Based on the resulting data, a probability distribution of this location was estimated for every age by applying the Kernel Smoothing Density procedure with a Gaussian kernel (Matlab).

2.3.4 Time-lapse imaging

Pregnant mothers were euthanized at E12.5, E14.5 and E17.5. Embryonic brains were isolated in ice-cold PBS-glucose (pH 7.4; 25mM), embedded in 3% low melting agarose (Fisher Scientific) and sliced coronally at a thickness of 300 μ m using a Microm HM650V Vibrating Blade Microtome. Slices were mounted on MilliCell organotypic inserts (Millipore) and maintained in semi-hydrous conditions at 37°C and 5% CO₂. The tissue was allowed to equilibrate for approximately 60 minutes before imaging. Migration media consisted of Neurobasal medium supplemented with 2mM L-glutamine, B27 supplement, N2 supplement and 0.5% penicillin-streptomycin (all from Invitrogen).

For live imaging, slices were transferred on their insert to a glass bottom microwell dish (MatTek) in semi-dry conditions. The microscope chamber was heated by constant air provision at 37°C. Humified air with 5% CO₂ was continuously applied to the slice. The eGFP positive microglia were excited by a Mai Tai DeepSee Ti:Sapphire pulsed laser (Spectra-Physics) with a central wavelength tuned at 900 nm and visualized using a KP 650 nm dichroic mirror. For the analysis of migration speed a z-stack, spanning 72 μ m with serial optical sections (1024 x 1024; 8-bit) every 8 μ m, was recorded every 10 minutes for a total duration of 5 – 7 hours. For the analysis of microglial behavior a z-stack, spanning 32 μ m with serial optical sections (1024 x 1024; 8-bit) every 8 μ m, was recorded every 2 minutes for a total duration of 1 hour. Each time imaging started from a minimum depth of 50 μ m under the cutting surface of the slice. A 20x EC plan-Neofluar objective (NA of 0.5 and 2 mm working distance) (Zeiss) was used, corresponding to a field of view measuring 450 x 450 μ m. The ImageJ (NIH, USA; <http://rsb.info.nih.gov/ij/>) plug-in "MTrackJ" was used to manually track movement paths of microglia in 4D and to calculate migration speed [181]. The average distance the cells travel per step is plotted as a cumulative frequency. The migration speed values are expressed as mean \pm S.E.M. Statistical significance was assessed by nonparametric Kruskal-Wallis test, p-values smaller than 0.05 were considered significant.

2.4 Results

In mice, neurogenesis and neuron migration start on E11 in the cortex and last to E17, when initiation of synaptogenesis and neuron differentiation begin [174, 176]. We focused our analysis on the cerebral cortex area located dorsally to the lateral ganglionic eminences (LGE) and medial ganglionic eminences (MGE), obtained from CX3CR1-eGFP +/- mouse embryos aged from E10.5 to E17.5. This region of the cortex is well characterized on the functional and cellular level and the two GE structures are the major sources of cortical interneurons during embryonic neurogenesis [182-184].

First we determined to what extent the CX3CR1-eGFP cells observed in the embryonic brain were effectively microglial cells. Most of the eGFP cells in the embryonic brain were immunoreactive for Iba-1. At E10.5 $91.7 \pm 8.3\%$ of the eGFP cells in the cortex were expressing Iba-1. This percentage remained stable between E10.5 and E17.5, ranging from $97.6 \pm 1.6\%$ at E11.5 to $99.8 \pm 0.2\%$ at E17.5 ($n = 4 - 9$ embryos) (E12.5, $99.1 \pm 0.9\%$; E13.5, $99.1 \pm 0.6\%$; E14.5, $99.2 \pm 0.5\%$; E15.5, $99.6 \pm 0.3\%$; E16.5, $100 \pm 0\%$). The percentage of eGFP cells expressing Iba-1 between E10.5 and E17.5 was not significantly different ($p > 0.1$). Like for the Iba-1 immunoreactivity, most of the eGFP cells in the embryonic cortex were expressing CD68. At E10.5 $\approx 100\%$ of the eGFP cells were CD68 positive and this percentage remained stable at all ages (E10.5, $100 \pm 0\%$; E11.5, $86.1 \pm 10.0\%$; E12.5, $85.8 \pm 3.3\%$; E13.5, $93.9 \pm 1.7\%$; E14.5, $88.2 \pm 3.6\%$; E15.5, $95.4 \pm 2.1\%$; E16.5, $98.2 \pm 1.4\%$; E17.5, $97.1 \pm 0.1\%$ ($n = 3 - 9$ embryos). The percentage of eGFP cells expressing CD68 between E10.5 and E17.5 did not change significantly ($p > 0.1$). These results demonstrate that the eGFP cells present in the developing brain parenchyma are microglial cells or microglial precursors and will from now on be referred to as microglia.

2.4.1 Invasion of the embryonic cortex and ganglionic eminences by microglia between E10.5 and E17.5

The number of microglial cells present in the cortex significantly increased ($p < 0.001$; Kruskal-Wallis test) between E10.5 and E17.5 (Fig. 2.2A). At the age of E10.5 (Fig. 2.1A, 2.2A) and E11.5 (Fig. 2.1B, 2.2A) almost no microglia could be observed in the cortex. At E10.5 and E11.5 we observed 0.5 ± 0.2 cells per slice ($n = 4$ embryos) and 2.6 ± 0.2 cells per slice ($n = 6$ embryos) respectively.

Many faint eGFP positive cells were present at the pial surface of the cortex, their round morphology and prominent nucleus suggest that these cells were likely to be monocytes [121, 185]. At E12.5 (Fig 2.1C, 2.2A), microglial cells were still rarely observed in the cortical parenchyma, although their number (5.0 ± 0.4 cells per slice; $n = 12$ embryos) had doubled when compared to E11.5. The distribution of the microglial cells throughout the cortical wall was random. Between E12.5 and E14.5 the number of microglia remained stable (E14.5: 8.8 ± 0.6 cells per slice; $n = 13$ embryos; $p > 0.05$) (Fig. 2.1D, 2.1E, 2.2A), to rise abruptly to 31 ± 2 cells per slice by the age of E15.5 ($n = 8$ embryos) (Fig. 2.1F, 2.2A). After this sudden rise at E15.5, the cell number remained stable (E17.5: 40 ± 1 cells per slice; $n = 6$ embryos; $p > 0.05$) (Fig. 2.1H, 2.2A). From E15.5 the cortical wall can be divided into three layers: the ventricular zone, intermediate zone and the cortical plate zone [186, 187]. Remarkably few microglia ($5 \pm 1\%$ of the eGFP cells per slice) were present in the cortical plate region from E15.5 to E17.5.

During embryonic development, the surface of the cortex increases and its morphology becomes more complex (Fig. 2.1A – H and Fig. 2.2B). The surface area of the cortex significantly increased 14-fold ($p < 0.001$; Kruskal-Wallis test) from E10.5 ($3.3 \times 10^4 \pm 0.6 \times 10^4 \mu\text{m}^2$; $n = 4$ embryos) to E17.5 ($47 \times 10^4 \pm 3.5 \times 10^4 \mu\text{m}^2$; $n = 6$ embryos).

To determine if the increase in microglial cell number with age (Fig. 2.2A) reflects a true colonization process or is related to the increase of cortex area only, we quantified the change in microglial cell density with embryonic age. The microglial density significantly increased ($p < 0.001$; Kruskal-Wallis test) 6-fold from E10.5 ($1.5 \times 10^{-5} \pm 0.6 \times 10^{-5}$ cells/ μm^2 ; $n = 4$ embryos) to E17.5 ($9.1 \times 10^{-5} \pm 0.7 \times 10^{-5}$ cells/ μm^2 ; $n = 6$ embryos) (Fig. 2.2C). During this developmental period microglial cell density significantly increased from E10.5 to E11.5 ($p < 0.05$), remained stable between E11.5 and E14.5 and then significantly increased after E14.5 ($p < 0.05$).

Throughout development the general morphology of the cortical microglial cells significantly changed ($p < 0.05$; Kruskal-Wallis test) from an amoeboid form in the early stages, towards a more ramified one later in development. At E12.5 ($n = 3$ embryos) the majority of the microglial cells had an amoeboid form (61 ± 5

%) (Fig. 2.2D). While at E16.5, $76 \pm 1\%$ of the microglial cells had 1 or more protrusions (Fig. 2.2D).

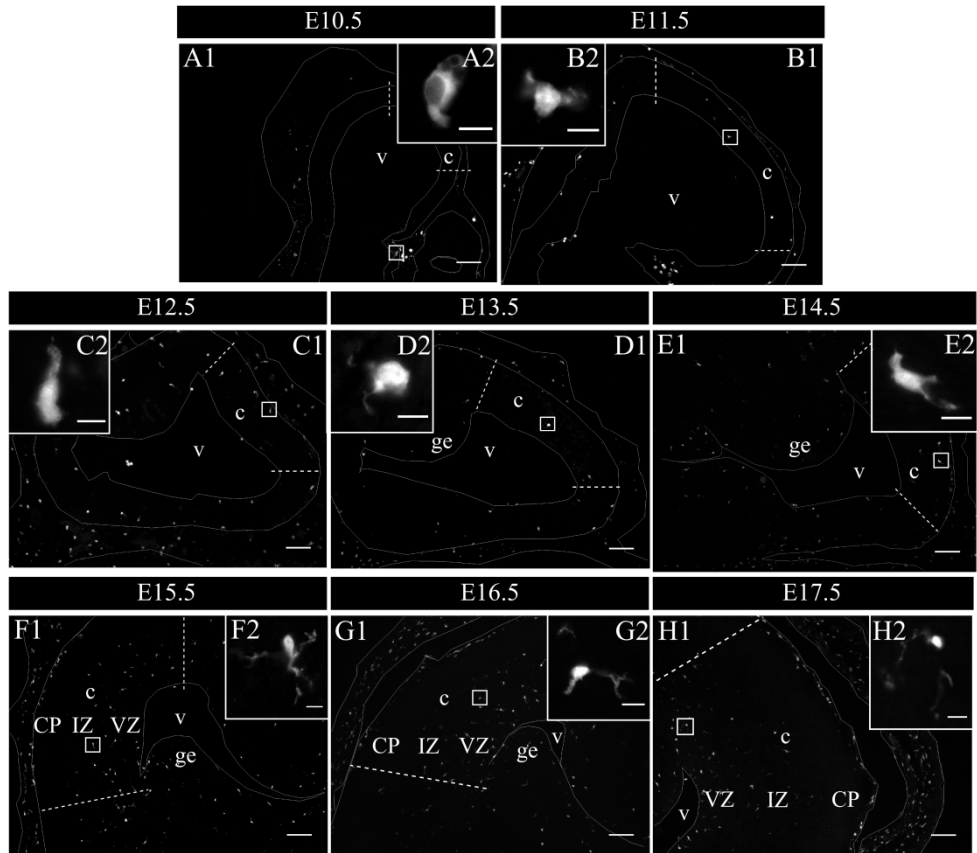


Figure 2.1. Invasion and distribution of microglial cells in the developing cortex. (A – H) Coronal sections of mouse E10.5 – E17.5 embryonic brains, eGFP cells in white. The DAPI channel was not shown to preserve the clarity of the pictures, instead the structures are contoured by a white line. The dotted lines mark out the investigated cortical areas (see Supplemental fig. 1 for a schematic description of these areas). The number of microglial cells gradually increases with the development of the cortex. Their morphology changed from a predominantly amoeboid form towards a branched one (figure insets). Many faint eGFP cells, probably monocytes, could be observed at the pial surface of the cortex. At all developmental stages single and groups of eGFP cells were present in the lateral ventricle, as free floating or attached to the ventricular wall, and many eGFP cells were lining the pial surface of the brain. Number of embryonic brains tested in each group: E10.5 n = 4; E11.5 n = 6; E12.5 n = 12; E13.5 n = 11; E14.5 n = 13; E15.5 n = 8; E16.5 n = 5; E17.5 n = 6. c, cortex; CP, cortical plate; ge, ganglionic eminence; IZ, Intermediate zone; v, ventricle; VZ, Ventricular zone. Scale bars = 100µm, inset = 10µm.

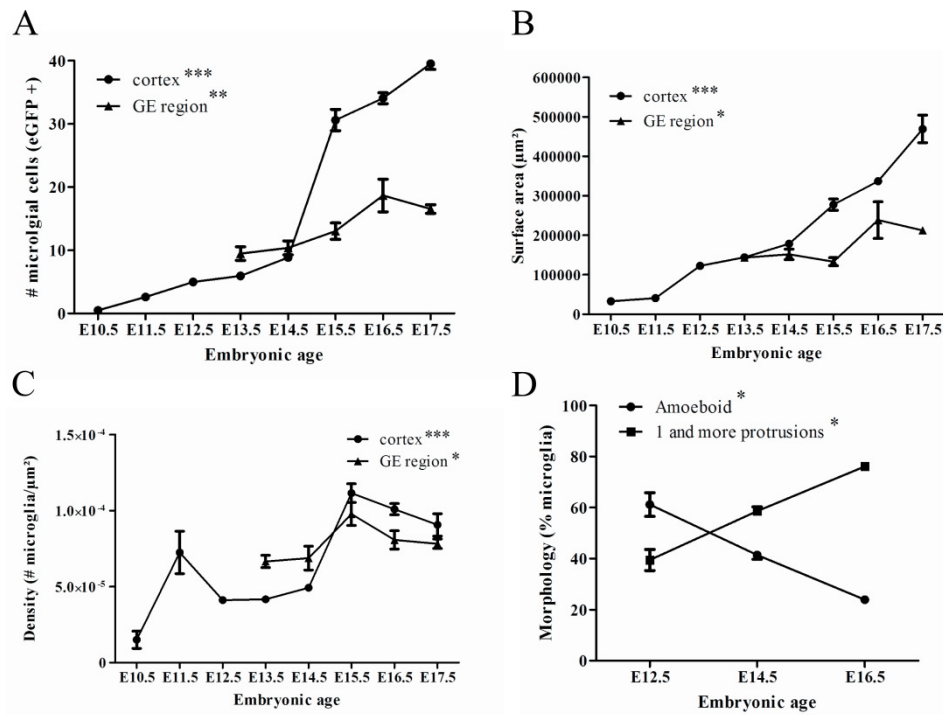


Figure 2.2. Quantification of microglial cell invasion. (A) The microglial cell number significantly increased during development in both the cortical wall as the GE region. At E10.5 almost no eGFP cells were observed in the cortical parenchyma. From E11.5 until E14.5, eGFP cells slowly invaded the cortex, afterwards there was a drastic increase in their cell number. In the ganglionic eminences the cell number slowly increased from E13.5 until E17.5. **(B)** The cortex surface area significantly increases during development. From E10.5 to E11.5 the area stays constant and gradually started to increase from E11.5 on. The surface area of the GE region also significantly increases when the embryo ages. The area of the region stays constant between E13.5 and E15.5, after E15.5 it increases. **(C)** Cell density significantly increased during development in both the cortical wall as the GE region. In the cortex, two phases could be observed in eGFP cell density, a first small increase at E11.5 after which the density remained stable up until E14.5, at E15.5 there was a second rise. In the ganglionic eminences a peak at E15.5 in eGFP cell density was also observed. Number of embryonic brains tested in cortex group: E10.5 n = 4; E11.5 n = 6; E12.5 n = 12; E13.5 n = 11; E14.5 n = 13; E15.5 n = 8; E16.5 n = 5; E17.5 n = 6. Number of embryonic brains tested in ganglionic eminence group: E13.5 n = 9; E14.5 n = 8; E15.5 n = 7; E16.5 n = 3; E17.5 n = 3. **(D)** The morphology of the eGFP cells present in the cortical parenchyma gradually changed from predominantly amoeboid cells towards branched cells. Number of embryonic brains tested : n = 3. (* $p < 0.05$; ** $p < 0.01$; *** $p < 0.001$).

When looking at the microglial invasion of the region comprising the LGE and MGE, a similar pattern was observed as in the cortex from E13.5 to E17.5. The number of microglial cells significantly increased ($p < 0.01$; Kruskal-Wallis test)

almost two-fold from E13.5 (10 ± 1 cells per slice; $n = 9$ embryos) to E17.5 (16.5 ± 0.7 cells per slice; $n = 3$ embryos) (Fig. 2.2A).

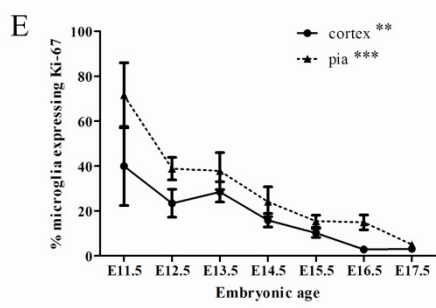
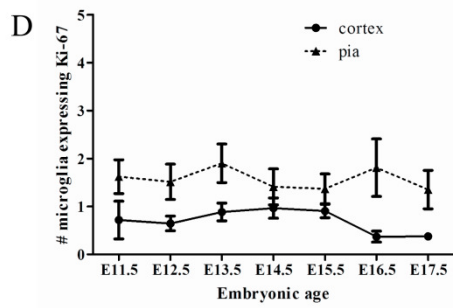
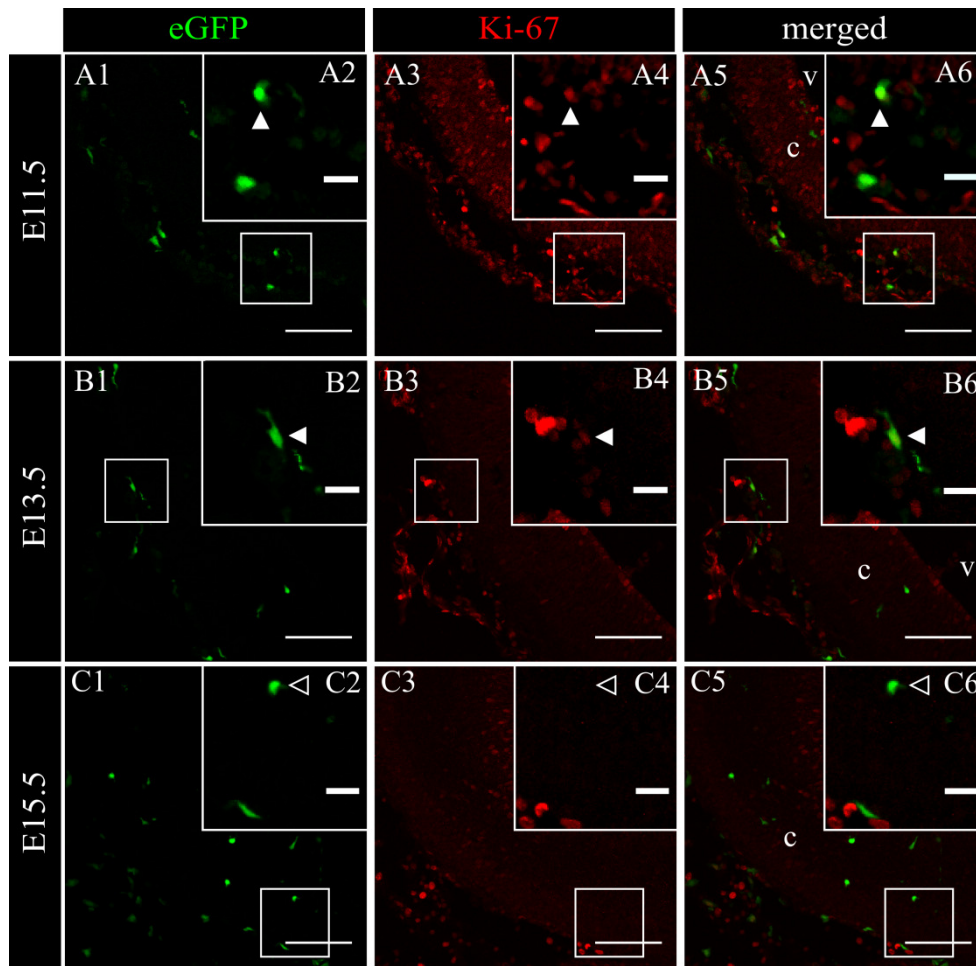
During embryonic development, the surface area of the GE region significantly increased 1.5 times ($p < 0.05$; Kruskal-Wallis test) from E13.5 ($14 \times 10^4 \pm 0.9 \times 10^4 \mu\text{m}^2$; $n = 9$ embryos) to E17.5 ($21 \times 10^4 \pm 0.2 \times 10^4 \mu\text{m}^2$; $n = 3$ embryos) (Fig. 2.2B).

Similarly as in the cortex, the microglial cell density was significantly different ($p < 0.05$; Kruskal-Wallis test) between E13.5 ($6.7 \times 10^{-5} \pm 0.4 \times 10^{-5}$ cells/ μm^2 ; $n = 9$ embryos) and E17.5 ($7.8 \times 10^{-5} \pm 0.3 \times 10^{-5}$ cells/ μm^2 ; $n = 3$ embryos) (Fig. 2.2C).

In the mouse embryonic spinal cord, microglia proliferate before entering the parenchyma [121]. Hence, the percentage of microglia that was actively proliferating in the cerebral cortex was determined using a Ki-67 staining. As shown in Fig. 3, actively proliferating cells could be observed between E11.5 and E17.5 (Fig. 2.3A3, B3, C3), with the majority located in the ventricular zone of the cortex where many precursors are located [174, 188, 189]. In addition, the embryonic brain was surrounded by proliferating cells during this time span in embryonic development (Fig. 2.3A3, B3, C3), likely indicating the growth of blood vessels and the development of the meninges [190, 191]. From E11.5 until E17.5, the number of microglial cells in the cortex that was positive for Ki-67 remained constant (Fig. 2.3D) (E11.5: 0.7 ± 0.4 Ki-67 positive microglial cells per slice; $n = 3$ embryos). However, the percentage of microglia that were actively proliferating in the cortex parenchyma significantly decreased ($p < 0.01$; Kruskal-Wallis test) during this period. At E11.5 (Fig. 2.3A2, A4, A6 and E), $40 \pm 18\%$ of the microglial cells ($n = 3$ embryos) were immunoreactive for the proliferation marker Ki-67. This percentage decreased to $28 \pm 5\%$ ($n = 6$ embryos) at E13.5 (Fig. 2.3B2, B4, B6 and E) and decreased even further to only $10 \pm 2\%$ at E15.5 (Fig. 2.3C2, C4, C6 and E). At E17.5 only $3 \pm 1\%$ ($n = 3$ embryos) of the eGFP cells were positive for Ki-67 (Fig. 2.3E). We observed many eGFP cells in the meninges that were immunoreactive for Ki-67, likely corresponding to microglial progenitors and suggesting that the majority of these cells proliferate in the periphery, before they enter the cortical parenchyma. The number and percentage of eGFP cells proliferating in the pia

followed the same tendency as that observed in the cortex. The absolute number of (Fig. 2.3D) proliferating microglia remained constant (E11.5: 1.6 ± 0.4 ki-67 positive microglial cells per slice; $n = 5$ embryos) while there was a significant decrease ($p < 0.001$; Kruskal-Wallis test) in the percentage (Fig. 2.3E) of proliferating microglial cells from E11.5 ($71.5 \pm 14.5\%$; $n = 5$ embryos) to E17.5 ($5.04 \pm 1.47\%$; $n = 6$ embryos).

Figure 2.3 (Next page). Proliferation in the developing mouse embryonic cortex and pia. (A1, B1, C1) Microglial cells (green) in coronal sections of E11.5 – E15.5 brains. **(A3, B3, C4)** Actively proliferating cells were identified using the Ki-67 antibody (red). The DAPI channel was not shown to preserve the clarity of the merged pictures (A5, B5, C5). **(A2, A4, A6)** At E11.5 and **(B2, B4, B6)** E13.5, a rather high percentage of microglial cells were Ki-67 positive. White arrowheads indicate Ki-67 expressing microglial cells. **(C2, C4, C6)** At E15.5 only a small percentage of the microglial cells were showing immunoreactivity against Ki-67. Open arrowheads indicate non-proliferating microglia in the cortex. **(D)** The absolute number of microglial cells that were actively proliferating in the cortical parenchyma and at the pia remained constant throughout development. **(E)** The percentage of proliferating microglia significantly decreased as the embryo develops. Number of embryonic brains tested in each group for cortex: E11.5 and E17.5 $n = 3$; E12.5 – E15.5 $n = 6$. Number of embryonic brains tested in each group for pia: E11.5 $n = 5$; rest $n = 6$. c, cortex; v, ventricle. Scale bars = $100\mu\text{m}$, insets = $20\mu\text{m}$. (** $p < 0.01$; *** $p < 0.001$).



2.4.2 Microglia accumulate in the region of the choroid plexus primordium and associate with dying cells

The choroid plexus primordium can be recognized from E11 on in the mouse embryonic brain [192]. An increased accumulation of microglial cells was observed in the region of the choroid plexus primordium from E11.5 until E14.5 (Fig. 2.4A1 and B1). The majority of microglial cells had an amoeboid morphology and endosomal-like compartments in their cell body (Fig. 2.4A2 and B2). The number (Fig. 2.4C) and density (Fig. 2.4D) of the microglial cells in this accumulation remained stable between E11.5 and E15.5 ($n = 13 - 15$ embryos). By the age of E15.5, this accumulation became less apparent and was no longer visible at E16.5. Accordingly, the density of microglial in this structure significantly decreased ($p < 0.05$) from E15.5 ($8.2 \times 10^{-4} \pm 6.0 \times 10^{-5}$ cells/ μm^2 ; $n = 15$ embryos) to E16.5 ($4.6 \times 10^{-4} \pm 6.7 \times 10^{-5}$ cells/ μm^2 ; $n = 14$ embryos) (Fig. 2.4D).

In rodents, it was shown that the choroid plexus is already mature at an early stage of embryonic development (E15 in rats) [193] and that a significant amount of apoptosis takes place during embryonic development of this structure [194-196]. Indeed, the presence of apoptosis in this structure was identified by cleaved caspase-3 immunoreactivity (Fig. 2.4A3-6). To the contrary, no immunoreactivity for cleaved caspase-3 was found in the cortical parenchyma (data not shown).

Based on the presence of apoptosis and the morphology of the microglia that we observed in the choroid plexus, we hypothesized that the microglial cells in this structure acquired a phagocyte phenotype and cleared cellular debris from the apoptotic cells. To determine to what extent the microglial cells are activated, we performed an immunostaining for Mac-2/Galectin-3. Increased expression of Mac-2/Galectin-3 is related to the phagocyte phenotype in immune cells [50-52]. When looking at Mac-2 expression, almost no Mac-2 immunoreactive microglial cells were observed in the cortex: at all ages tested, less than 5% of the microglia were positive for Mac-2 (data not shown). At E11.5 only a few cells showed Mac-2 reactivity in the choroid plexus ($7 \pm 7\%$; $n = 5$ embryos). After E11.5 this percentage increased, to reach a peak at E14.5 ($48 \pm 6\%$; $n = 4$

embryos) (Fig. 2.4B3-6). Subsequently this percentage decreased to $11 \pm 2\%$ ($n = 6$ embryos) at E16.5.

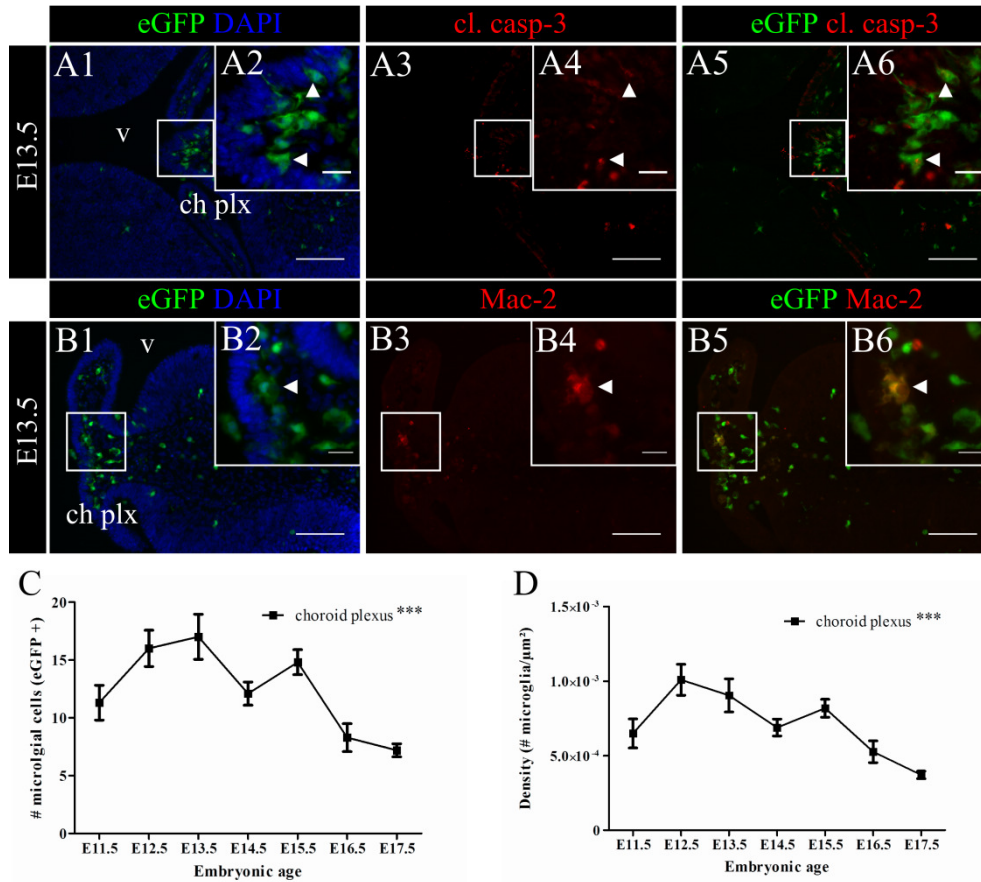
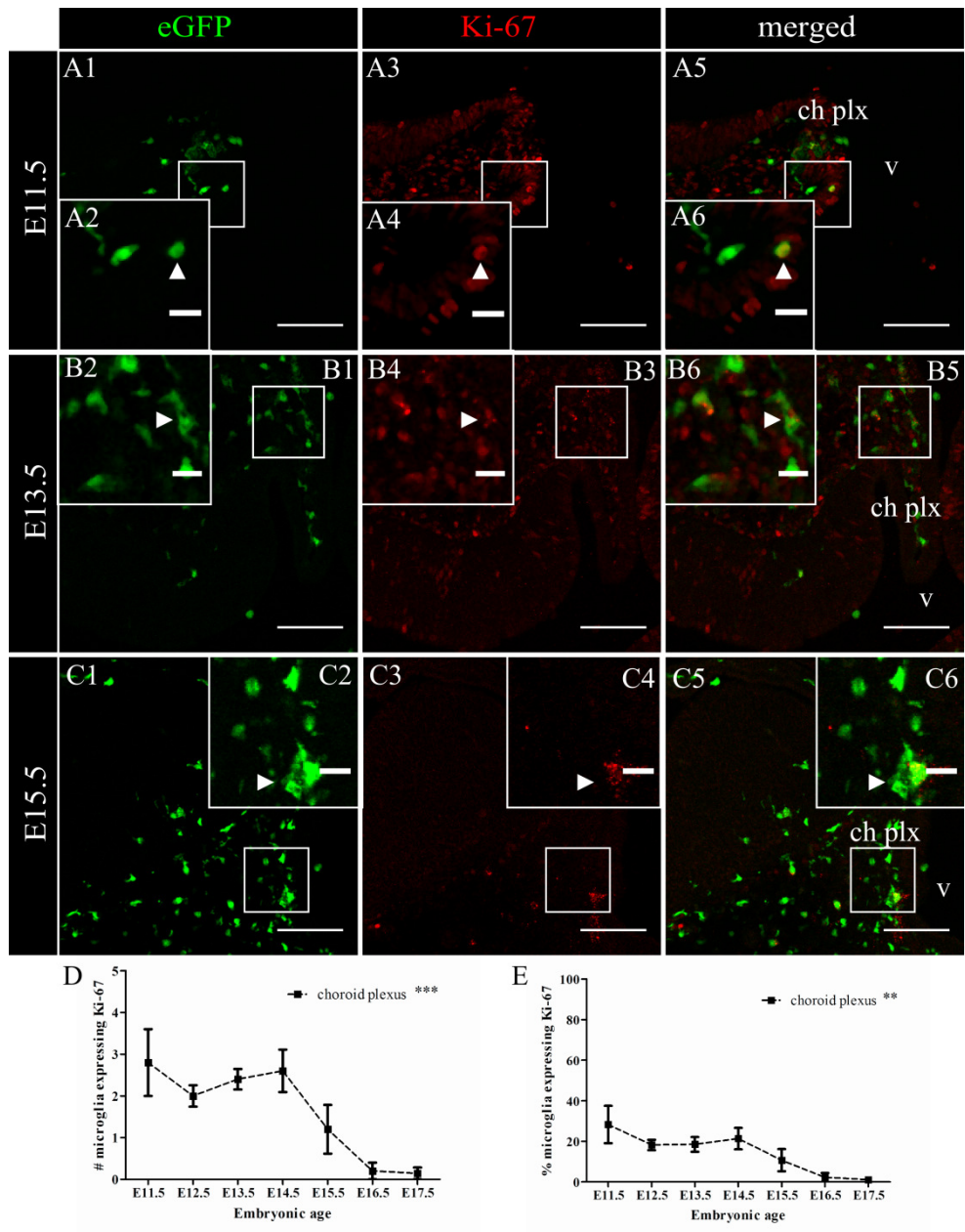


Figure 2.4. Activated microglia accumulate in the choroid plexus region during developmental cellular death. (A1, B1) Coronal sections of mouse E13.5 embryonic brains with cell nucleus staining in blue (DAPI) and eGFP cells in green. From E11.5 until E14.5, an accumulation of eGFP cells in the choroid plexus primordium was observed. These eGFP cells had a predominantly amoeboid or unipolar morphology with endosomal-like compartments in their cell body (A2, B2). **(A3, A4)** Apoptotic cells were identified using the cleaved caspase-3 antibody (red). **(A5, A6)** At E13.5 apoptotic cells were found in the region comprising the choroid plexus (primordium), especially at the epithelial lining. Microglial cells present in the accumulation were in close proximity of these apoptotic cells (A2, A4, A6 white arrowheads). Several of them showed endosomal-like compartments and extended one or two processes through the epithelial lining of the plexus or around cleaved caspase-3 immunoreactive cells. **(B3, B4)** Immunohistochemical staining using a Mac-2 antibody (red) showed that the microglia present in this aggregate and close to the apoptotic cells are positive for the activation marker Mac-2 (B5, B6 white arrowhead). **(C – D)** In the choroid plexus primordium, the

eGFP cell number (C) and density (D) significantly decreased throughout development. Number of embryonic brains tested in each group: E11.5 n = 5; E12.5 n = 6; E13.5 n = 6; E14.5 n = 9; E15.5 n = 6; E16.5 n = 3; E17.5 n = 3. ch plx, choroid plexus; v, ventricle. Scale bars = 100µm, inset = 20µm. (***) $p < 0.001$).

As observed in the cortex and its periphery, many proliferating cells could be observed in the choroid plexus primordium (Fig. 2.5A3, B3, C3). Some microglial cells localized in the choroid plexus were also immunoreactive for Ki-67 (Fig. 2.5A6, B6, C6 white arrowheads), indicating active proliferation. The absolute number of microglial cell positive for Ki-67 significantly decreased ($p < 0.001$; Kruskal-Wallis test) from 2.8 ± 0.8 Ki-67 positive microglial cells per slice at E11.5 (n = 5 embryos) to 0.1 ± 0.1 at E17.5 (n = 7 embryos) (Fig. 2.5D). A same significant decrease ($p < 0.01$; Kruskal-Wallis test) was observed for the percentage of proliferating microglial cells in this area (Fig. 2.5E), being $28 \pm 9\%$ at E11.5 (n = 5 embryos) (Fig. 2.5A5, A6) and $1 \pm 1\%$ at E17.5 (n = 7 embryos).

Figure 2.5 (Next page). Proliferation in the developing mouse embryonic choroid plexus primordium. (A1, B1, C1) Microglial cells (green) in coronal sections of E11.5 – E15.5 brains, the DAPI channel was not shown to preserve the clarity of the pictures. **(A3, B3, C3)** Actively proliferating cells were identified using the Ki-67 antibody (red). **(A2, A4, A6)** At E11.5 and **(B2, B4, B6)** E13.5 a relative high percentage of the microglial cells in the plexus primordium were positive for Ki-67, white arrowheads indicate Ki-67 expressing microglial cells. **(C2, C4, C6)** At E15.5 a smaller percentage of the microglial cells were showing immunoreactivity against Ki-67. However, Ki-67 positive microglia could still be detected in the plexus primordium, white arrowheads indicate proliferating microglia. **(D - E)** The number (D) and the percentage (E) of microglia that were actively proliferating in the choroid plexus primordium significantly decreased as the embryo matures. Number of embryonic brains tested in each group: E12.5 and E14.5 n = 4; rest n = 3. ch plx, choroid plexus; v, ventricle. Scale bars = 100µm, insets = 20µm. (** $p < 0.01$; *** $p < 0.001$).



2.4.3 Migration behavior of microglial cells in the embryonic cortex

To study the dynamic behavior of microglia in the neocortex at the onset of their colonization process, we first quantified their location within the cortex and then analyzed their migration and behavior in acutely prepared brain slices of embryos using two-photon excitation time-lapse microscopy. In order to look at the developmental change in the distribution of microglia in the embryonic cortex, we analyzed the distribution of these eGFP cells within the parenchyma with respect to the ventricular lining as a position reference (Fig. 2.6). At the onset of their invasion process (E12.5), the microglial cells accumulated at the ventricular wall (Fig. 2.6, dark bulb in E12.5 column at 0-20% region) and to the pial surface (Fig. 2.6, dark bulb in E12.5 column at 80-100% region). Afterwards, they became randomly distributed within the cortical wall. During the second phase of invasion (E14.5 to E15.5), characterized by an abrupt increase in cell density (Fig. 2.2B), the relative density of microglia at the pial side of the cortex progressively decreased, while most microglia accumulated in the area close to the ventricle at E17.5 (Fig. 2.6, dark bulb in E17.5 column at 0-20% region). These observations suggest that microglia enter the cortex at early stages, both from the ventricular lining and pial surface. After E14.5 there was a reorganization of microglia distribution, which could be the result from changes in their dynamic behavior during this developmental window.

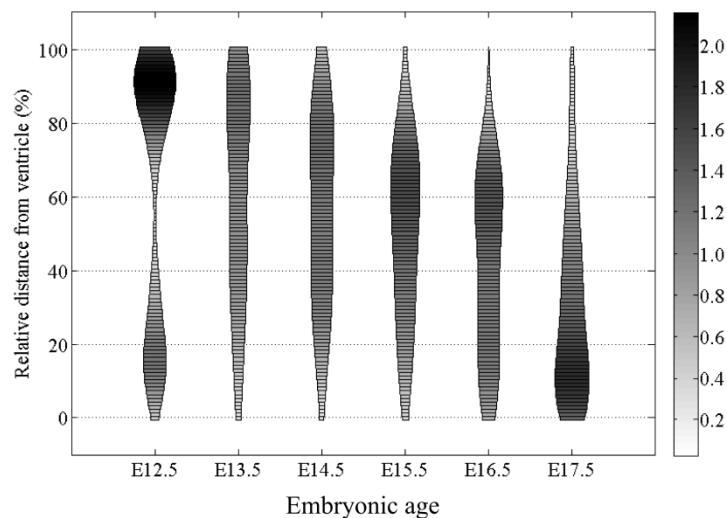


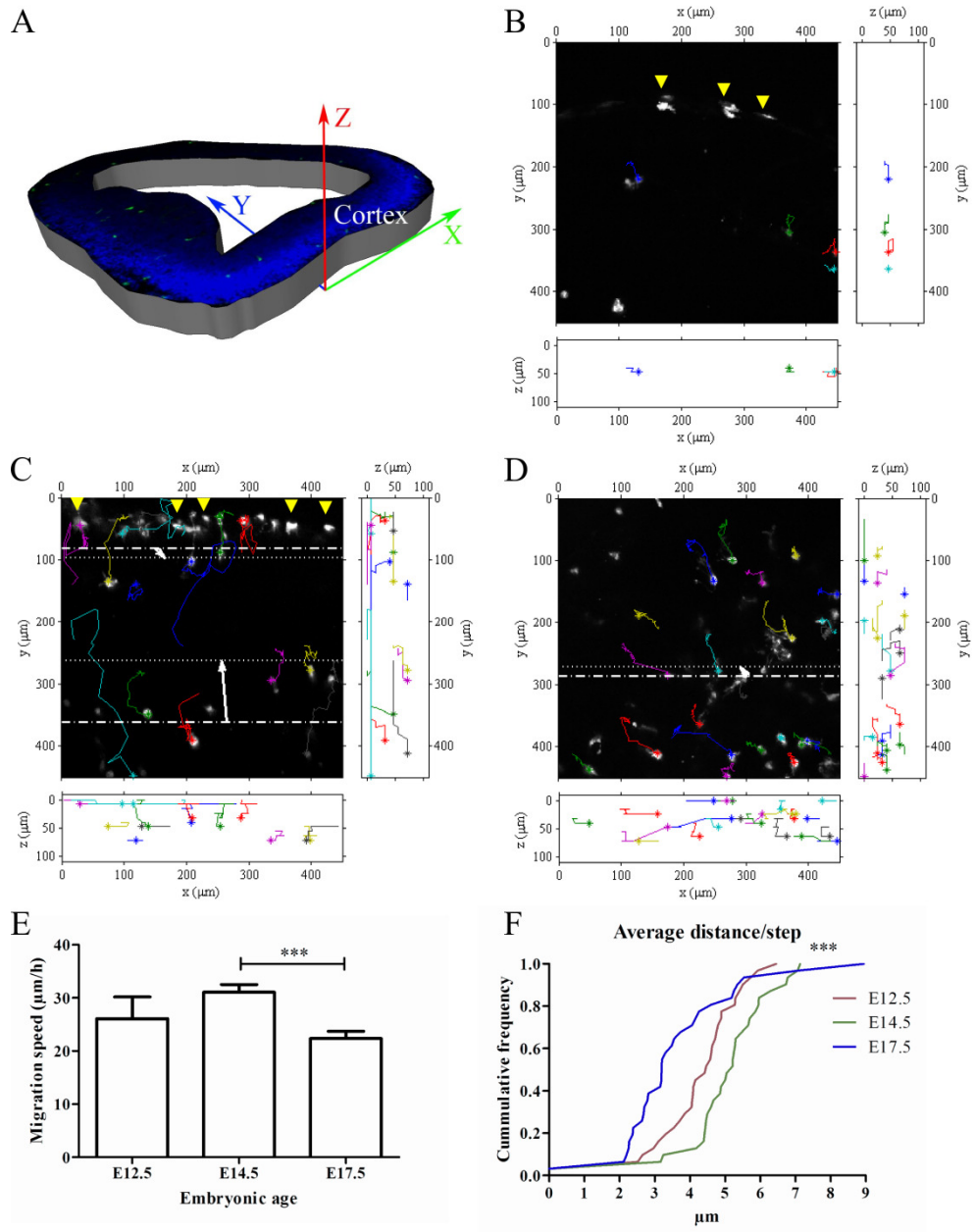
Figure 2.6 (Previous page). Microglial distribution in the embryonic cortical wall. Absolute localization of the microglial cells in the cortical wall. The left axis represents the location of the microglia within the cortex relative to the entire thickness of the cortex (the distance between the ventricular lining and cell soma divided by the straight distance between ventricular lining and pia) shown in %, with 0% corresponding to the ventricular lining and 100% to the pia. The right grey scale axis indicates by its darkness the percentage of microglial cells that are located at a specific position in the cortical wall. The darker the color is and the wider the width of the column, the higher the percentage of cells at that position in the cortical wall. At E12.5, microglial cells are mostly located close to the ventricular lining and to the pial surface (indicated by the dark groups between 0-20% and 80-100%). From E13.5, these cells start to spread in order to populate the cortical layers in between. From E15.5 on the developing cortical plate is marked by an almost complete absence of microglial cells (indicated by the small, light groups between 80-100%). Measurements were performed on 3 embryos per age; number of cells in each age group: E12.5 n= 50; E13.5 n= 66; E14.5 n= 102; E15.5 n= 70; E16.5 n= 137 and E17.5 n= 142.

Time series analysis in live brain slices at E12.5, E14.5 and E17.5 revealed the heterogeneous and dynamic nature of the embryonic microglial cells. At E12.5, few microglial cells were present in the cortex and most of them had a predominant amoeboid morphology, however some cells displayed motile processes. The mean microglial migration speed was $26 \pm 4 \mu\text{m/h}$ (11 cells) (Fig. 2.7B and E). At E14.5, the migration speed was increased to $31 \pm 2 \mu\text{m/h}$ (39 cells) (Fig. 2.7C and E). Cells located close to the pial surface were seen to exit this structure and enter the cortical parenchyma. Conversely, microglial cells located in the parenchyma were seen to migrate into the pial surface, suggesting a complex behavior that cannot reflect the colonization process leading to the invasion of the cortex only. The main migration direction of the cells was from the outside (being the region at the pial surface and the region next to the ventricle) to the middle of the wall (Fig. 2.7C white arrow). At E17.5 the migration speed ($22 \pm 1 \mu\text{m/h}$; 37 cells) had significantly decreased ($p < 0.001$; Kruskal-Wallis test) compared to E14.5 (Fig. 2.7D and E). Again the main migration direction of the cells was from the outside (being the region next to the ventricle) to the middle of the wall (Fig. 2.7D white arrow). Plotting for each age the cumulative frequency of the average distance the microglial cells travel per step (Fig. 2.7F) shows that this is significantly smaller at E17.5 compared to E14.5 ($p < 0.001$; Kruskal-Wallis test).

In these relatively long imaging experiments (5 to 7 hours, with 10 minutes interval) we observed that microglial movement did not occur continuously, but

was characterized by phases of active migration interspersed with stationary phases, a pattern that can be described as saltatory locomotion and, at E14.5 and E17.5, the cells displayed highly motile processes. Imaging for one hour with a 2 minute interval at E14.5 (Fig. 2.8) confirmed that the embryonic microglia are very dynamic cells, constantly sending out (Fig. 2.8 closed arrowheads) and retracting (Fig. 2.8 open arrowheads) processes, which suggests they can already survey their local environment, as observed in the adult [5].

Figure 2.7 (Next page). Microglial migration in the embryonic cortical wall. (A) Representation of the different axes in the tissue slice for time-lapse imaging experiments. **(B)** Representation of microglial migration at E12.5 (length recording = 5 hours). The pial surface is located closest to the coordinate 0 on the y-axis. Many eGFP cells are present at this pial surface (yellow arrowheads). Asterisks indicate the start position of the microglial cells. **(C)** Representation of microglial migration at E14.5 (length recording = 7 hours). The orientation and marks are as described in panel B. There is some heterogeneity between microglia concerning their movement; some microglial cells migrate long distances whilst others remain approximately at their start position. White arrows indicate the main migration direction for cells located at the pial surface and cells located at the ventricular side. Dashed-dotted lines and dotted lines indicate respectively the beginning and ending positions in the y-direction. **(D)** Representation of microglial migration at E17.5 (length recording = 5 hours). The pial surface is located at the same side of the coordinate 0 on the y-axis however not visible due to the thickness of the wall at this age. Asterisks indicate the start position of the microglial cells. White arrow indicates the main migration direction for cells located at the ventricular side, dashed-dotted line and dotted line indicate respectively the begin and end position in the y-direction. **(E)** Migration speed of the microglial cells significantly changed during development with a peak at E14.5. **(F)** Plot showing the cumulative frequency of average distance the microglial cells migrate in between two steps during the whole recording session at E12.5 (red), E14.5 (green) and E17.5 (blue). The distance travelled by the cells significantly changed during development with a peak at E14.5. (E-F) Number of cells in each age group: E12.5 n= 6; E14.5 n= 39 and E17.5 n= 37. The imaging for the time-lapse experiments always started from a minimum depth of 50 μm under the cutting surface of the slice. (***) $p < 0.001$.



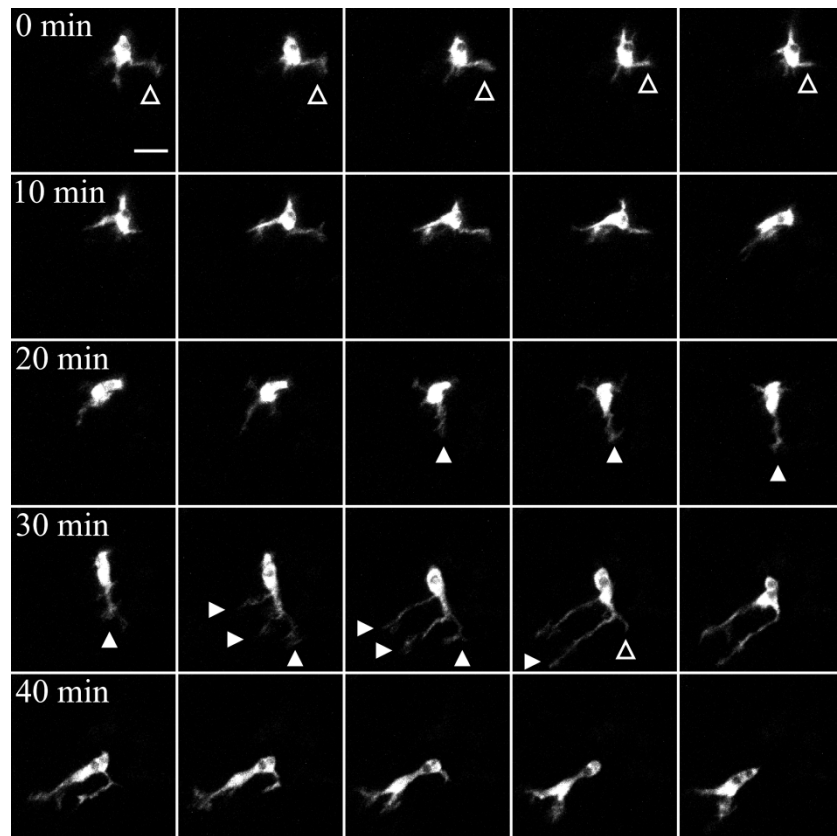


Figure 2.8. Time-lapse confocal imaging demonstration of microglial cell behavior at E14.5. A microglial cell showing highly dynamic behavior. It seems to be scanning the environment by constantly sending out (closed arrowheads) and retracting (open arrowheads) protrusions. At 30 minutes the cell starts sending out more protrusions in the same direction after which it drags the cell soma in the same path resulting in a displacement of the cell. Images are cropped z-projections (5 optical slices with a z-step of 8 μm and time interval of 2 minutes). Scale bar = 20 μm.

2.5 Discussion

In this work, we show that cortical invasion by embryonic microglia is a complex process. We provide evidence that microglial cells and/or precursors accumulate at the pial surface of the cortex before they invade the parenchyma. Within the parenchyma they display a "resting" immunohistochemical phenotype but they are far from being static cells. An accumulation of microglial cells is also present in the choroid plexus primordium, which is related to the presence of cell death in this structure. Consequently, microglial cells in the proximity of the dying cells present a phagocytic phenotype.

2.5.1 Initial invasion of the embryonic cortex occurs in different phases

The colonization of the embryonic cortex by microglia occurs in three phases. The first one is characterized by a slow increase of microglial cells between E10.5 and E14.5. From E14.5 to E15.5 there is a rapid phase with a massive increase in microglia being followed by a second slow phase from E15.5 until E17.5. The increase in microglia cells during early development of the cortex could result from both microglia precursor cell invasion and microglial proliferation during invasion as suspected in the brain of the human fetus [124, 125]. Early in development (E11.5 – E13.5), more than 20% of the microglial cells in the cortex are actively proliferating. After E14.5 there was a drastic increase in microglial cell number, which could not be explained by cell proliferation alone, since the percentage of proliferating microglia steeply decreased from E14.5 on. These observations suggest that proliferation of resident microglia plays an important role in the first invasion phase but lesser in the second one, which is probably the result of microglia entering the parenchyma from peripheral sources. These results are consistent with findings made by others in mouse embryos. In the embryonic mouse retina, the colonization occurs in two invasion waves, although at earlier developmental stages than in the cortex, with the first one occurring between E11.5 and E12.5, and the second one from E12.5 on [46]. In the embryonic mouse spinal cord the massive rise in cell number and cell density was observed earlier (around E12.5) than in the cortex [121].

At E12.5, most microglial cells in the cortex were located close to the pial surface and to the lateral ventricles. In addition, at all developmental stages

single and groups of microglial cells were present in the lateral ventricle, as free floating or attached to the ventricular wall, and many eGFP cells were lining the pial surface of the brain. This suggests that microglia have entered the cortical parenchyma by crossing the pial membrane and ventricular wall, as suggested earlier by others [122]. Afterwards they spread throughout the entire cortical wall. From E15.5 on, when the third invasion phase takes place, the microglial cells are mainly located in the ventricular and intermediate zones of the cortical wall, avoiding the cortical plate region. This suggests that microglia could play a role in the proliferation and development of the progenitor cells located in the ventricular zone of the cortex. Indeed, studies on primary cultures indicate that microglial cells can influence progenitor proliferation, at least in vitro, as well as neurogenesis and astrogenesis [19, 25].

Since only a small number of microglial cells were present in the cortical plate region from E15.5 on we suggest that at these later ages the microglial cells use a different route to enter the cortical parenchyma than just the "simple" crossing of the pial surface. Based on our observations (data not shown) we hypothesize that, when the complexity of the cortical wall increases, the microglia travel along the pial surface towards the interhemispheric fissure and enter the cortex via the hippocampal primordium, whereupon they travel tangentially and radially to reach their final position in the cortical parenchyma.

2.5.2 Microglial cells accumulate in a region where developmental cell death occurs

At early developmental stages, an accumulation of activated microglial cells was observed in the choroid plexus primordium. In mice, the choroid plexus structure first appears at E11 and subsequently undergoes major morphological changes, which in turn results in an already well differentiated and quite extensive structure by the age of E14. [192, 194, 195]. The presence of this microglial aggregation and activation coincides with the occurrence of developmental cell death in this structure, as was visualized by cleaved caspase-3. The phagocytic morphology of the microglia in the choroid plexus primordium and their immunoreactivity for Mac-2 indicate that these cells have acquired a phagocytic phenotype in order to clear the apoptotic cells. An observation that has also been made in the brain of zebrafish embryos [197] and mouse

embryonic spinal cord [121]. It has been shown that microglial cells promote neuronal cell death in the developing mouse cerebellum [32] and hippocampus [49]. Accordingly, it is reasonable to hypothesize that the microglia observed in the choroid plexus primordium can also influence the developmental apoptosis in this structure.

2.5.3 Embryonic microglial cells are highly dynamic cells that scan their local environment during their migration process

Time-lapse imaging demonstrates that embryonic microglia have a highly dynamic nature with a high motility during their invasion process, a property that has also been described in the embryonic zebrafish [115, 198]. This is in contrast with microglia in the healthy, adult brain in which they are generally randomly localized and display no migration pattern. Surprisingly, besides the wandering of these cells throughout the parenchyma, live imaging showed that the embryonic microglial cells were constantly sending out and retracting processes during their migration process. This behavior has already been described for microglia in the adult mammal CNS [5] but not in the embryonic brain. This scanning property of embryonic microglia processes was observed at E14.5 and E17.5 (and to a lesser extent also at E12.5) and probably reflects their capability to continuously scan their local environment, as described in the adult [5, 199]. During development, we saw an increase in the proportion of microglia with extensions; in addition to a simple change in their morphology and activation state this could also reflect a change in their dynamic nature. This suggests that classification of microglia according to their morphology highly reflects their momental shape, and thus not necessarily reflects their maturation. Accordingly, quantitative analysis of microglial morphology showed that at the age of E14.5, approximately 60% of the microglial cells had a branched morphology.

In conclusion, our results demonstrate that microglial cells invade the cortical parenchyma in three waves. During this colonization process the microglia display a dynamic behavior. Our data indicate that although the embryonic microglial cells have the same origin, their invasion pattern and behavior differ depending on the CNS structure they invade. Probably, the local environment

plays an important role in determining their function during embryonic development.

3 Microglia proliferation is controlled by P2X7 receptors in a Pannexin-1-independent manner during early embryonic spinal cord invasion

this chapter is based on:

Microglia proliferation is controlled by P2X7 receptors in a Pannexin-1-independent manner during early embryonic spinal cord invasion.

Rigato C*, Swinnen N*, Buckinx R, Couillin I, Mangin JM, Rigo JM, Legendre P*, Le Corrionc H*. (*C.R., N.S., P.L. and H.L.C. contributed equally to this work)
J Neurosci. 2012 Aug 22;32(34):11559-73.

Declaration of own contribution:

Conduction and analysis of the microglia isolation, FACS and qPCR. Conduction of a part of the patch-clamp experiments on embryonic spinal cord microglia of CX3CR1 mice. Participation in writing and revision of the manuscript.

3.1 Abstract

Microglia are known to invade the mammalian spinal cord (SC) at an early embryonic stage. While the mechanisms underlying this early colonization of the nervous system are still unknown, we recently found that it is associated, at least partially, with the ability of microglia to proliferate at the onset of motoneuron developmental cell death and of synaptogenesis in mouse embryo (E13.5). *In vitro* studies have shown that the proliferation and activation of adult microglia can be influenced by the purinergic ionotropic receptor P2X7 via a coupling with Pannexin-1. By performing patch-clamp recordings *in situ* using a whole-mouse embryonic SC preparation, we show here that embryonic microglia already express functional P2X7R. P2X7R activation evoked a biphasic current in embryonic microglia, which is supposed to reflect large plasma membrane pore opening. However, although embryonic microglia express pannexin-1, this biphasic current was still recorded in microglia of pannexin-1 knockout embryos, indicating that it rather reflected P2X7R intrinsic pore dilatation. More important, we found that proliferation of embryonic SC microglia, but not their activation state, depends almost entirely on P2X7R by comparing wild type and P2X7R^{-/-} embryos. Absence of P2X7R led also to a decrease in microglia density. Pannexin-1^{-/-} embryos did not exhibit any difference in microglial proliferation, showing that the control of embryonic microglial proliferation by P2X7R does not depend on pannexin-1 expression. These results reveal a developmental role of P2X7R by controlling embryonic SC microglia proliferation at a critical developmental state in the SC of mouse embryos.

3.2 Introduction

Microglia are the resident immune cells of the central nervous system (CNS), which begin to colonize at early embryonic developmental stages [108, 111, 112, 121]. In the mouse embryo, the colonization of the SC by microglia involves several processes, including microglia proliferation at the periphery of the parenchyma [121]. Remarkably, microglia accumulate in the motoneuron (MN) area at 13.5 days of embryonic age (E13.5), a time at which they reach an activated state, proliferate and phagocyte dying MNs [121]. However, the molecular mechanisms underlying microglia proliferation during SC invasion in the embryo remain unknown. In addition it is unclear whether the proliferation and the activation state of microglia are controlled by the same signals and mechanisms at this early developmental stage. In the adult, *in vitro* studies have shown that a number of factors, among which purinergic receptors, such as P2X7R [200], evoke both microglia activation and proliferation [3]. While P2X7R, in addition to P2X4R and P2X1R, is also expressed by embryonic microglia [88], its functions remain unknown at these developmental stages. In the adult, P2X7R is involved, in addition to microglia activation and proliferation, in a variety of important effector functions of microglia [3], including the release of interleukin (IL)-1 β , IL-1 α and TNF- α [201-204]. A remarkable feature of P2X7R is that it promotes the formation of a large pore permeable to hydrophilic moieties up to 900 Da [205], which has been proposed to evoke IL-1 β release, to mediate P2X7R effects on the control of microglia activation and proliferation and to mediate the detrimental effect of continuous P2X7R activation [205-208]. Initially, it was proposed that dilatation of the integral pore of the P2X7R channel accounts for this large pore formation [205], but, later, experimental evidence indicated that large molecule uptake can occur through the formation of an independent plasma membrane pore [209], which might be related to a functional coupling of P2X7R to the hemi-channel pannexin-1 (Panx1) [206]. Using multiple approaches, we determined to which extent P2X7R influences embryonic microglia proliferation during their colonization of the embryonic SC at E13.5 [121] and whether this needs an association to Panx1. We show that, already at E13.5, microglia express P2X7R and that P2X7R activation evokes a biphasic current, even in Panx1 knockout (KO) (-/-) mice. Microglia proliferation is strongly reduced in P2X7R-/- mice, but not in Panx1-/- mice. Our results

provide direct evidence that P2X7Rs strictly control embryonic microglia proliferation independently of their activation state and without involving a coupling to Panx1. Our study discloses the function of P2X7R during embryonic SC colonization by microglia.

3.3 Materials & Methods

3.3.1 Animals

The experiments were performed in accordance with the European Community guiding principles on the care and use of animals (86/609/CEE; *Official Journal of the European Communities* no. L358; December 18, 1986), French Decree no. 97/748 of October 19, 1987 (*Journal Officiel de la République Française*; October 20, 1987) and the recommendations of the Centre National de la Recherche Scientifique. We used transgenic CX3CR1eGFP mice from CNRS/CDTA. P2X7R^{-/-} mice were derived from Pfizer and from GlaxoSmithKline. Given the questionable specificity of the available P2X7R antibodies [210], we performed β -galactosidase immunostainings on the SC of GlaxoSmithKline P2X7R^{-/-} mice as an indirect assay for P2X7R protein expression and cellular localization. Panx1^{-/-} C57B1/6N mice were from the Knockout Mouse Project (KOMP). Panx1 immunostaining was no longer observed in Panx1^{-/-} C57B1/6N mice (see Fig. 3.7B). Mice were coupled overnight and females were examined for vaginal plugs in the morning. Mice in which a vaginal plug was observed, were considered as E 0.5. The developmental stage of the embryos was confirmed using the e-Mouse Atlas from EMAP (<http://www.emouseatlas.org/emap/ema/home.html>). At the intended embryonic age (E13.5), SCs of mouse embryos were isolated as previously described [121]. Briefly, pregnant mice were anesthetized by intramuscular injection of a mix of ketamine and xylazine. Pregnant mice were then killed using CO₂ and the embryos were removed immediately and the SC was isolated. Isolated SCs were then maintained for 1 h before recording in an artificial cerebrospinal fluid (ACSF) containing (in mM): 130 NaCl, 25 NaHCO₃, 1 NaH₂PO₄, 4.5 KCl, 10 glucose, 2 CaCl₂, and 1 MgCl₂, at 32°C, continuously bubbled with a 95% O₂-5% CO₂ gas mixture.

Pharmacological experiments with P2XR agonists and antagonists and hemi-channel blockers were performed on transgenic C57Bl/6 CX3CR1eGFP mice [41, 121] to record microglia in the SC of wild-type mouse embryos. CX3CR1eGFP mouse embryos were also used to analyze the passive electrophysiological properties of microglia in the SC of wild-type mouse embryos. Homozygous C57BL/6 CX3CR1eGFP mice were obtained from the CNRS/CDTA via the European Mouse Mutant Archive. The CX3CR1eGFP ^{-/+} embryos used

throughout this study were obtained by crossing CX3CR1eGFP^{+/+} male mice with C57BL/6 wild-type female mice. Two lines of transgenic C57Bl/6 P2X7R KO mice were also used: P2X7R^{-/-} mice derived from Pfizer and from GlaxoSmithKline [210]. P2X7R^{-/-} mouse lines were kindly provided by E. Audinat (INSERM U603, CNRS UMR 8154, Université Paris Descartes, France) and by Micaela Galante (IBBMC, CNRS UMR 8619, France). Pfizer mice were preferentially used instead of GlaxoSmithKline mice for patch-clamp recordings and for studying microglia cell activation and proliferation, since a P2X7R variant can still be expressed in GlaxoSmithKline homozygous P2X7R^{-/-} mice [211]. P2X7R^{+/-} mice were obtained by crossing C57BL/6 P2X7R^{-/-} Pfizer mice with C57BL/6^{+/+} mice. Briefly, Pfizer mice were constructed by a deletion in the region containing amino acids 506–532, followed by insertion of a neomycin cassette in a 3' to 5' direction. The GlaxoSmithKline P2X7R^{-/-} mice have a *lacZ* gene inserted at the beginning of the exon 1 region of the P2X7R gene. We also used Pannexin-1-targeted homozygous C57Bl/6N mice from the KOMP [212]. Disruption of *Panx1* was generated by insertion of a trapping cassette splice acceptor-beta-geo-polyA flanked by Flp-recombinase target sites within intron 2 upstream of the critical exon 3, where it tags the gene with the *lacZ* reporter. This creates a constitutive null mutation in the target gene through efficient splicing to the reporter cassette, resulting in truncation of the endogenous transcript (*pannexin1tm1a(KOMP)Wtsi*). Reverse-transcription-PCR (RT-PCR) of mouse ear punches and Western blot analysis of the brain confirmed the absence of *Panx1* expression in this *Panx1*^{-/-} mouse [213]. Our immunohistochemical experiments showed a lack of *Panx1* expression in the SC of *Panx1*^{-/-} mouse embryos (Fig. 3.7B). Primers used for PCR analysis for genotyping P2X7R^{-/-} and *Panx1*^{-/-} mice are listed in Table 3.1. PCR results for *Panx1*^{-/-} and P2X7R^{-/-} mice are shown in Fig. 3.6A and Fig. 3.8A, respectively.

Table 3.1. Primers used for PCR analysis for genotyping P2X7 and Panx1 KO mice

Primers	Sequence
Primers P2X7	
P2X7 wt-F	5'-GCAGCCCAGCCCTGATACAGACATT-3'
P2X7 wt-R	5'-TCGGGACAGCACGAGCTTATGGA-3'
NEO-F	5'-GCAGGATCTCCTGTCATCTCACC-3'
NEO-R	5'-GATGCTCTTCGTCAGATCATCC-3'
Primers Panx1	
CSD-comLoxP-F	5'-GAGATGGCGCAACGCAATTAAT-3'
CSD-panx1-R	5'-CTGGCTCTCATAATTCTTGCCCTG-3'
CSD-panx1-wtF	5'-CTGTATCACACAACCACTTCAGAGAAGG-3'
CSD-panx1-wtR	5'-GAGCTGACCCCTTCCATTCAATAG-3'

3.3.2 Whole-cell recordings and analysis

The isolated SC was placed in a recording chamber and continuously perfused at room temperature (20-24°C) with oxygenated ACSF (2 ml/min). Standard whole-cell patch-clamp and voltage-clamp recordings of fluorescent microglia were made under direct visualization using an infrared-sensitive CCD video camera. In CX3CR1eGFP mice embryo, all eGFP cells localized in the SC are microglial cells [121]. We recorded microglia localized in the ventrolateral region of the spinal since at E13.5. At this age activated microglial cells (Mac-2 staining) accumulated in the ventro-lateral region close to motor columns where they proliferated at the onset of the developmental cell death of MNs [121]. Recordings of microglia in the ventrolateral part of the SC fiber zone of Pfizer P2X7R^{-/-}, of Pfizer P2X7R^{+/-}, and of Panx1^{-/-} mouse embryos were performed using infrared microscopy. Microglia in this SC area can be easily recognized by their morphology. Their electrophysiological profile was identical to those of CX3CR1eGFP microglia (Fig. 3.2, 3.6B and 3.8B).

Whole-cell patch-clamp electrodes were pulled from thick-wall borosilicate glass using a Brown-Flaming puller (Sutter Instrument Co., USA). The tip of the electrode was fire-polished using a microforge (Narishige, Japan). Patch-clamp electrodes had resistances of 5-7 MΩ. For voltage-clamp experiments, the electrode was filled with a solution containing (in mM): 130 KCl, 4 MgCl₂, 4 Na₂ATP, 10 EGTA, and 10 HEPES (pH adjusted to 7.2 with KOH, osmolarity 290 mosmol/kg-H₂O, equilibrium potential for chloride ions $E_{Cl} \approx 0$ mV). In some

experiments with low $[Cl^-]_i$, the electrode contained (in mM): 113 potassium methyl sulfate, 17 KCl, 4 MgCl₂, 4 Na₂ATP 4, 10 HEPES and 1 EGTA (pH adjusted to 7.2 with KOH, osmolarity 290 mosmol/kg-H₂O, equilibrium potential for chloride ions $E_{Cl} \approx -40$ mV).

Current fluctuations were recorded and lowpass filtered (2 KHz) using an Axopatch 1D amplifier, digitized (20 kHz) on-line using a Digidata 1322A interface card and analyzed off-line with the PClamp10 software package or the Axograph X.1.3.5 software (Axograph).

Because embryonic microglia are rapidly damaged by voltage steps, voltage-dependent currents were analyzed using 2 s voltage ramps from -100 mV to +100 mV from a holding potential of -60 mV. An initial voltage step (100ms) to -100 mV was applied before the onset of the ramp. To control the stability of the recordings, 3 ramps were applied at 2 s intervals. The resulting evoked currents were then averaged for analysis using the Axograph X software. In the large majority of the recordings, outward voltage-gated currents evoked by voltage ramps slowly increased with time (run-up), reaching a steady state and then decreasing (run-down) as previously described in cultures of murine microglia [75]. The steady state period lasted for 10-15 min, being the period during which the pharmacological experiments were performed. To estimate the stability of the recordings, voltage ramp-evoked currents in the presence of carbenoxolone (CBX) were compared to currents evoked by voltage ramps applied 1 min before and 3 min after application of the drug. A set of three ramps (2 s time interval) was applied before, during and after drug applications. The resulting evoked currents for each voltage ramp set were then averaged for analysis. Recordings without evidence of recovery after drug treatment were discarded.

To analyze concentration-response relationships in these conditions, different ATP concentrations were applied alternatively with 1 mM ATP to control changes in response amplitudes due to rundown (see below). The responses evoked by different ATP concentrations were compared to the responses evoked by 1 mM ATP applied before and after each test application. The amplitude of the test response was normalized to the value obtained by the sum of the amplitudes of the response evoked by 1 mM ATP before and after the test response divided by two. Normalized concentration-response curves were fitted using the Hill

equation : $I/I_{\max} = 1/(1 + (EC_{50}/[ATP])^{nH})$, where I/I_{\max} is the normalized response amplitude, EC_{50} is the ATP concentration producing half of the maximal response and nH is the Hill coefficient. For each concentration tested, the amplitude of the current, I , was measured at the peak of the response.

For pharmacological experiments with P2XR antagonists, P2XR activation was evoked through application of 500 μ M ATP in $[Ca^{2+}]_o$ and $[Mg^{2+}]_o$ free ACSF ($V_h = -60$ mV). All experiments were performed using the first three responses elicited by ATP after inducing the enlarged inward (biphasic) current (Fig. 3.3C). The first response was used as the control, the second response being the test response and the third response corresponding to the recovery of antagonist effects. Application of the antagonist started between the control and the test responses and ended between the test response and the third ATP application (recovery) (3 min interval between ATP applications). To determine antagonist efficiency, the amplitude of the test response was compared to the amplitude of the control response (100%). Current amplitude was measured at the peak of the responses. Recovery from antagonist block was evaluated by comparing the amplitude of the third response to the amplitude of the test response. However, when microglia were exposed to successive ATP applications after inducing a biphasic inward current, the amplitude of the following responses showed a progressive decline with time, the extent of which was similar in all microglial cells (see 3.4 Results). Accordingly, such a rundown can give rise to an overestimation of the efficiency of the antagonist tested. To overcome this problem, the percentage change in response amplitude observed during the application of the antagonist was compensated according to the averaged decrease in the corresponding responses observed on different cells in the absence of the antagonist in $[Ca^{2+}]_o$ and $[Mg^{2+}]_o$ -free ACSF (13 % : see 3.4 Results).

3.3.3 Drug application and pharmacological agents

All drugs were applied using a 0.5 mm diameter quartz tubing positioned 1 mm away from the recording area [214]. The quartz tubing was connected using a manifold to reservoirs filled with a control solution or with P2X receptor agonists and/or channel blockers or P2X receptor antagonists.

Adenosine triphosphate disodium salt (Na_2ATP), 2'(3')-O-(4-Benzoylbenzoyl) adenosine 5'-triphosphate triethylammonium salt (bzATP), α,β -methylene ATP (α,β -Me-ATP), Brilliant Blue G (BBG), 4,4'-Diisothiocyanatostilbene-2,2'-disulfonic acid disodium salt hydrate (DIDS) and the hemi-channel blocker carbenoxolone (CBX) [215, 216] were purchased from Sigma-Aldrich. CuCl_2 and ZnCl_2 (0.1 M stock solution) were also purchased from Sigma-Aldrich. 2',3'-O-(2,4,6-Trinitrophenyl)adenosine-5'-triphosphate tetra(triethylammonium) (TNP-ATP), suramin, Pyridoxalphosphate-6-azophenyl-2',4'-disulfonic acid (PPADS), 3-[[5-(2,3-Dichlorophenyl)-1*H*-tetrazol-1-yl)methyl]pyridine hydrochloride (A438079), *N*-[1-[[[(Cyanoamino)(5-quinolinylamino)methylene]amino]-2,2-dimethylpropyl]-3,4-dimethoxybenzeneacetamide (A740003) were all purchased from Tocris Bioscience. Na_2ATP , bzATP, α,β -Me-ATP, BBG, CuCl_2 , ZnCl_2 , TNP-ATP, suramin, PPADS, A438079 and A740003 were dissolved in the bathing solution. DIDS and CBX were dissolved in dimethylsulfoxide (0.1% final concentration). ATP solutions were prepared the day of the experiment.

3.3.4 Immunohistochemistry and confocal microscopy

All primary antibodies used and their dilutions are listed in Table 3.2. To visualize P2X4R, we used rabbit polyclonal P2X4R antibodies (kindly provided by Francois Rassendren ; CNRS UMR 5203/INSERM U661, Montpellier, France). P2X4R staining was abolished in P2X4R^{-/-} mice indicating that this antibody specifically recognizes P2X4R [217]. To perform multiple staining in the SC of mouse embryos other than CX3CR1eGFP mouse embryos, microglia were marked using anti-Iba1 (Wako), anti-CD11b (Serotec) or anti-CD68 (Serotec) antibodies (see [121] for antibody specificity). Activated caspase-3 Asp175 antibody (Cell Signaling) was used to detect apoptotic cells. The Asp175 antibody recognizes two bands of 17 and 19 kDa on Western blot corresponding to large fragments of activated caspase-3. This antibody does not recognize full-length caspase-3 or other cleaved caspases [180]. We used a purified mouse anti-human Ki-67 antibody to determine the proliferation state of microglial cells (BD Pharmingen) [218]. To determine to which extent microglial cells can be activated, we used a monoclonal antibody directed against Mac-2 [66]. This antibody (hybridomas TIB-166; American Type Culture Collection-LGC Standards) was originally used to isolate the protein Galectin3/Mac-2 [219]. In

Microglia proliferation is controlled by P2X7 in the embryonic spinal cord

GlaxoSmithKline P2X7R^{+/-} mice, we used anti- β -galactosidase antibody (MP Biomedical, Aurora, USA) as an indirect probe to visualize cells expressing P2X7Rs. This antibody was produced by hyperimmunizing rabbits with the enzyme β -galactosidase from *Escherichia coli*. To detect Panx1 in microglia, we used a polyclonal chicken anti-mouse Panx1 antibody from Diatheva (ANT0027) [220]. Panx1 staining was no longer observed in Panx1 knockout mice (Fig. 7B).

Table 3.2. Primary antibodies

Primary antibody	Company	Reference	Dilution
anti-Ki67	BD Pharmingen	556003, clone B56	1:200
anti-Caspase3	Cell Signaling	9661	1:500
Anti-pannexin-1	Diatheva	ANT0027	1:100
Anit-P2X4	Provided by F.Rassendren, INSERM U661, Montpellier, France	Sim JA, et al. (2006). J Neurosci 26: 9006-9009.	1:500
anti-Mac-2	American Type Culture Collection	clone M3/38.1.2.8 HL.2	1:1000
anti-CD68	Serotec	MCA1957, clone FA-11	1:400
anti-IBA1	Wako	019-19741	1:500
anti-CD11b	Serotec	MCA74GA, clone M1/70.15	1:400
Anti- β galactosidase	MP Biomedicals	55976	1:500

Whole embryonic SCs were fixed in 4% paraformaldehyde for 1 hour at 4 °C and subsequently incubated in 30% sucrose overnight at 4 °C for cryoprotection. Sucrose was dissolved in a phosphate buffer. After overnight incubation, the tissue was embedded in optimal cutting temperature compound (VWR) and quickly frozen to -50 °C in isopentane (Sigma-Aldrich). The embedded tissue was then stored at -80 °C. Fifty micrometer transverse cryosections were made using a Leica Cryostat (Leica Microsystem). Tissue sections were washed three times in PBS for 5 minutes, in PBS-NH₄Cl for 20 minutes and again three times in PBS for 5 minutes. SC sections were permeabilized with 0.2% Triton X-100 (Sigma-Aldrich) and 0.25% fish gelatin (PBS-G-T) for 1 hour at room temperature, before incubation with primary antibodies (18-20 h) at 4°C. After three washes in PBS-G-T for 5 minutes, sections were incubated with the secondary antibodies and with DAPI nuclear stain (Sigma-Aldrich, 1/1000) for 2

hours at room temperature. Sections were washed three times in PBS for 5 minutes and rinsed in distilled water before addition of Mowiol 4-88 (475904, Calbiochem). Confocal images were taken on a Leica SP5 platform (Leica Microsystems). Preparations were analyzed using a Leica SP5 confocal microscope. For quantitative analysis of microglial cells on isolated SC or in total embryo transverse sections, serial optical sections were obtained with a Z-step of 1 μm and observed using a 20X oil-immersion objective with a numerical aperture (NA) of 0.7. A Z-step of 0.3 μm was performed when using a 63X oil-immersion objective (NA 1.32), plus a 3x digital zoom magnification. Images (1024 x 1024; 8-bit grayscale) were stored using Leica software LAS-AF. Images were analyzed using ImageJ 1.41 (National Institutes of Health [NIH]; <http://rsb.info.nih.gov/ij/>) and Photoshop CS3 (Adobe software). Quantification was performed on 50- μm -thick transverse sections ($N = 10$ slices per SC) of the embryonic lumbar SC ($N = 3-5$ SCs). Only eGFP cell bodies were taken into account. Microglial cells immunoreactive (ir) to specific antibodies were counted manually in 10 optical sections per embryo. The threshold used to determine whether a microglial cell was coimmunolabeled was set at twice the intensity of background noise measured between eGFP-positive cells.

As cleaved caspase-3 is not only detectable in the cytoplasm of dying cells but also in apoptotic bodies, as a result of cell dismantling, it was not possible to quantify the exact number of cells that were undergoing apoptosis. For this reason, we performed a statistical analysis by measuring the area fraction of anti-caspase-3 fluorescence, setting the ventral region area as constant at all SC analyzed (347x260 μm). Thirty micrometer stack images for each SC slice were made using ImageJ 1.41 (NIH; <http://rsb.info.nih.gov/ij/>), and then transformed into binary images on a black background, by adjusting the threshold. If necessary, the option fill holes was selected and the area fraction checkbox was checked. The percentage of white area, corresponding to anti-caspase-3 fluorescence, was calculated, permitting comparisons of area fraction of anti-caspase-3 fluorescence between wild type and mutant P2X7R SCs. Background noise for activated caspase-3-ir was measured around the central canal.

3.3.5 Microglia isolation

Embryonic SCs were isolated and transferred into 2 ml Neurobasal media (Invitrogen), supplemented with N2 (100x), B27 (50x), L-glutamine (100x) and penicillin/streptomycin (200x), containing papain at a concentration of 48 U/ml (Sigma; 31 U/mg protein). After being cut into small pieces, they were incubated at 37 °C for 30 min. Afterwards, the tissue was allowed to settle for 5 min, the media was removed and 1 ml of media was added. By making use of a 1 ml pipette, the tissue sections were quickly triturated 10 times. The larger pieces were allowed to settle for 2 min. Afterwards, the supernatant was transferred to a fresh Falcon tube. These steps were repeated twice and the supernatants were combined. The obtained cell suspension was centrifuged at 400 *g* for 5 min at room temperature. The supernatant was discarded and the pellet resuspended in 1 ml fresh media. Large pieces were filtered away using a 70 µm cell strainer (BD Falcon – BD Biosciences). The cell strainer was prewet with 1 ml medium; afterwards another 2 ml of medium was used to rinse the cell strainer. This cell suspension was centrifuged at 350 *g* for 10 minutes at room temperature, supernatant was discarded and the pellet resuspended at 10x10⁶ cells/ml.

The microglial cell suspension was sorted out by means of their eGFP expression. The emitted fluorescence was detected using a fluorescence-activated cell-sorting (FACS) Aria flow cytometer (BD Biosciences) equipped with a 488 nm argon-ion laser. The eGFP-positive cells were sorted out and collected. Afterwards, they were centrifuged at 350 *g* for 10 min at room temperature and the cell pellet was washed with PBS and re-pelleted. The cell pellet was kept at -80 °C until RNA isolation was performed. Approximately 3500-5500 microglia were obtained per SC upon FACS sorting. Thirty-two SC were used to perform quantitative PCR (qPCR) experiments.

3.3.6 RNA isolation, reverse transcription-PCR and qPCR

Total RNA was isolated using the PicoPure RNA isolation kit (Arcturus) according to the manufacturer's protocol. The RNA was reversed transcribed into cDNA with oligo(dT)₁₅ primers in a 20 µl reaction using the Promega Reverse Transcription System. Quantitative real-time PCR (qRT-PCR) was performed in duplicate using four independent RNA samples. The cDNA was quantified using

the SYBR green mix (Applied Biosystems) and Quantitect Primer Assay kit (Qiagen). Primer references are listed in Table 3.3.

Table 3.3. Primers used for real time PCR analysis

Gene	Product size	Company (ref)	Acc. number
HPRT	168 bp	Qiagen (QT00166768)	NM_013556
P2X1	100 bp	Qiagen (QT00120694)	NM_008771
P2X4	73 bp	Qiagen (QT00163149)	NM_011026
P2X7	80 bp	Qiagen (QT00130900)	NM_011027, NM_001038839, NM_001038845
Panx1	108 bp	Qiagen (QT00138845)	NM_019482
Panx2	133 bp	Qiagen (QT01773737)	NM_001002005

The PCR was run in 10 μ l on 10 ng cDNA generated from total RNA using a 7900 HT Fast Real-Time PCR System (Applied Biosystems). Reaction conditions for the PCR amplification were 20 s at 95 °C, followed by 40 cycles, each consisting of 1 second at 95 °C and 20 s at 60 °C. For the analysis, we used the comparative Ct method, and normalized the cycle threshold (Ct) value of each sample to the endogenous housekeeping gene HPRT (hypoxanthineguanine phosphoribosyltransferase), which gives the Δ Ct value of the sample. This estimates the fold change in expression of the other genes relative to the housekeeping gene. The results of the quantitative PCR were run on a 2% agarose gel at the end of the PCR process to verify the product sizes.

3.3.7 Statistics

Data are presented as mean \pm SEM; N expresses the number of recorded cells or the number of independent experiments in each of which multiple cells were measured. Mean effects of drugs applied on the same cell or on the same group of cells were compared using nonparametric Wilcoxon rank sign test for paired data. Means for each group of cells treated in the same way were compared using the nonparametric Mann-Whitney U test for continuous and unpaired variables. Differences were considered significant at $P < 0.05$. Statistics were performed using Graph Pad Prism 4 (2003) and Kaleidagraph 4.04 (2006 Synergy software, USA). Graphics were prepared using Kaleidagraph software.

3.4 Results

3.4.1 P2X1R, P2X4R and P2X7R expression in embryonic microglia

Microglia are known to express ionotropic P2X1R, P2X4R and P2X7R in the adult [3] and during substantia nigra pars compacta development [88]. We first determined the expression of these P2XRs using qPCR in FACS-sorted microglia of E13.5 CX3CR1eGFP mouse embryonic SCs. We also investigated the expression of the mRNAs coding for Panx1 and pannexin-2 (Panx2) since P2X7R can interact with Panx hemi-channels [221]. P2X1R mRNAs were poorly expressed when compared to P2X4R and P2X7R mRNAs. We observed a significant ($p < 0.01$) 19- and 7-fold larger expression of the mRNAs coding for P2X4R and for P2X7R respectively (Fig. 3.1A), when compared to the expression of mRNAs coding for P2X1R. We observed a significant ($p < 0.01$) 2.25-fold larger expression of the mRNAs coding for Panx1 (Fig. 3.1A), when compared to the expression of mRNAs coding for P2X1R. To the contrary, Panx2 mRNAs were poorly expressed in microglia. We observed a significant ($p < 0.01$) 12.9-fold lower expression of the mRNAs coding for Panx2 (Fig. 3.1A), when compared to the expression of mRNAs coding for Panx1.

When analyzing P2X4R expression in the ventral part of the SC using immunostaining (Fig. 3.1B2, C2, D2, C2 and C3) we observed that 63.7 ± 2.2 % ($N = 5$ SCs) of microglia localized in the ventral SC expressed P2X4R. However, at E13.5, 67.8 ± 1.9 % ($N = 5$ SCs) of the ventral microglia were localized in the ventrolateral region (the MN area) of the SC (Fig. 3.1B1 and B3) [121] and a significant higher proportion ($p < 0.01$) of these microglia expressed P2X4R (81.3 ± 2.9 % ; $N = 5$ SCs) when compared to the other areas of the ventral SC (27.1 ± 5.1 % ; $N = 5$ SCs) (Fig. 3.1B2 and D2). The motoneuron area ($12000 \mu\text{m}^2$) was set as constant in all SCs analyzed as previously described [121].

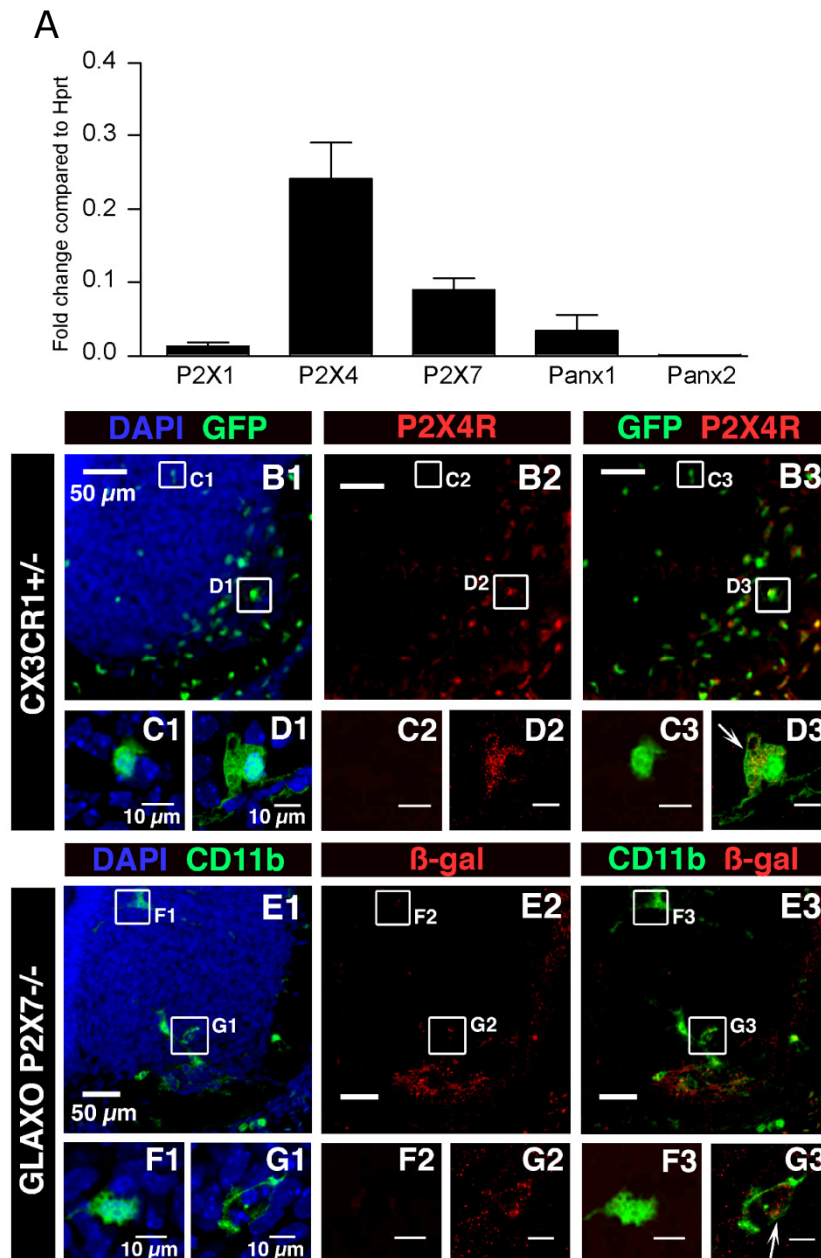


Figure 3.1. P2X1R, P2X4R, P2X7R, Panx1 and Panx2 expression in microglia. A) P2X1R, P2X4R, P2X7R, Panx1 and Panx2 expression was analyzed on FACS-sorted SC microglia using qPCR. For each gene, the expression level corresponds to the x-fold change relative to the housekeeping gene Hprt. Note that P2X4R and P2X7R are the main P2XR transcripts expressed. The P2X1R transcript expression level is significantly ($p < 0.01$) lower than those of P2X4R and P2X7R. Note that low levels of Panx2 mRNAs were detected when compared to Panx1 mRNAs (≈ 13 -fold significantly lower; $p <$

Microglia proliferation is controlled by P2X7 in the embryonic spinal cord

0.01). **B-D)** P2X4R immunostaining in the ventral region of the SC of E13.5 CX3CR1eGFP mouse embryos. B1) Representative pictures of the SC ventral region. Note the accumulation of microglia (green) in the ventrolateral part of the SC. B2) P2X4R immunostaining. B3) Superimposed images shown in B1 and B2. C1) Enlarged image showing an example of eGFP microglia localized in the dorsomedial region of the ventral SC. C2) Note the lack of P2X4R immunostaining in the area shown in C1 (arrow red). C3) Superimposed images (C1 and C2) showing lack of P2X4R immunostaining within eGFP-positive microglia localized in the dorsomedial region. D1) Enlarged image showing an example of eGFP microglia localized in the ventrolateral region of the ventral SC. D2) P2X4R immunostaining in the area shown in D1 (red). D3) Superimposed images (D1 and D2) showing P2X4R immunostaining within eGFP-positive microglia localized in the ventro-lateral region (arrow). Note that the staining is mainly located within the cytoplasm (single confocal section). **E-G)** β -galactosidase immunostaining in the ventral region of the SC of E13.5 GlaxoSmithKline P2X7R^{-/-} mouse embryos where the LacZ reporter gene has been inserted into the P2X7R gene. E1) Representative pictures of the ventral SC in E13.5 GlaxoSmithKline P2X7R^{-/-} mouse embryos. Microglia were stained using CD11b antibody. E2) β -galactosidase staining in the ventral SC. E3) superimposed images shown in E1 and E2. F1) Enlarged image showing an example of microglia localized in the dorsomedial region of the ventral SC. F2) β -galactosidase immunostaining in the area of the microglia shown in F1. Note the lack of galactosidase immunostaining. F3) superimposed images shown in F1 and F2. G1) Enlarged image showing an example of microglia localized in the ventrolateral region of the ventral SC. G2) Galactosidase immunostaining in the area shown in G1. G3) Superimposed images (G1 and G2) showing galactosidase immunostaining within CD11b-positive microglia localized in the ventrolateral region (arrow; single confocal section), which indicates P2X7R gene expression in microglia. B1, C1, D1, E1, F1 and G1) Cell nuclei are visualized with DAPI staining.

P2X4R immunostaining was mainly localized in the cytoplasm (Fig. 3.1D3), as also observed in peritoneal macrophages [222]. Due to the lack of a specific antibody for P2X7R, we used GlaxoP2X7R^{+/-} mice, in which the *LacZ* gene has been inserted into the *P2X7* gene, to analyze P2X7R cellular expression [210]. Double immunostaining using antibodies directed against CD11b (Fig. 3.1E1, F1 and G1) to stain microglia [121] and against β -galactosidase encoded by the *LacZ* gene (Fig. 3.1E2, E3, F2, F3, G2 and G3), showed that 77.1 ± 1.6 % ($N = 5$ SCs) of microglia expressed P2X7R in the ventral part of the embryonic SC at E13.5. But as mentioned above most microglia accumulate within the ventrolateral region at E13.5 (72.2 ± 1.7 % of ventral microglia in this set of experiments; $N = 5$ SCs) (Fig. 3.1E1). Moreover, 88.1 ± 1.4 % ($N = 5$ SCs) of microglia localized in the ventro-lateral region of the SC expressed galactosidase while only 47.7 ± 4.1 % ($N = 5$ SCs) of microglia localized in other areas of the ventral SC were immunoreactive to galactosidase antibody (Fig. 3.1E2, F2, F3,

G2, G3), indicating that P2X7R was significantly ($p < 0.01$) more likely to be expressed by microglia localized in the MN area compared with other parts of the ventral SC.

3.4.2 ATP evokes biphasic membrane currents in embryonic microglia that result from P2X7R activation

To evaluate the functionality of the purinergic receptors expressed at the cell membrane of microglia, we performed an electrophysiological study of embryonic microglia *ex vivo* using whole-cell patch-clamp. We first investigated the passive electrophysiological properties of microglia in the embryonic SC. At E13.5, microglia had an irregular cell body shape and short processes (branched microglia) or an amoeboid morphology (Fig. 3.2C). The input resistances of the branched cells and of the amoeboid cells were $3.6 \pm 0.3 \text{ G}\Omega$ and $4.3 \pm 0.5 \text{ G}\Omega$, respectively, being not significantly different ($p > 0.1$). The input capacitances of the branched cells ($12 \pm 1 \text{ pF}$; $N = 56$) and of the amoeboid cells ($11 \pm 1 \text{ pF}$; $N = 26$) were not significantly different either ($p > 0.1$). Almost all cells with an amoeboid morphology (96.2 % ; 24 of 26 recorded cells) displayed inward rectifying current (IrC), while only 57.1 % (32 of 56 recorded cells) of the branched cells exhibited IrC (Fig. 3.2A and C). In contrast, all cells, irrespective of their morphology, displayed outward rectifying current (OrC; Fig. 3.2A and B). Because outward rectification in the I/V relationship obtained on embryonic microglia (Fig. 3.2A and B, and 3.6B) was reminiscent of that described for a Panx1 voltage-dependent current [216], we tested the effect of the hemichannel blocker CBX [216] on currents evoked by voltage ramps from -100 mV to + 100 mV. 100 μM CBX had no significant effect ($p > 0.1$) on the outward rectification (Fig. 3.2D): it inhibited only $8.4 \pm 4.8 \%$ of the current ($N = 8$). This clearly indicates that the voltage-activated current in embryonic microglia does not reflect Panx1 activation.

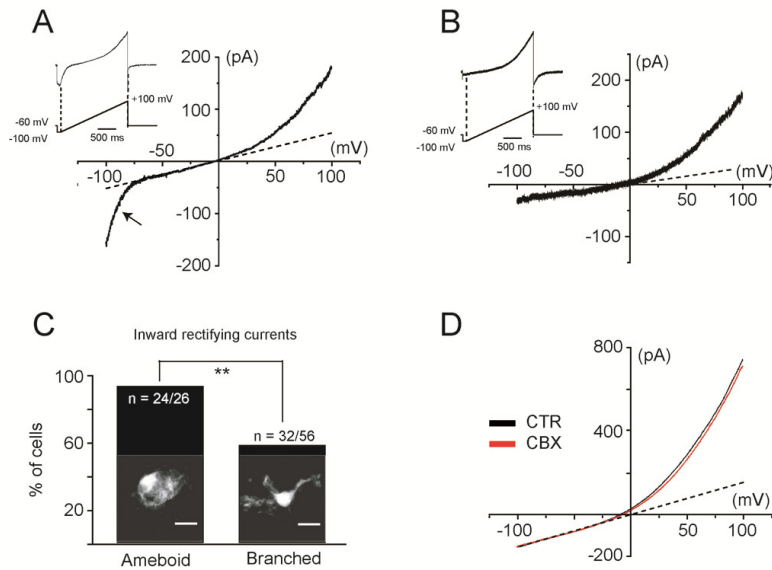


Figure 3.2. Voltage-activated current profile in microglia of the developing SC. Voltage-activated current was analyzed using voltage ramps ranging from -100 to +100 mV over 2 s. Two different voltage-activated current patterns could be distinguished: an IrC, observed at membrane potentials lower than ≈ -70 mV (**A**), and an OrC (**B**). **C**) The absence or the presence of IrC was significantly correlated ($p < 0.05$) to the morphology of the recorded microglia (Fisher's exact test, $p < 0.05$). **C**) Confocal images (Z-stack) showing amoeboid microglia (left) and branched microglia (right) in the ventral SC area of CXCR1 EGFP mice. **D**) The gap junction/hemichannel blocker CBX (100 μ M) had no effect on the OrC ($P > 0.1$). This current was 8.4 ± 4.8 % inhibited in the presence of 100 μ M CBX ($N = 8$). CTR, Control.

Next, we assessed the presence of functional P2XRs. The threshold concentration of ATP to elicit a response was 0.5 mM suggesting that P2XR involved in this current had a low affinity for ATP as previously described for P2X7R [221]. Applications of 0.5 mM and 1 mM ATP evoked currents of 0.3 ± 0.1 pA/pF ($N = 9$), and of 1.21 ± 0.41 pA/pF ($N = 5$), respectively, while 3 mM ATP evoked a biphasic current of 30.7 ± 4.4 pA/pF ($N = 7$) (Fig. 3.3A). Such a biphasic response may reflect P2XR channel pore dilatation [223, 224] and/or the formation of a large plasma membrane pore [221]. Since calcium and/or magnesium are known to modulate P2X7R and P2X4R activation [225], we determined to which extent lowering their extracellular concentration could modify ATP-evoked responses. Responses evoked by ATP in the absence and in

the presence of $[Ca^{2+}, Mg^{2+}]_{out}$ were analyzed in different cells. In free $[Ca^{2+}, Mg^{2+}]_{out}$ solution, the minimal ATP concentration necessary to evoke a current was 10 times lower (50 μ M) than in normal $[Ca^{2+}, Mg^{2+}]_{out}$ (Fig. 3.3B). Similarly, a biphasic current was evoked by 0.3 mM ATP in free $[Ca^{2+}, Mg^{2+}]_{out}$ (Fig. 3.3B). ATP (0.3 mM) elicited a current of 25.97 ± 3.17 pA/pF ($N = 5$), being not significantly different ($p > 0.05$) from the one measured with 3 mM ATP in normal $[Ca^{2+}, Mg^{2+}]_{out}$ (30.7 ± 4.4 pA/pF; $N = 7$). In free $[Ca^{2+}, Mg^{2+}]_{out}$, 0.05 mM ATP ($N = 9$) and 0.1 mM ATP ($N = 9$) evoked currents of 0.42 ± 0.6 pA/pF and of 0.65 ± 0.14 pA/pF, respectively. Input capacitance of recorded microglia in normal $[Ca^{2+}, Mg^{2+}]_{out}$ (13.3 ± 1 pF; $N = 9$) and in free $[Ca^{2+}, Mg^{2+}]_{out}$ (13.8 ± 1.4 pF; $N = 5$) were not significantly different ($p > 0.1$).

ATP-induced biphasic responses occurred only at the first application, while subsequent responses did not display a biphasic activation phase anymore (Fig. 3.3C). These subsequent responses had a significantly ($p < 0.01$) faster 20-80% rise time (20-80 % RT = 1.9 ± 0.4 s; $N = 8$) than the first response (20-80 % RT = 10.1 ± 1.4 s; $N = 8$). In free $[Ca^{2+}, Mg^{2+}]_{out}$, these values were not significantly modified ($p > 0.05$): they were 13.7 ± 1.3 s and 3 ± 0.4 s ($N = 16$) for the biphasic current and the subsequent responses, respectively. We also observed a small rundown of the current amplitude with time of the responses after evoking a biphasic current (Fig. 3.3C). We compared the amplitude of the currents evoked after obtaining a biphasic response. When the responses were evoked on the 3 min (Fig. 3.3C), the amplitude of the second current was decreased by 6.8 ± 4 % ($N = 7$) in normal $[Ca^{2+}, Mg^{2+}]_{out}$, and by 13 ± 8 % ($N = 12$) in free $[Ca^{2+}, Mg^{2+}]_{out}$, being not significantly different ($p > 0.1$). The amplitude of the third current was decreased by 26.6 ± 3.2 % ($N = 7$) in normal $[Ca^{2+}, Mg^{2+}]_{out}$, and by 15.4 ± 3.8 % ($N = 12$) in free $[Ca^{2+}, Mg^{2+}]_{out}$ being significantly different ($p < 0.05$). Large inward currents evoked by long application of ATP (140 s) slowly decreased with time, indicating that these P2XRs have slow desensitization kinetics (Fig. 3.3D1 and D2). In addition, responses evoked by application of different concentrations of ATP after evoking a biphasic current could be fitted with the Hill equation, yielding an EC_{50} of 0.47 mM and a Hill coefficient of 2.6 (Fig. 3.3E). Finally, ATP-induced inward current versus voltage relationship yielded a reversal potential of 3 ± 3 mV ($N = 7$) (E_{Cl}

= -40 mV), indicating that ATP application caused an increase in cationic conductance (Fig. 3.4A).

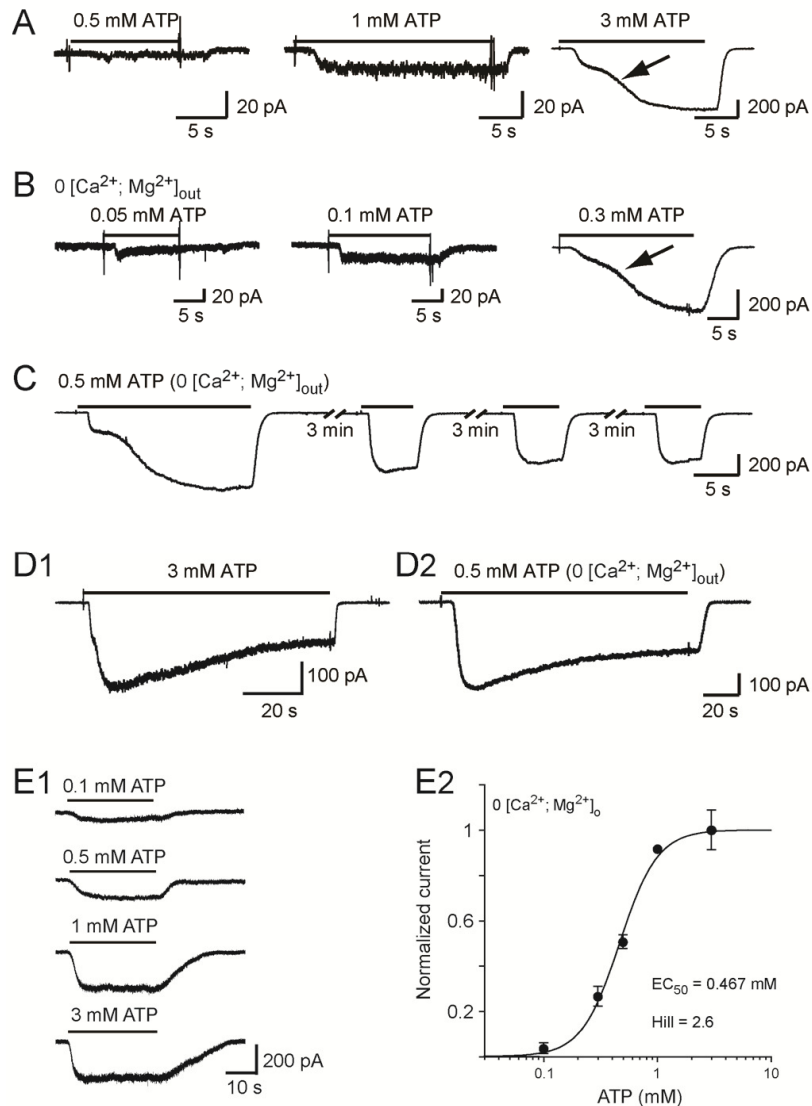


Figure 3.3. ATP evokes inward currents in embryonic microglia. A) Example of responses evoked by 0.5 mM, 1 mM and 3 mM ATP in the presence of 1.3 mM $[Ca^{2+}]_o$ and 3 mM $[Mg^{2+}]_o$. Note the biphasic activation phase (arrow) of the response evoked by 3mM ATP. **B)** Currents evoked by 0.05, 0.1 and 0.3 mM ATP in $[Ca^{2+} + Mg^{2+}]_o = 0$. **C)** Currents evoked by repetitive applications of 0.5 mM ATP in $[Ca^{2+} + Mg^{2+}]_o = 0$. **D)** Current evoked by long application of 3 mM ATP in the presence (D1) and of 0.5 mM ATP in the absence (D2) of $[Ca^{2+} + Mg^{2+}]_o$. This response slowly desensitized (half-amplitude

decay time = 26.9 s in the presence of $[\text{Ca}^{2+} + \text{Mg}^{2+}]_o$ and 41.9 s in free $[\text{Ca}^{2+} + \text{Mg}^{2+}]_o$ solution). Large inward currents evoked by 140 s application of ATP after eliciting a biphasic response slowly decreased with time in both normal $[\text{Ca}^{2+}, \text{Mg}^{2+}]_{out}$ (3mM ATP) and free $[\text{Ca}^{2+}, \text{Mg}^{2+}]_{out}$ (0.5mM ATP) solutions and reached a plateau representing $50.5 \pm 3.1\%$ ($N = 5$) of the peak current in normal $[\text{Ca}^{2+}, \text{Mg}^{2+}]_{out}$ solution and $64.7 \pm 5.2\%$ ($N = 8$) in free $[\text{Ca}^{2+}, \text{Mg}^{2+}]_{out}$. The half-desensitization time was 25.9 ± 3.3 s ($N = 5$) in normal $[\text{Ca}^{2+}, \text{Mg}^{2+}]_{out}$ and 36.9 ± 6.5 s ($N = 8$) in free $[\text{Ca}^{2+}, \text{Mg}^{2+}]_{out}$. **E1**) Example of currents evoked by increasing ATP concentrations after having obtained a biphasic response ($[\text{Ca}^{2+} + \text{Mg}^{2+}]_o = 0$). **E2**) Dose-response curve of ATP-evoked currents as shown in E1 ($EC_{50} = 467 \mu\text{M}$; Hill coefficient = 2.6). Each point represents the average of 5-10 measurements. The amplitude of the ATP-evoked responses has been normalized to the current amplitude of the responses evoked by 1 mM ATP (see 3.3 Materials and methods). ($V_h = -60$ mV). Error bars indicate SEM.

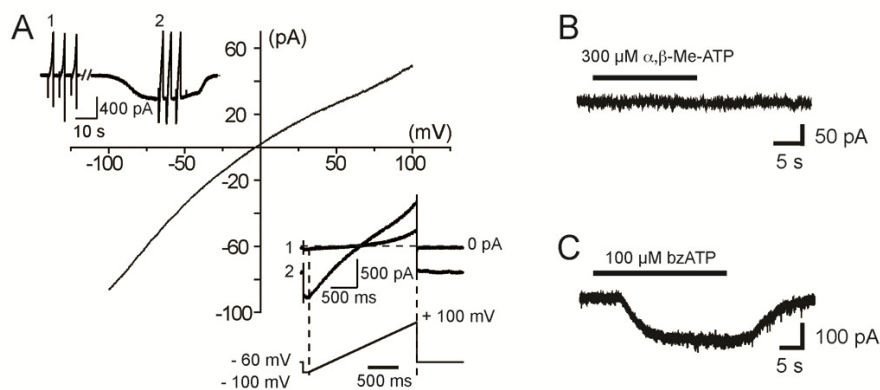
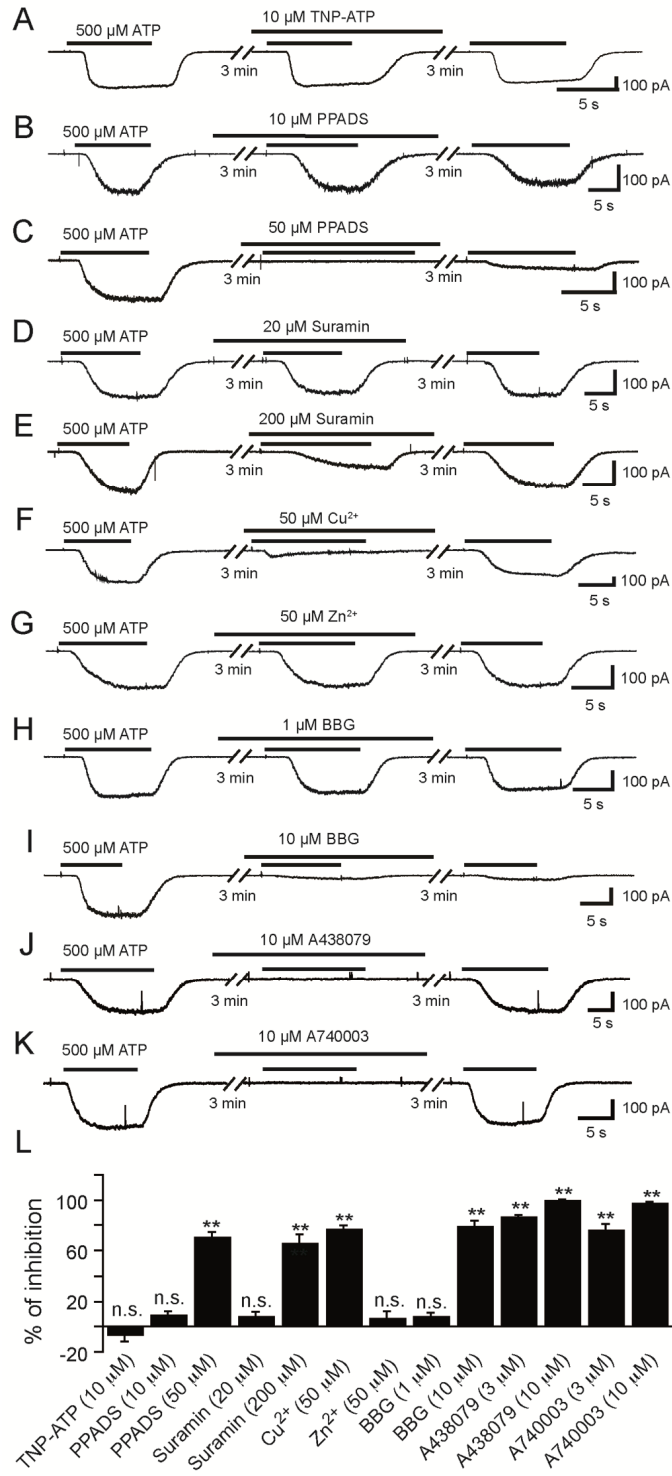


Figure 3.4. Whole-cell currents evoked by ATP and P2XR agonists in embryonic microglia *in situ*. **A**) A voltage ramp protocol (-100 mV +100 mV; 2 s) was used to determine the reversal potential of ATP evoked currents (insert lower right). A set of three voltage ramps from -100 to 100 mV (interval) was applied before and during the response to 3 mM ATP (inset upper left) and the resulting currents were averaged. The averaged currents evoked before ATP application were subtracted from the averaged currents evoked during ATP application to obtain the current-voltage relationship of the current evoked by ATP. In this example, 3 mM ATP evoked inward currents with a reversal potential of -3.2 mV. **B**) Application of α, β -Me-ATP (300 μM), a P2X1R and P2X3R agonist, failed to evoke a response in embryonic SC microglia ($V_h = -60$ mV). **C**) In contrast, bzATP (100 μM), a compound acting as an agonist on P2X7Rs and being also effective on P2X1Rs and P2X2Rs, induced inward currents ($V_h = -60$ mV). bzATP (100 μM) evoked a current of 9 ± 2 pA/pF ($N = 6$).

These functional characteristics of ATP-evoked currents are compatible with the activation of P2X4R and/or of P2X7R, but not of P2X1R [226]. To have an estimation of the pharmacological profile of these microglia P2XRs, we then analyzed the effect of two agonists and eight antagonists on the response evoked by repetitive applications of 500 μM ATP in free $[\text{Ca}^{2+}, \text{Mg}^{2+}]_{\text{out}}$ (See 3.3 Materials & Methods). Agonist α, β -Me-ATP (300 μM), a P2X1R and P2X3R agonist [227], did not induce any current ($N = 4$) (Fig. 3.4B) unlike 100 μM bzATP ($N = 6$), a strong agonist on P2X7Rs that can also be effective on P2X1Rs and P2X2Rs, but not on P2X5Rs [227] (Fig. 3.4C). TNP-ATP (10 μM), a potent antagonist at concentrations ≥ 2 μM on P2X1R, P2X2R, P2X3R, P2X4R [227] and on P2X4/P2X7R [228], (Fig. 3.5A and L) and 10 μM PPADS (Fig. 3.5B and L) being known to antagonize P2X1R, P2X2R, P2X3R and P2X5R [227], and to weakly antagonize mouse P2X7R [229], had no significant effect ($p > 0.1$) on the ATP-evoked response, while 50 μM PPADS significantly ($p < 0.01$) blocked (≈ 70 %) the response evoked by ATP (Fig. 3.5C and L). Similarly, 20 μM suramin, being known to fully antagonize all P2XR except P2X4R and P2X7R [227], had no significant inhibitory effect ($p > 0.05$) on the ATP-evoked current (Fig. 3.5D and J), while 200 μM suramin evoked a significant ($p < 0.01$) ≈ 66 % inhibition (Fig. 3.5E and L). We then tested the effect of Cu^{2+} and Zn^{2+} on ATP-evoked currents. Cu^{2+} inhibits both P2X7Rs and P2X4Rs whereas Zn^{2+} increases the activity of P2X4R and is virtually without effect on rat P2X7R expressed in oocytes [226] or fully blocks the activity of these two receptors expressed in transfected human embryonic kidney (HEK) cells [230]. Then 50 μM Cu^{2+} evoked a significant ($p < 0.01$) ≈ 77 % inhibition (Fig. 3.5F and 5L), while ATP-evoked responses were insensitive to 50 μM Zn^{2+} (Fig. 3.5G and L). Although this pharmacological profile was apparently consistent with P2X7R expression, 1 μM BBG, known to fully antagonize P2X7R [231], had no significant effect ($p > 0.1$) (Fig. 3.5H and L), whereas 10 μM BBG, known to also inhibit P2X4R [231], evoked a significant ($p < 0.01$) ≈ 79 % inhibition (Fig. 3.5I and L). Accordingly, this pharmacological profile of ATP-evoked current did not allow discriminating clearly between P2X4R and P2X7R. To further address this issue we analyzed the effects of A438079 and A740003, two novel highly selective P2X7R antagonists [232]. Three (data not shown) and 10 μM (Fig. 3.5J) A438079 resulted in significant ($p < 0.01$) ≈ 87 % and ≈ 100 % inhibition, respectively (Fig. 3.5L) while 3 (data not shown)

and 10 μM (Fig. 3.5K) A740003 resulted in significant ($p < 0.01$) $\approx 76\%$ and $\approx 97\%$ inhibition, respectively (Fig. 3.5L). These results are consistent with the hypothesis that ATP-evoked currents were due to the activation of P2X7R on embryonic SC microglia. To confirm this hypothesis, we then compared the effect of ATP on microglia in the isolated SC of E13.5 P2X7R^{-/-} and P2X7R^{+/-} mouse embryos. In microglia of P2X7R^{-/-} embryos, the current evoked by a voltage ramp in microglia curve displayed both inward and outward rectifications as observed in wild type (Fig. 3.6B), but the application of 3 mM ATP evoked a very small transient inward current (≤ 1 pA/pF; $N = 5$) only (Fig. 3.6C1), whereas it was larger and showed a biphasic activation time course in the SC of P2X7R^{+/-} embryos ($N = 7$) (Fig. 3.6C2) as observed in C57Bl/6 CX3CR1eGFP^{+/-} mouse embryos. The current density in P2X7R^{-/-} was significantly (≈ 16 times) smaller ($p < 0.01$) than the current measured in P2X7R^{+/-} ($N = 7$) (Fig. 3.6C3). Together, these results demonstrate that ATP-evoked biphasic current in embryonic microglia requires the expression of P2X7R.

Figure 3.5 (Next page). Effects of TNP-ATP, PPADS, suramin, copper, zinc, BBG, A438079 and A740003 on ATP-evoked currents in SC microglia. All compounds were applied before and during ATP application (500 μM ; free $[\text{Ca}^{2+}$, $\text{Mg}^{2+}]_i$; $V_h = -60$ mV). **A)** ATP-evoked current was poorly sensitive to TNP-ATP (10 μM), a selective antagonist of P2X1R, P2X3R and P2X4R ($p > 0.05$). **B)** PPADS (10 μM) did not prevent ATP-evoked currents. **C)** PPADS (50 μM) fully blocked ATP-evoked currents. Note that ATP-evoked responses were poorly reversible 3 min after the end of the PPADS application. **D)** Suramin (20 μM) did not inhibit ATP-evoked responses as expected for P2X7Rs. **E)** Suramin (200 μM) partially blocked ATP-evoked currents. **F)** Copper (50 μM), known to block P2X7R activity, reversibly inhibited ATP-evoked currents. **G)** Zn^{2+} (50 μM) was poorly effective on ATP-evoked currents. **H)** BBG (1 μM) at this concentration was poorly effective on ATP-evoked currents. **I)** BBG (10 μM), known at this concentration to inhibit both P2X7R and P2X4R, irreversibly inhibited ATP-evoked currents. **J)** A438079 (10 μM) known at this concentration to inhibit selectively murine P2X7R fully inhibited ATP-evoked currents. **K)** A740003 (10 μM) also known to inhibit selectively murine P2X7R fully blocked ATP-evoked currents. **L)** Quantification of the inhibitory effects of the antagonists on ATP-evoked responses. Inhibitions of ATP responses were as follows: $-6.8 \pm 5.5\%$ ($N = 6$) for 10 μM TNP-ATP, $8.7 \pm 3\%$ ($N = 5$) for 10 μM PPADS, $70.3 \pm 4.4\%$ ($N = 6$) for 50 μM PPADS, $7.2 \pm 3.9\%$ ($N = 6$) for 20 μM suramin, $65.7 \pm 7.4\%$ ($N = 5$) for 200 μM suramin, $76.8 \pm 3.4\%$ ($N = 13$) for 50 μM Cu^{2+} , $5.9 \pm 5.6\%$ ($N = 10$) for 50 μM Zn^{2+} , $7.2 \pm 3.4\%$ ($N = 10$) for 1 μM BBG, $79.3 \pm 4.5\%$ ($N = 5$) for 10 μM BBG, $86.8 \pm 1.5\%$ ($N = 5$) for 3 μM A438079, $76 \pm 5\%$ ($N = 5$) for 3 μM A740003, $99.8 \pm 0.8\%$ ($N = 5$) for 10 μM A438079 and $97.4 \pm 1.6\%$ ($N = 5$) for 10 μM A740003. (Statistical significance: * $p < 0.05$, ** $p < 0.01$). Error bars indicate SEM.



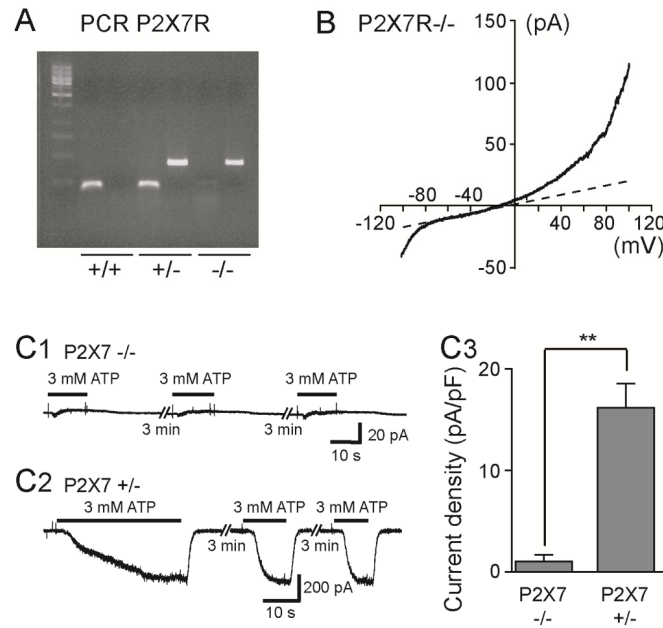


Figure 3.6. ATP-evoked biphasic currents were not observed in SC microglia of P2X7R-/- mouse embryos. A) PCR results for wild type (+/+) mice, heterozygote mice (+/-) and P2X7R KO mice (-/-). **B)** Voltage-current relationship of microglia recorded in the SC of E13.5 P2X7R-/- mouse embryos. A voltage ramp protocol (-100 mV +100 mV; 2 s) was used to investigate voltage-activated currents. **C1)** Application of 3 mM ATP on microglia recorded in the SC of P2X7R -/- mouse E13.5 embryo failed to evoke large biphasic inward currents. **C2)** Examples of currents evoked by 3 mM ATP on microglia of a P2X7R +/- mouse E13.5 embryo. **C3)** Histogram showing differences in current density of 3 mM ATP-evoked responses in SC microglia of P2X7R -/- (0.93 ± 0.43 pA/pF; $N = 5$) and P2X7R +/- (16.5 ± 2.12 pA/pF; $N = 7$) mouse embryos. ($V_h = -60$ mV). Input capacitance of recorded microglia in P2X7R-/- embryos (11.9 ± 1.4 pF; $N = 5$) and in P2X7R +/- embryos (10.3 ± 1 pF; $N = 7$) were not significantly different ($p > 0.1$). Error bars indicate SEM.

3.4.3 P2X7R activation does not need Panx1 expression to generate a biphasic current.

Large biphasic currents evoked in response to ATP might result from the interaction between P2X7R and Panx1 [221]. Embryonic microglia express both Panx1 mRNAs (Fig. 3.1A) and proteins, as shown by immunohistochemistry (Fig. 3.7A); 61 ± 3 % ($N = 5$ SCs; 249-282 cells tested per SC) of the microglia located in the ventral area of the SC were immunoreactive to the Panx1 antibody. Panx1 staining was not observed in SC microglia of E13.5 Panx1-/- mouse embryos (Fig. 3.7B). Microglia obtained from Panx1-/- still express the

voltage-dependent current ($N = 5$) observed in wild-type (Fig. 3.2A, B and D), further supporting its independence on Panx1 expression (Fig. 3.8B).

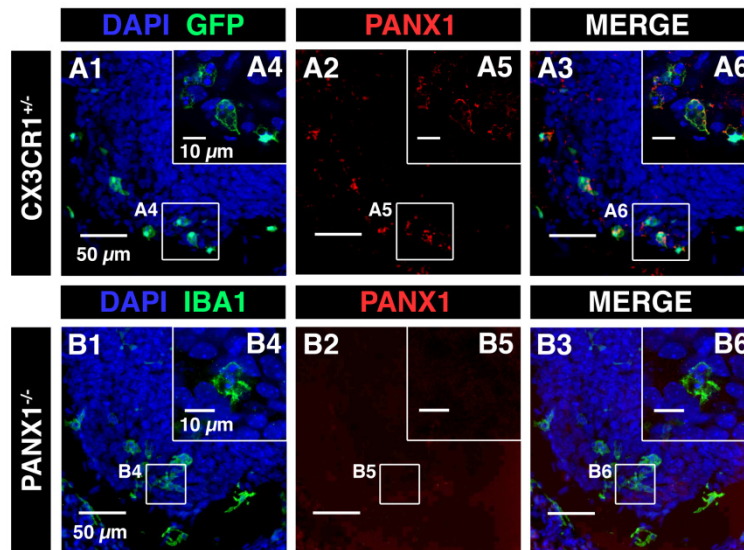


Figure 3.7. Panx1 immunostaining was not observed in the SC of Panx1^{-/-} mouse embryos.

A) Confocal image of immunostaining against Panx1 (red; A2, A3, A5 and A6) in the ventral SC of CX3CR1eGFP mouse embryo. A3, B3) Superposition of Iba1 and Panx1 immunostainings. A4 and A6) Single confocal sections showing microglia located in the ventrolateral area of the SC. A2 and A5) Panx1 immunostaining in the ventral SC of CX3CR1eGFP mouse embryo. A3) superimposed images (A1 and A2) showing Panx1 staining in microglia. A6) Superimposed images showing Panx1 staining in microglia localized in the ventrolateral region. **B)** Confocal image of immunostaining against Panx1 (red; B2, B3, B5 and B6) in the ventral SC of Panx1^{-/-} mouse embryo. B1 and B4) Microglia were stained using IBA1 antibody. B1, B2 and B3) Panx1 immunostaining in the SC of E13.5 Panx1^{-/-} mouse embryos. B1, B3, B4 and B6) Microglia were revealed using IBA1 antibody (green). Note that Panx1 immunostaining was no longer observed in the SC of E13.5 Panx1^{-/-} mouse, indicating that this antibody specifically recognizes Panx1. A1, A3, A4, A6, B1, B3, B4 and B6) Cell nuclei are visualized with DAPI staining.

To determine to what extent the biphasic currents evoked by ATP applications might reflect Panx1 opening, we first tested the effect of two putative hemi-channel blockers, DIDS and CBX [215, 216], on successive responses evoked by 3 mM ATP in normal $[Ca^{2+}, Mg^{2+}]_{out}$ on SC microglia of CX3CR1eGFP mouse embryos. High concentration (100 μ M) of DIDS had little but significant ($p < 0.01$) effect (20-30 % inhibition) on ATP-evoked current whereas 100 μ M CBX

had no significant effect ($p < 0.1$) on ATP-evoked current (Fig. 3.8C1, C2 and C3). Because the pharmacological profile of Panx1 could have been modified by its interaction with P2X7Rs [216], we then determined if ATP could evoke a biphasic response on microglia of Panx1^{-/-} embryos (Fig. 3.8D), although 3 mM ATP still evoked biphasic currents (27.7 ± 3.5 pA/pF; $N = 10$), indicating that the biphasic response to ATP did not reflect functional coupling of P2X7R to Panx1.

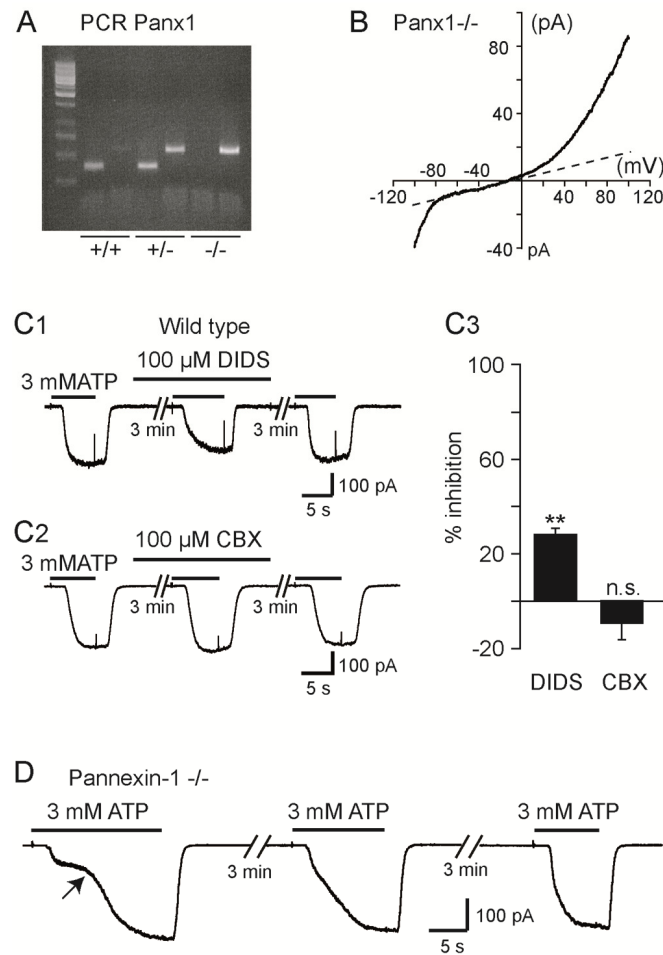


Figure 3.8. ATP-evoked biphasic currents did not result from Panx1 activation. **A)** PCR results for wild-type (+/+), heterozygote (+/-) and Panx1 KO mice (-/-). **B)** Voltage-current relationship of currents recorded in microglia obtained from the SC of E13.5 Panx1^{-/-} mouse embryos. A voltage ramp protocol (-100 mV +100 mV; 2 s) was used to investigate voltage-activated currents. **C1 and C2)** Effect of high concentrations of the hemi-channel blockers DIDS and CBX on ATP-evoked

currents (3 mM ATP; $V_h = -60$ mV) in CXCR1eGFP mice. **C3**) 100 μ M DIDS significantly ($p < 0.01$) inhibits 28.3 ± 2.9 % ($N = 11$) of ATP responses while 100 μ M CBX had no significant effect ($p > 0.1$) (9.9 ± 6.6 % increase ; $N = 7$). The percentage change in response amplitude observed during the application of the blockers was compensated according to the averaged decrease (rundown: 6.8 %) in the corresponding responses observed on different cells in the absence of the blockers (Normal $[Ca^{2+}]_o$ and $[Mg^{2+}]_o$ ACSF: see Materials and methods and Results). **D**) Currents evoked by 3 mM ATP on microglia recorded from the SC of E13.5 Panx1 $-/-$ mouse embryos. Note that ATP application evoked a biphasic current as observed in CX3CR1eGFP and in P2X7 $+/-$ mouse embryos (see Fig. 3 and 6).

3.4.4 Embryonic microglia proliferation requires the expression of P2X7R but not of Panx1.

P2XRs have been proposed to promote both microglia activation and proliferation [200]. At E13.5, microglia in the ventral area of the embryonic SC proliferate while they are activated when interacting with apoptotic MNs [121]. To determine whether P2X7R is involved in these processes, we compared Ki67 staining (a proliferation marker) and Mac-2 staining (an activation marker for microglia) on microglia at E13.5 in the ventral SC area of P2X7R $-/-$, P2X7R $+/-$ and wild-type mouse embryos (Fig. 3.9A-C, 3.10A and B). Because microglia activation within the lateral motor column was associated with MN developmental cell death at E13.5 [121], we also determined to what extent MN developmental cell death was altered in P2X7R $-/-$ mouse embryos using activated caspase-3 immunostaining (Fig. 3.10C). The proportion of proliferating microglia (Ki67 staining) was dramatically decreased in P2X7R $-/-$ mouse embryos (2.1 ± 0.4 %; $N = 5$) when compared to P2X7R $+/-$ mouse embryos (25.4 ± 1.5 %; $N = 5$) ($p < 0.01$) or to P2X7R $+/+$ mouse embryos (26.9 ± 0.8 %; $N = 5$) (Figures 3.9A-C). The difference between P2X7R $+/-$ and P2X7R $+/+$ was not significant ($p > 0.1$). Accordingly, the number of microglial cells was significantly decreased (by 12.5 %; $p < 0.05$) in the ventral area of the lumbar SC of E13.5 P2X7R $-/-$ mouse embryos (225 ± 3 cells; $N = 5$) when compared to P2X7R $+/+$ (257 ± 5 cells; $N = 5$). Similarly the density of microglia aggregating in the lateral motor column (LMC) at the onset of MN developmental cell death was also significantly decreased by 13.5% ($p < 0.01$) in E13.5 P2X7R $-/-$ mouse embryos ($4.7 \pm 0.1 \times 10^{-4}$ cells/ μ m², $N = 5$) when compared to wild type ($5.4 \pm 0.2 \times 10^{-4}$ cells/ μ m², $N = 5$). We did not find any difference ($p > 0.1$) in microglia proliferation between wild-type and Panx1 $-/-$ mice (24.8 ± 0.9 %; N

= 5) (Fig. 3.9C), indicating that the control of embryonic microglia proliferation by P2X7Rs did not involve coupling of P2X7Rs to Panx1.

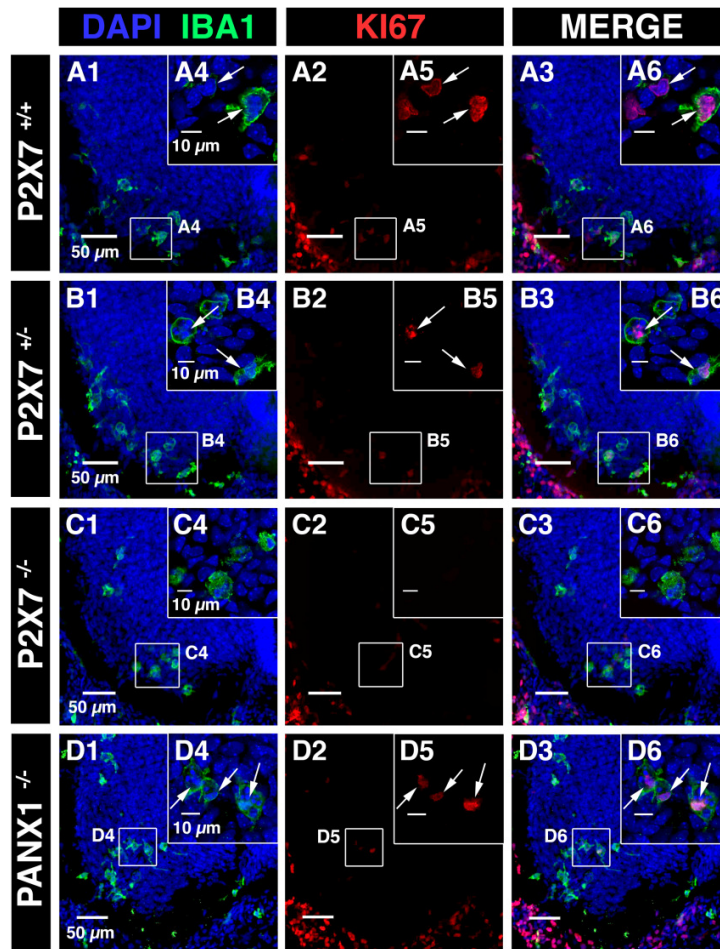


Figure 3.9. Microglia proliferation was dramatically reduced in the SC of P2X7R^{-/-} mouse embryos but was unchanged in the SC of Panx1^{-/-} mouse embryos. A1, B1, C1 and D1) DAPI staining (blue) and microglia accumulation (Iba1 immunostaining, green) in the ventral region of P2X7^{+/+}, P2X7^{+/-}, P2X7^{-/-} and Panx1^{-/-} E13.5 SCs. A2, B2, C2 and D2) Nuclear staining of KI67-expressing cells (red). A3, B3, C3 and D3) Superposition of Iba1 and KI67 immunostainings. A4, B4 and C4) Examples of microglia localized in the ventrolateral region of the SCs. A5, B5 and C6) Example of KI67 staining in the ventro-lateral region of the SC. A6 and B6) White arrows indicate KI67 staining (single confocal section). Contrary to P2X7^{+/+} SC (A6) and P2X7^{+/-} SC (B6) LMC microglia are not stained for KI67 in P2X7^{-/-} SC, (C6, single confocal section). D1) example of microglia localized in the ventral SC of E13.5 Panx1^{-/-} mouse embryos. D2) Immunostaining for KI67 in the ventral SC of E13.5 Panx1^{-/-} mouse embryos. D3) superimposed images shown in D1 and D2.

D4) Example of microglia localized in the ventrolateral region of the SC of E13.5 *Panx1*^{-/-} mouse embryos. **D5)** KI67 staining in the ventrolateral region of the SC of E13.5 *Panx1*^{-/-} mouse embryos. Note that KI67 immunostaining (arrows; D5) co-localized with Iba1 immunostaining (arrows; D6), indicating that microglia proliferated in the ventrolateral region of the SC of E13.5 *Panx1*^{-/-} mouse embryos. **D4, D5, D6)** single confocal section.

Microglia localized in the LMC have been previously shown to be in an activated state (Mac-2 staining) [121], but the proportion of activated microglia in the LMC was not significantly different ($p > 0.1$) between *P2X7R*^{-/-} (20 ± 0.5 %; $N = 5$) and wild-type (20.5 ± 0.6 %; $N = 5$) (Figures 3.5A and B). Accordingly, *P2X7R* was not involved in embryonic microglia activation at E13.5. Finally, MN developmental cell death at E13.5 was not affected in *P2X7R*^{-/-} mouse embryo. No difference ($p > 0.1$) in activated caspase-3 staining in the ventral region of the SC was found between wild-type (3.18 ± 0.12 % fluorescence/area; $N = 4$) and *P2X7R*^{-/-} (3.24 ± 0.15 % fluorescence/area; 40 slices, $N = 4$) (Fig. 3.10C and D).

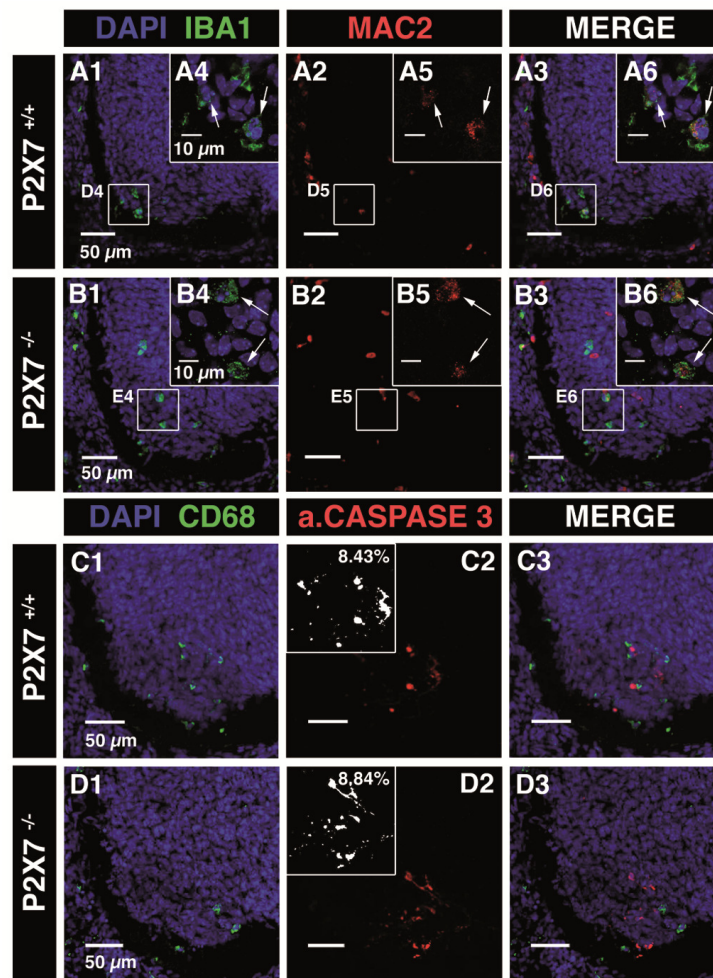


Figure 3.10. Microglia activation and motoneuron developmental cell death were not altered in the SC of E13.5 P2X7R^{-/-} mouse embryos. A-B) Confocal image of immunostainings against Iba1 (A1, B1) and Mac-2 (red; A2, B2) in the SC of wild-type (A) and P2X7R^{-/-} (B) mouse embryos. **A1, B1)** DAPI staining (blue) and microglia staining (Iba1 immunostaining, green) in the ventrolateral region of the SC. **A3, B3)** Superposition of Iba1 and Mac2 immunostainings. Note that Mac2 immunostaining co-localized with Iba1 immunostaining (arrows; B6), indicating that microglia were activated in the LMC of the SC of E13.5 P2X7R^{-/-} mouse embryos. **A4, B4)** single confocal section showing microglia located in the ventrolateral region of the SC. **C-D)** Confocal image of immunostainings against CD68 (C1, D1) and activated caspase-3 (red; C2, D2) in the ventral SC of wild type (C) and of P2X7R^{-/-} (D) mouse embryos. **C1, D1)** DAPI staining (blue) and microglia staining (CD68 immunostaining, green) in the ventrolateral region of the SC. **C3, D3)** Superposition of CD68 and activated caspase-3 immunostainings. Inserts in C2 and D2 are measurements of the percentage of fluorescence in the ventro-lateral region of the SC (see 3.3 Materials and methods).

3.5 Discussion

Our results demonstrate a new physiological role of P2X7R during SC embryonic development. Microglia in the SC of the mouse embryo already express functional P2X7R at the onset of MN developmental cell death and synaptogenesis [121, 214]. P2X7R activation by high concentration of ATP evokes a biphasic current in embryonic microglia, but our results indicate that although these cells express Panx1, there is no functional coupling of P2X7R to Panx1 in the embryo. Our results also demonstrate that P2X7R expression is required for the proliferation, but not for the activation of embryonic spinal microglia at the onset of MN developmental cell death. Since proliferation of nonactivated microglia is also affected in the SC of P2X7R^{-/-} mouse embryos, our results also suggest that embryonic microglia proliferation and activation are controlled by two independent mechanisms.

3.5.1 Functional P2XRs expressed by embryonic microglia in situ

It is now well accepted that microglia express P2X1R, P2X4R and P2X7R, both *in vitro* and *in vivo* in the adult [3]. Their expression in prenatal microglia [88], let alone their function, was, however, unknown. Although we found low P2X1R mRNA expression in embryonic microglia, we cannot exclude the possibility that functional P2X1Rs are expressed on the cell membrane. P2X1Rs have fast desensitization kinetics [233], which render their detection difficult due to the relatively slow drug exchange in our *ex vivo* preparations (0.5-1 s). In embryonic SC microglia, P2X4R transcripts were the most abundantly expressed, as shown by qPCR, but our immunohistochemical results indicate that most P2X4Rs are rather located within the cytoplasm. This can result from a fast turnover of this receptor at the cell membrane [234]. Our results contrast with recent data showing that P2X4R are functional in BV2 microglia cell lines and in cultured postnatal microglia [235]. This was unlikely to be the case in embryonic SC microglia of E13.5 mouse embryo, according to the pharmacological profile of ATP-evoked currents and to experiments performed on microglia of P2X7R^{-/-} mouse embryos. Such an apparent discrepancy between our results obtained *in situ* and those recently described in culture could be explained by the activation state of cultured microglia. Cultured microglia adopt an activation state that can be variable depending on the culture conditions [3], which could favor the

membrane expression of P2X4R. Effectively, surface expression of P2X4R is increased by exposure of microglia to proinflammatory bacterial lipopolysaccharides, which mimic microglial activation observed in pathological conditions [236].

Although our data demonstrate that P2X7R expression is required for ATP-evoked biphasic responses, the pharmacological profile of P2X7R is somewhat different from that classically described, especially with regard to the BBG potency in inhibiting ATP-evoked currents in transfected cells [231]. However, BBG efficiency on P2X7R largely depends on the method used to measure P2X7R activation and on animal species. [232]. We cannot completely rule out the possibility that BBG concentrations reaching the receptors were lower *in situ* than expected, but BBG has been applied 3 min before ATP, which is > 40 times longer than necessary to reach equilibrium for other molecules in our preparation. Alternatively, a low BBG efficiency might indicate the expression of heteromeric P2X7/P2X4Rs, which is also consistent with the low efficiency of Zn²⁺ on ATP-evoked current [228]. However, this hypothesis is not supported by our experiments (Fig. 3.5A) showing a lack of inhibition of ATP-evoked current by TNP-ATP [228]. Another possibility might be that homomeric P2X7Rs and homomeric P2X4Rs directly interact, as previously proposed in cultured microglia [237], but the pharmacological consequences of such an interaction remain unknown. A lack of effect of Zn²⁺ on ATP-evoked current was surprising (Fig. 3.5G), but the Zn²⁺ effect on P2X7R remains controversial and depends on the preparation used. Indeed, Zn²⁺ has a low potency on rat P2X7R expressed in oocytes [226, 238], when compared to rat P2X7R expressed in transfected HEK cells [230].

3.5.2 P2X7R is not coupled to Panx1 in embryonic microglia

Our results indicate that P2X7R is not coupled to Panx1 in embryonic microglia *in situ*, which contrasts with results previously obtained in the adult and *in vitro*. Accordingly, the biphasic ATP response reported in our experiments rather reflects integral pore dilatation of P2X7Rs [239]. However our data do not rule out the possibility that P2X7R activation can evoke the formation of Panx1 plasma membrane pore in more mature microglia, as proposed in BV2 microglial cell line and in cultured microglia [235]. It could be envisioned that the

difference in P2X7R/Panx1 interaction between embryonic microglia and adult microglia reflects a developmental process. Another consequence of the interaction of P2X7R with Panx1 is their induction of cell death [240]. In that respect, immature T-cells are less sensitive to cell death evoked by P2X7R activation when compared to mature T-cells [241]. A lack of coupling between P2X7R and Panx1 in embryonic microglia may prevent this detrimental effect without affecting other P2X7R functions. Nevertheless, recent data also suggest that there is no functional coupling of P2X7R to Panx1 in mature macrophages. Effectively, the activation of P2X7R by ATP increases bone marrow-derived macrophages membrane permeability independently of Panx1, indicating that Panx1 is not essential for P2X7R channel formation [242]. Panx1 activation independently of P2X7R signaling [242] was proposed to release a nucleotide “find me” signal from apoptotic cells [242, 243] allowing purinergic receptor activation on phagocytes. This nucleotide release pathway is unlikely to be involved in the embryonic SC, at least at the onset of MN developmental cell death. Indeed, we did not observe any Panx1 expression in MNs at E13.5. The activation of P2X7R by an autocrine release of ATP by microglia through Panx1 activation seems also unlikely, since we did not find evidence for spontaneous activation of Panx1 expressed by embryonic microglia.

3.5.3 P2X7Rs control microglia proliferation independently of microglia activation.

It has been previously proposed that microglia proliferation is an important mechanism that allows an increase in activated microglia density in response to brain injury [3]. By showing that P2X7R can control microglia proliferation during their early embryonic SC colonization, our results reveal a new physiological role of P2X7R on microglia *in vivo* that does not require pathological events leading to microglia activation. Although experiments performed in cultured microglia cell line and primary microglia have suggested that P2X7R activation promotes both microglia proliferation and activation [200, 244], our results clearly indicate that P2X7R is not involved in embryonic microglia activation. The reduction in microglia proliferation marker (Ki67) observed in P2X7R^{-/-} embryonic SC microglia was not restricted to Mac-2-positive cells, but was also observed in nonactivated cells, which lends further

support to the conclusion that *in vivo* P2X7R controls microglia proliferation, either independently of its activation, or through a different mechanism. We determined the microglia activation state using Mac-2 staining [121]. Because Mac-2 (also named galectin-3) marks a unique state of activation in microglia that correlates to phagocytosis behaviour [54, 55] and promotes phagocytosis by macrophages [245], we can ascertain that P2X7R was not required to engage embryonic microglia in a phagocytic phenotype. An increase in cytosolic calcium level is known to induce proliferation of primary microglia cultures [246] and of cultured N9 murine microglia cell line in response to P2X7R activation [244]. Accordingly, it is possible that embryonic microglia proliferation requires an increase in cytosolic calcium level provided by P2X7R activation [247]. The regional distribution of microglia within the parenchyma and their aggregation close to dying MN was not affected in P2X7R^{-/-} embryonic mice, demonstrating that P2X7R is not involved in embryonic microglia migration and attraction by dying cells. At least in the adult, microglia migration and aggregation at damaged sites are regulated by several chemokines receptors [3]. In addition, microglia localized in the MN area showed an amoeboid morphology at the onset of MN developmental cell death. This morphological change is unlikely to result from P2X7R expression by microglia as amoeboid cells were still observed in P2X7R^{-/-} embryonic mice SC. Such a morphological change of activated microglia in the embryonic SC could result from the activation of adenosine A2 receptors by adenosine as recently shown in culture and in the adult brain [99].

In conclusion, our experiments revealed that embryonic microglia activation and proliferation can be controlled independently and that embryonic microglia proliferation is mainly under the control of P2X7Rs. Our data thus reveal a new role of this receptor during the SC development by regulating embryonic microglia proliferation without the need of its interaction to Panx1 during their initial SC colonization.

4 Electrophysiological characterization of microglia in the embryonic cortex and choroid plexus

4.1 Abstract

Microglia invade the embryonic brain at early embryonic stages (chapter 2). During this invasion there is a massive increase in cortical microglial cell number from E13.5 to E15.5. With increasing age they adopt a more ramified morphology but immunohistochemically there was no difference in activation level. In the choroid plexus, at the age of E13.5 there were more activated microglial cells present when compared to E15.5. It has been shown that the expression of K^+ currents can be linked to microglial activation state, therefore we investigated the presence of IK_{IR} and IK_{DR} . In addition, it is to be expected that microglia express certain neurotransmitter receptors since these cells are present in the developing CNS at stages when neurotransmitters are already playing a role in circuit development, migration or act as a trophic factors. By performing patch-clamp recordings in tissue slices, we show here that embryonic microglia in the cortex express few to no IK_{IR} . However, when they are in close association with apoptotic cells, they are in an alerted activation state marked by an increased expression of IK_{IR} . Embryonic microglial cells also express a small stretch-activated outward current and functional P2X7 receptors. Our results suggest that embryonic microglia have a resting phenotype, although their morphology does not resemble that of resting microglial cells. Like in the adult CNS, microglia can transform into an alerted state when encountering activation signals, like apoptotic cells, in their immediate surroundings. Proliferation of microglia in the embryonic spinal cord was dependent on P2X7 receptors (chapter 3), suggesting a similar role for these receptors in cortical microglia.

4.2 Introduction

In the CNS the microglial cells belong to the non-excitabile cell types. However, studies on cell lines, primary cultures and tissue slices have found that microglia can express a variety of ion channels and neurotransmitter receptors [3, 61, 62, 84, 85, 248]. Most of the information we have has been obtained from cultured microglia. However, these cells are always in an alerted/activated state due to the isolation procedure [61]. As a consequence, they are not a true representation for resting microglia in the intact CNS. Acute brain slices have been shown to be a good model to study microglial properties and this *in situ* approach lies closest to the *in vivo* situation.

In primary cultures, microglial cells show the presence of proton currents [249]. Microglial cells of acute brain slices also express these proton channels that are activated in a time- and voltage-dependent way, influenced by the pH and inhibited by Zn^{2+} [64]. Another current identified in primary cultured and acute slice microglia is a stretch-activated Cl^- channel [74, 79] which is responsible for microglial process formation. There has been some special attention to K^+ channels and more in particular the inward and delayed outward rectifying K^+ channels. In acute slices, microglial cells displayed almost no voltage-gated currents, only a small inward rectifying K^+ current (IK_{IR}) (Fig. 1.2) [61, 62, 64]. Upon microglial activation by facial nerve axotomy the K^+ channel pattern changed. Twelve hours after the nerve transection the IK_{IR} increased in amplitude (Fig. 1.2), resembling "resting" microglia *in vitro*. This state is referred to as "alerted". After 24 hours, the microglia additionally displayed a delayed outward rectifying K^+ current (IK_{DR}), one that is similar to *in vitro* LPS-stimulated microglial cells, and represents fully activated microglial cells (Fig. 1.2). Three days after induction of the lesion the current amplitude decreased and by day 7 they had returned to the normal levels (Fig. 1.2) [61]. The same time-dependent changes of these currents were also present after induction of status epilepticus and ischemia [65, 66, 250]. These results show that the expression of certain K^+ channels is linked to the microglial activation level.

Besides ion channels, microglial cells also express receptors for neurotransmitters such as glutamate (mostly AMPA), $GABA_B$ and purinergic receptors [84, 86, 251]. Of all the neurotransmitter systems, the purinergic pathways gained the strongest attention in the last years. Microglial cells

express a variety of the ligand-activated P2X receptors and the G protein-coupled P2Y and P1 receptors. Activation of P2X results in a non-selective cationic current while activation of P2Y and P1 receptors results in modulation of ion channels. Purinergic receptor activation influences migration behavior, dynamic behavior and cytokine release [6, 62, 66, 88, 93, 96, 98, 99, 252]. However, as was the case for the voltage-gated ion channels, most of what we know today is derived from microglial cell cultures. There are some studies that used acute brain slices to study microglia electrophysiology however none have ever looked at the characteristics of embryonic microglia. Therefore we decided to investigate the presence of IK_{IR} and IK_{DR} , the swelling sensitive Cl^- current and a subset of neurotransmitter receptors in fetal microglial cells since these channels are important for microglial function.

4.3 Materials & Methods

4.3.1 Animals

Transgenic CX3CR1-eGFP knock-in mice [41] were used in order to visualize microglia in the embryonic cortex *in vivo*. In these animals, eGFP is expressed under the promoter of CX3CR1, also known as the fractalkine receptor, rendering all monocyte-derived cells, including microglia, green fluorescent [41]. All experiments were conducted in accordance with the European Community guiding principles on the care and use of animals and with the approval of the Ethical Committee on Animal Research of the Hasselt University; the French Decree no. 97/748 of October 19, 1987 and the recommendations of the Centre National de la Recherche Scientifique. The heterozygous CX3CR1-eGFP +/- embryos that were used in this study were obtained by crossing homozygous CX3CR1-eGFP +/+ mice (mice were obtained from the European Mouse Mutant Archive – EMMA with the approval of Stephen Jung [41]) with wild type C57BL/6 mice. Females were checked for vaginal plugs each morning, the day of conception was designated as embryonic day 0.5 (E0.5).

Pregnant mothers were euthanized at E13.5 and E15.5. Embryonic brains were isolated in ice-cold PBS-glucose (pH 7.4; 25mM), embedded in 3% low melting agarose (Fisher Scientific) and sliced coronally at a thickness of 300 μm .

Acute brain sections were then maintained for 30 min - 1 h before recording in an artificial cerebrospinal fluid (ACSF) containing (in mM): 126 NaCl, 25 NaHCO₃, 1 NaH₂PO₄, 4.5 KCl, 10 glucose, 2 CaCl₂, and 1 MgCl₂ (normal saline), at 32°C, continuously bubbled with a 95% O₂-5% CO₂ gas mixture.

4.3.2 Whole-cell recordings and analysis

The acute brain slice was placed in a recording chamber and continuously perfused at room temperature (20-24°C) with oxygenated ACSF. Standard whole-cell patch-clamp recordings of fluorescent microglia were made under direct visualization using an infrared-sensitive CCD video camera.

Whole-cell patch-clamp electrodes were pulled from thick-wall borosilicate glass using a pipette puller (Sutter Instrument Co., USA). The tip of the electrode was fire-polished using a microforge (Narishige, Japan). Patch-clamp electrodes had resistances of 5-7 M Ω . For our experiments, the electrode was filled with a solution containing (in mM): 130 KCl, 4 MgCl₂, 4 Na₂ATP, 10 EGTA, and 10

HEPES (pH adjusted to 7.2 with KOH, osmolarity 290 mosmol/kg-H₂O, equilibrium potential for chloride ions $E_{Cl} \approx 0$ mV).

Current fluctuations were recorded and lowpass filtered (2 kHz) using an Axopatch 1D or 200B amplifier, digitized (20 kHz) on-line using a Digidata 1322A or 1440A interface card, stored on hard disk and analyzed off-line.

The voltage-dependent currents were analyzed using a voltage step protocol and a ramp protocol. The 10 mV steps lasted 200 ms and started at -150 mV to +30 mV from a holding potential of -60 mV. The 2 s voltage ramps from -100 mV to +100 mV from a holding potential of -60 mV, an initial voltage step (100ms) to -100 mV was applied before the onset of the ramp. To control the stability of the recordings, 3 ramps were applied at 2 s intervals. The resulting evoked currents were then averaged for analysis. Outward voltage-gated currents evoked by voltage ramps slowly increased with time (run-up) after applying a membrane stretch, reaching a steady state and then decreasing (run-down) as previously described in cultures of murine microglia [75]. The steady state period lasted for 5-10 min and was obtained after approximately 5 min, being the period during which the experiments were performed. A set of three ramps (2 s time interval) was applied before, during and after drug applications. The resulting evoked currents for each voltage ramp set were then averaged for analysis. Recordings without evidence of recovery after treatment were discarded.

To eliminate inward K⁺ currents we used K⁺-free ASCF (CsCl saline) containing in mM: 126 NaCl, 25 NaHCO₃, 1 NaH₂PO₄, 4.5 CsCl, 10 glucose, 2 CaCl₂, and 1 MgCl₂. To study the dependence of the outward current on Cl⁻ we used an ASCF solution with a lower amount of Cl⁻ (low Cl⁻ out) containing in mM: 17.8 NaCl, 108.2 Methylsulfate Na⁺, 25 NaHCO₃, 1 NaH₂PO₄, 4.5 CsCl, 10 glucose, 2 CaCl₂, and 1 MgCl₂. Drugs that were applied to the ramp were: 10 mM Tetraethylammonium chloride (TEA) and 5 mM 4-Aminopyridine (4-AP), dissolved in the CsCl saline.

Neurotransmitters were applied for 15 s at a concentration of 1 mM and a holding potential of -60 mV. The transmitters tested were: serotonin, glutamate, GABA, glycine and ATP, dissolved in normal saline. To analyze concentration-response relationships, different ATP concentrations were applied. The responses evoked by different ATP concentrations were compared to the responses evoked by 1 mM ATP. Normalized concentration-response curves were fitted using the

Hill equation. For each concentration tested, the amplitude of the current was measured at the peak of the response. For the pharmacological experiments with the P2X7R antagonist, A438079 (10 μ M), all experiments were performed using the first three responses elicited by ATP after inducing the enlarged inward (biphasic) current. The first response was used as the control, the second response being the test response and the third response corresponding to the recovery of antagonist effects. Application of the antagonist started between the control and the test responses and ended between the test response and the third ATP application (recovery) (3 min interval between ATP applications). To determine antagonist efficiency, the amplitude of the test response was compared to the amplitude of the control response (100%). Current amplitude was measured at the peak of the responses. Recovery from antagonist block was evaluated by comparing the amplitude of the third response to the amplitude of the test response.

4.3.3 Statistics

Data are presented as mean \pm SEM; N expresses the number of recorded cells. Statistical significance was assessed by the appropriate statistical test, p-values smaller than 0.05 were considered significant.

4.4 Results

Microglial cells were investigated in the cortex and choroid plexus of embryonic mice, aged E13.5 and E15.5. The mean cell capacitance of E13.5 microglia was significantly lower in the cortex (10.6 ± 0.5 pF; $N = 35$) when compared with microglia in the choroid plexus (15.4 ± 1.5 pF; $N = 9$) ($p < 0.01$; Kruskal-Wallis test). The same significant difference ($p < 0.05$; Kruskal-Wallis test) was observed at E15.5 (cortex: 11.1 ± 0.7 pF ($N = 27$); choroid plexus: 16.2 ± 2 pF ($N = 11$)). The mean input resistance of microglia in the cortex (E13.5: 3.3 ± 0.4 G Ω and E15.5: 3 ± 0.4 G Ω) was not significantly different from that of those present in the choroid plexus (E13.5: 3.8 ± 0.6 G Ω and E15.5: 5 ± 0.9 G Ω).

4.4.1 The expression of K⁺ currents is linked to the microglial activation state

Our previous results (chapter 2) have indicated that between E13.5 and E15.5 there is a massive increase in the number of cortical microglial cells and the microglia transformed to a more ramified morphology; however there was no difference in activation level based on immunohistochemistry. In the choroid plexus, there was a difference in activation level based on Mac-2 staining (chapter 2, Fig. 2.4B). At the age of E13.5 there were more activated microglial cells present when compared to E15.5, which correlated with the presence of apoptotic cells. Since the expression of K⁺ currents can be linked to the activation state of microglia in the adult and juvenile CNS we investigated the presence of the IK_{IR} and IK_{DR} in cortical and choroid plexus microglia in the embryo. A voltage-step protocol ranging from -150 mV to +30 mV was applied. At hyperpolarizing potentials more negative to -80 mV an inward rectifying current could be observed at E13.5 in the choroid plexus microglia (Fig. 4.1). There were no outward rectifying currents observed at potentials more positive than -40 mV [64].

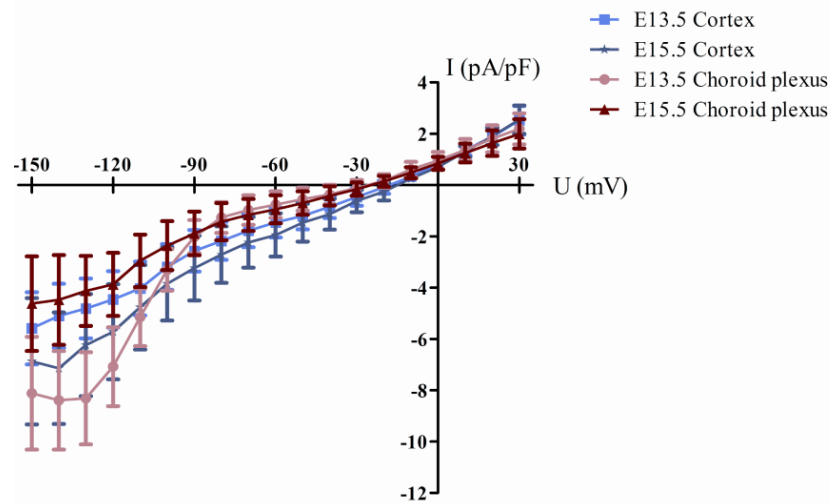


Figure 4.1. Inward and outward currents expressed by microglia in the embryonic brain. Current density of the peak amplitudes of currents elicited by 200 ms-lasting voltage pulses ranging from -150 mV to +30 mV. The holding potential was -60 mV. E13.5 cortex N = 14; E15.5 cortex N = 6; E13.5 choroid plexus N = 7; E15.5 choroid plexus N = 5.

In order to determine what part of the inward rectifier is carried by K^+ , the KCl in the extracellular solution was replaced by CsCl, since it has been shown that Cs^+ selectively inhibits the inward current [253, 254]. By subtracting the current present in presence of Cs^+ from the current recorded in the K^+ -containing extracellular solution, the inward K^+ current could be isolated. Microglial cells present in the cortex at E13.5 and E15.5 and in the choroid plexus at E15.5 displayed a small to none IK_{IR} (Fig. 4.2A). However, in the choroid plexus at E13.5 a clear IK_{IR} was present (Fig. 4.2A). At the more negative potentials (from -130 mV on) the current showed signs of inactivation, as has been described for IK_{IR} . The current density of the peak amplitude was significantly larger at -130 mV ($p < 0.05$; Mann Whitney test) in E13.5 choroid plexus microglial cells when compared to E15.5 cells (Fig. 4.2B). Similarly, the peak current density of microglia at the same age (E13.5) but in a different structure, in the choroid plexus or the cortex, is also significantly different ($p < 0.01$; Mann Whitney test). This higher current density peak amplitude at E13.5 choroid plexus microglia correlates to our previous findings on the expression of the activation marker Mac-2 (chapter 2, Fig. 2.4B).

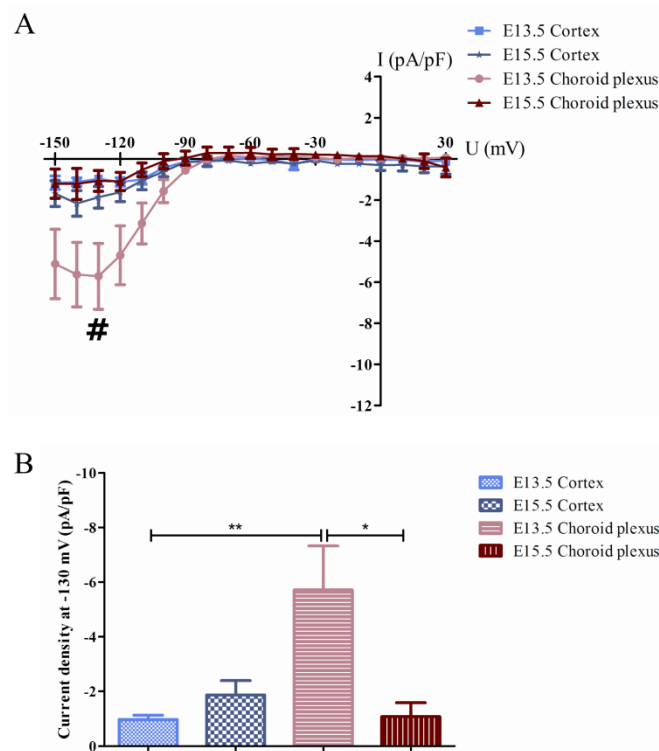


Figure 4.2. Inward rectifying K^+ currents expressed by microglia in the embryonic brain. A) Current density of the peak amplitudes of currents elicited by 200 ms-lasting voltage pulses ranging from -150 mV to +30 mV. The holding potential was -60 mV. Inward K^+ currents were identified by subtracting the currents in presence of Cs^+ from the ones recorded in presence of normal saline. In the cortex (E13.5 and E15.5) and E15.5 choroid plexus there were only very small $I_{K_{IR}}$ present. In the choroid plexus microglia at E13.5 the $I_{K_{IR}}$ was larger. **B)** The current density at -130 mV (# in part A) indicates that the peak amplitude of the inward K^+ current is significantly larger in E13.5 choroid plexus microglia. E13.5 cortex N = 14; E15.5 cortex N = 6; E13.5 choroid plexus N = 7; E15.5 choroid plexus N = 5. (* $p < 0.05$; ** $p < 0.01$).

4.4.2 Stretch-sensitive ion channels

Microglial cells in primary cultures and slice preparations have been shown to express stretch-activated Cl^- channels. Studies that investigated the effect of inhibition of these Cl^- channels indicated that they are important in microglial morphology, migration and phagocytosis [75, 79, 255-257].

Stretching of the cell membrane was induced by applying a 2 mmHg positive pressure via the patch pipette after the whole cell configuration was achieved. A 2 s voltage ramp from -100 mV to +100 mV, with an initial voltage step

(100ms) to -100 mV was applied. The holding potential was -60 mV. To control the stability of the recordings, 3 ramps were applied at 2 s intervals. After application of the stretch approximately 50 % of the microglial cells developed a run up that reached a steady state period (lasted for 5-10 min) after 5 min (Fig. 4.3A); in the cortex at E13.5 6 out of 10 microglial cells and at E15.5 10 out of 18, in the choroid plexus 3 out of 6 microglial cells at E13.5 and 5 out of 10 at E15.5. However the amplitude of the observed run up was not as big as the ones described in literature by others [75, 257]. The cells that did not show the run up only displayed a small outward current when the ramp was applied (Fig. 4.3B).

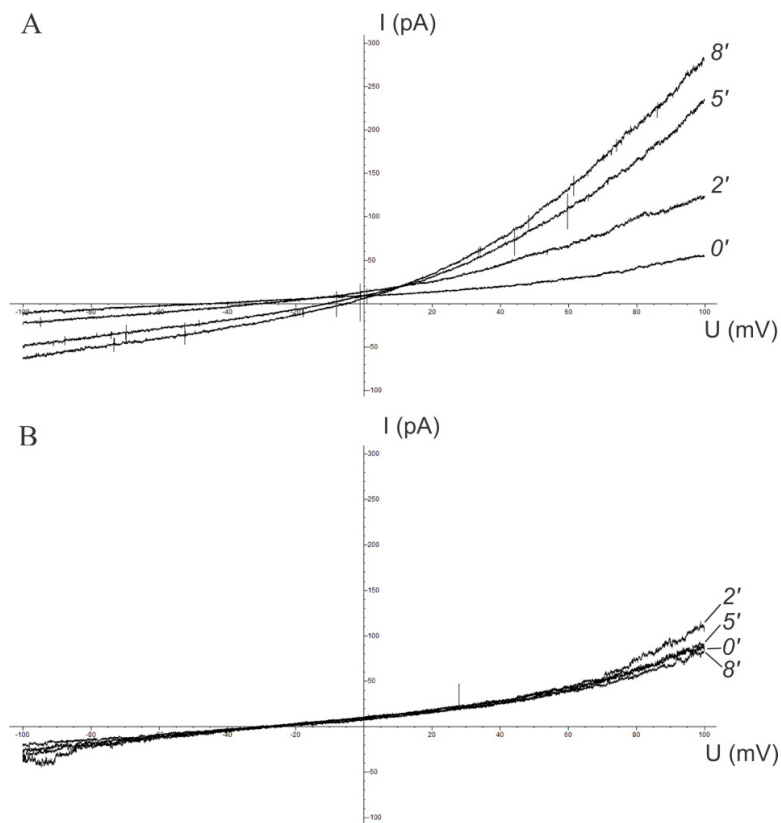


Figure 4.3. Run up development in E13.5 cortical microglia after application of 2 mmHg via the patch pipette. Example of a microglial cell that developed the run up current (A) and one that did not showed a run up (B). Two second lasting voltage ramp protocol from -100 mV to +100 mV, holding potential -60 mV.

The mean current density during development of the run up in the cortex at E13.5 and E15.5 was comparable to that of microglia in the choroid plexus (Fig. 4.4). After 5 min the steady state was reached. At E15.5 the current density of cortical microglia would even rise further 8 min after application of the pressure; however this rise was not significant when compared to the density at 5 min. Eight min after applying the membrane stretch to cortical microglial cells resulted in a mean peak current density of 13.7 ± 2.4 pA/pF ($N = 14$) and 27.5 ± 7.3 pA/pF ($N = 11$) on E13.5 and E15.5 respectively. In the choroid plexus the mean peak current density was 6.8 ± 1.5 pA/pF at E13.5 ($N = 5$) and 10.3 ± 3.8 pA/pF at E15.5 ($N = 5$) (Fig. 4.4).

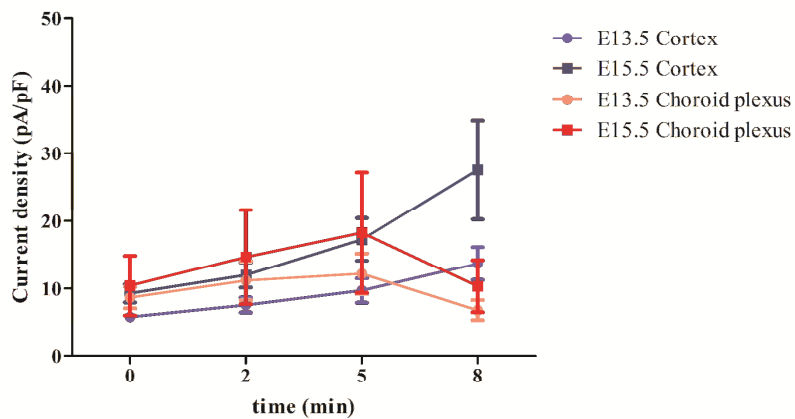


Figure 4.4. Mean peak current density at 100 mV at different time point during development of the run up. At both ages (E13.5 and E15.5) microglial cells in the cortex and choroid plexus reached their steady state maximum approximately 5 min after application of the pressure.

An extracellular solution with a low Cl^- concentration was applied to check whether the small current induced by the membrane stretch was the result of a stretch-activated Cl^- channel. In this low Cl^- solution the calculated E_{Cl} shifted to +40 mV, in contrast to the E_{Cl} of ~ 0 mV in the control saline. In the low extracellular Cl^- saline the mean peak current density decreased significantly (Fig. 4.5A). In the cortex, at E13.5 the peak was significantly decreased to $72 \pm 5\%$ ($N = 9$) of the control ($p < 0.01$; Kruskal Wallis test) (Fig. 4.5B) and at E15.5 this was $64 \pm 4\%$ ($N = 10$) ($p < 0.001$; Kruskal Wallis test). The same effect was observed when microglial cells were recorded in the choroid plexus.

At E13.5 the peak was significantly decreased to $65 \pm 8\%$ ($N = 5$) of the control ($p < 0.01$; Kruskal Wallis test) (Fig. 4.5B) and at E15.5 this was $69 \pm 3\%$ ($N = 8$) ($p < 0.01$; Kruskal Wallis test).

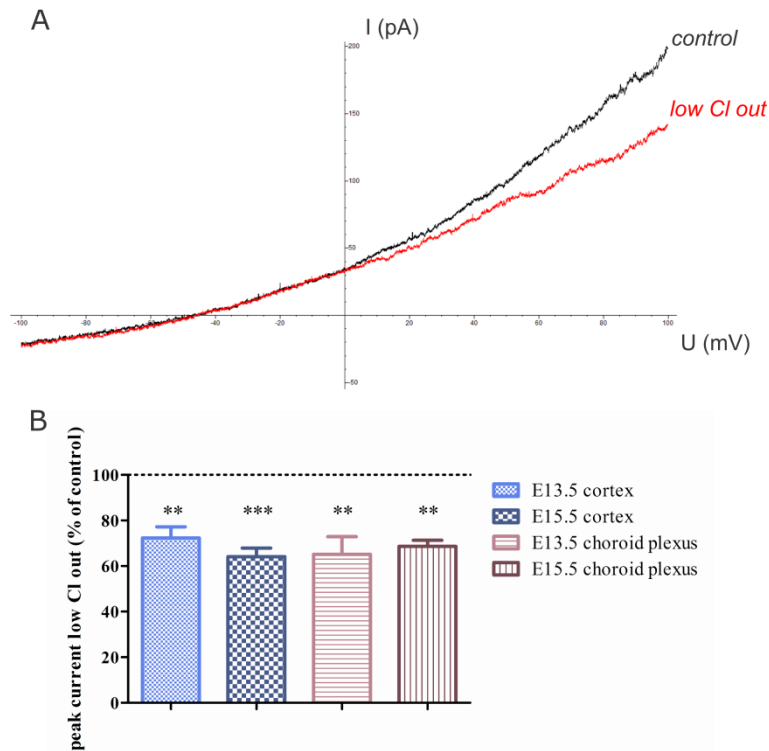


Figure 4.5. Effect of low extracellular Cl^- concentration on the outward current. A) Example of a recording of a microglia in the cortex at E13.5 in presence of low extracellular Cl^- . There was a decrease of the peak current when a low concentration of Cl^- (low Cl^- out) was applied when compared to normal Cl^- (control). 2 s ramp from -100 mV to $+100$ mV, holding potential -60 mV. **B)** A decrease in extracellular Cl^- significantly decreased the mean peak current density at 100 mV. (** $p < 0.01$; *** $p < 0.001$).

However there was no change in the reversal potential as expected. The mean reversal potential in control saline was at both ages and structures approximately -35 mV (data not shown). In the cortex, the reversal potential shifted 3 ± 1 mV at E13.5 and 7 ± 2 mV at E15.5 when the saline with low Cl^- was applied. The same small shift was observed in the choroid plexus, at E13.5 this was 10 ± 3 mV and at E15.5 7 ± 3 mV. A study by Martin in 1995 showed that human monocyte-derived macrophages contain a K^+ channel that is

sensitive to stretch. This outwardly rectifying K^+ channel could be blocked by 4-AP [258]. To eliminate the possibility that the outward current was evoked by K^+ rectifiers a combination of K^+ channel blockers, TEA and 4-AP, was applied (Fig. 4.6A). Application of the blockers only significantly decreased ($p < 0.05$; Kruskal Wallis test) the mean peak current density of the outward current in choroid plexus microglia at E13.5 to $60 \pm 10\%$ ($N = 4$) of the control (Fig. 4.6B). There was no significant decrease of the mean peak current density in microglia recorded in the cortex (E13.5: $80 \pm 9\%$ ($N = 8$); E15.5: $75 \pm 11\%$ ($N = 9$)) or at E15.5 in the choroid plexus ($91 \pm 13\%$ ($N = 6$)).

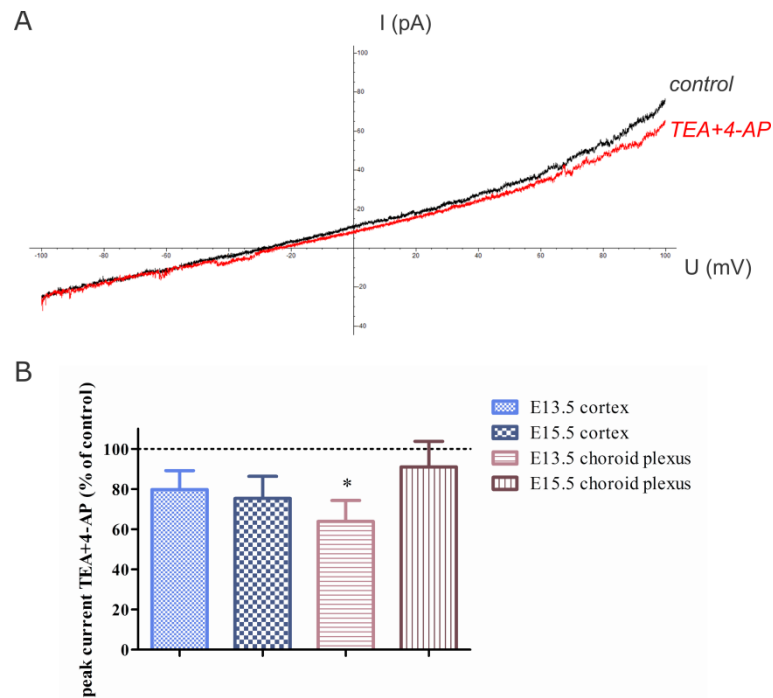


Figure 4.6. Effect of TEA and 4-AP on the outward current. A) Example of a recording of a microglia in the cortex at E13.5 in presence of 10 mM TEA and 5 mM 4-AP. There was no significant decrease of the peak current when TEA and 4-AP (TEA+4-AP) was applied when compared to normal saline (control). 2 s ramp from -100 mV to +100 mV, holding potential -60 mV. **B)** Application of TEA and 4-AP only significantly decreased the mean peak current density of the outward current (at 100 mV) in microglia of the E13.5 choroid plexus. (* $p < 0.05$).

4.4.3 Embryonic microglia express few ligand-gated ion channels

Neurotransmitters are already produced and secreted during embryonic development of the CNS. Their secretion is dependent on the surrounding microenvironment. In general, their levels increase with increasing synapse formation. Serotonergic cells are among the first to be produced in the mouse CNS [259]. Amino acid transmitters like glutamate, GABA and glycine are present in high levels in the embryonic murine CNS. During development their effects will differ as receptor expression and composition can change because of CNS plasticity [259, 260]. Besides neuron signaling, neurotransmitters are also important in the development of the circuit and cytoarchitecture of the CNS and can act as trophic factors [261-264]. As experiments on adult or juvenile microglia have shown that these cells possess several neurotransmitter receptors [6, 62, 84, 86, 251] we checked for the presence of ligand-gated ion channels on the microglial cells in the cortex of E13.5 and E15.5 embryos. Application of 1 mM of serotonin, glutamate, GABA or glycine did not evoke a current in E13.5 microglia (Fig. 4.7 left) nor in E15.5 microglia (Fig. 4.7 right).

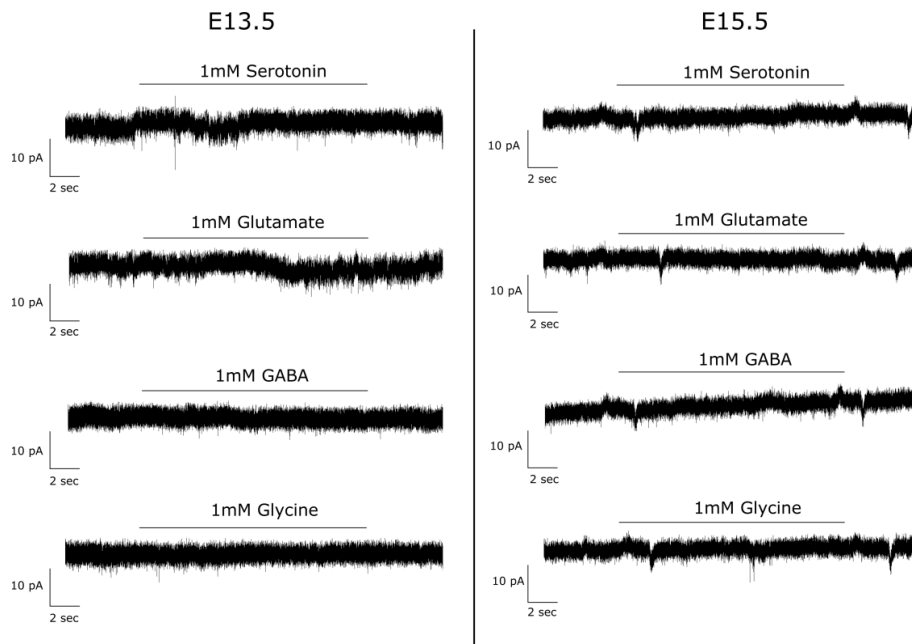


Figure 4.7. Embryonic microglia expression of ligand-gated ion channels. Application of 1 mM serotonin, glutamate, GABA or glycine did not evoke any ligand-gated ion current in embryonic microglia in the E13.5 (left) and E15.5 (right) cortex. Holding potential -60 mV.

Microglia have been shown to express several types of purinergic receptors of the P1 and P2 family. Their expression depends on the functional state of the microglial cell [66, 88, 93, 98]. In the P2 group, the P2X receptors are ligand-gated ion channels; seven subunits are known and the different P2X receptors can be distinguished by their sensitivity to ATP and specific agonists/antagonists [87].

Different ATP concentrations were applied to microglial cells in the E13.5 and E15.5 cortex. On both ages tested, at a concentration of 100 μ M and 300 μ M ATP there were no currents elicited. A very small inward current was observed when 1 mM ATP was applied, being -0.5 ± 0.2 pA/pF (N = 13) at E13.5 and -0.5 ± 0.1 pA/pF (N = 5) at E15.5. Upon the first application of 3 mM ATP a large, biphasic inward current was induced (Fig. 4.8A). This biphasic response was not observed again in the same cell at later applications of 3 mM. The second application of 3 mM of ATP induced a mean current density of -9.2 ± 2.2 pA/pF (N = 7) at E13.5 and -26.2 ± 4.5 pA/pF (N = 9) at E15.5. The evoked responses were normalized to the responses evoked by 1 mM ATP, fitting of these normalized currents yielded an EC₅₀ value larger than 1 mM.

The biphasic response upon a first application of 3 mM ATP was also observed in microglia of the embryonic spinal cord (chapter 3, Fig. 3.3A). This biphasic response and the high concentration of ATP suggest that the ATP-induced current in cortical microglia was the result of P2X7 receptor activation [87]. Application of the P2X7 specific blocker, A438079 (10 μ M), significantly reduced ($p < 0.01$; Friedman test) the ATP current to $3.8 \pm 0.7\%$ of the control (N = 5) in microglia of the E15.5 cortex (Fig. 4.8B).

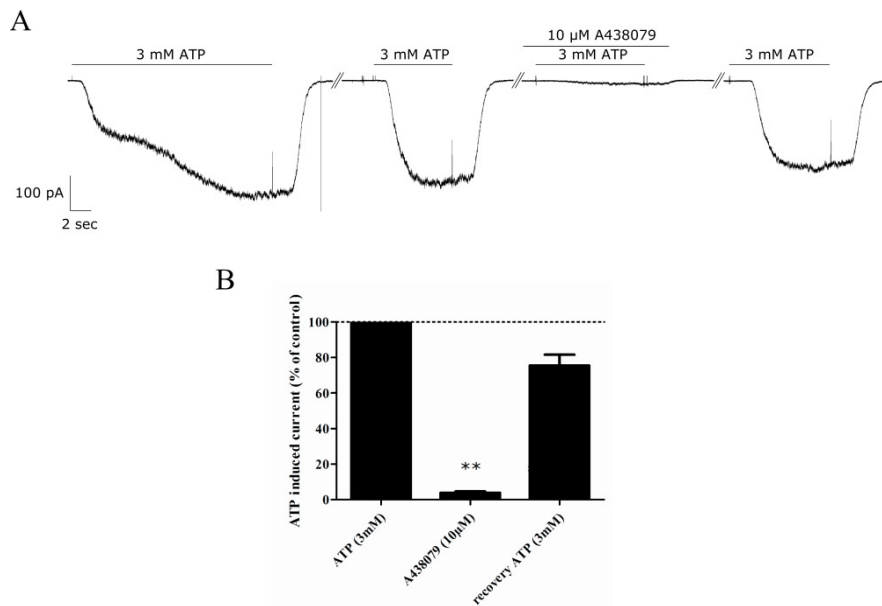


Figure 4.8. ATP (3 mM) induced a biphasic current in cortical microglia. A) Example of the biphasic current induced by 3 mM ATP in microglia of the E15.5 cortex. The P2X7 blocker A438079 (10 μM) nearly blocked the current completely **(B)**. Holding potential -60 mV. (** $p < 0.01$).

4.5 Discussion

In this chapter we show that embryonic microglia in the cortex express few inward rectifying K^+ channels, a stretch-sensitive current that is partially carried by Cl^- and P2X receptors, probably P2X7. Microglia located in the choroid plexus at E13.5 show a larger inward rectifying K^+ current than those at E15.5. At both ages they express a stretch-sensitive current.

4.5.1. The expression of IK_{IR} correlates with microglial activation level

The expression of K^+ currents can be linked to the activation state of microglia in the adult and juvenile CNS [61, 64, 66]. Previous results (chapter 2) have indicated that from E13.5 to E15.5 there is a massive increase in the number of cortical microglial cells and that microglia transformed to a more ramified morphology. However, immunohistochemical staining for activation markers (Mac-2 and MHC class II) showed no difference in activation level. In the choroid plexus, a difference in activation level based on Mac-2 staining was observed (chapter 2, Fig. 2.4B). At the age of E13.5 there were more activated microglial cells present in the choroid plexus when compared to E15.5. To see whether the activation stage of cortical and choroid plexus microglia in the embryo correlates with the presence of certain K^+ channels we investigated the presence of the IK_{IR} and IK_{DR} by means of patch clamp recordings in the first part of this chapter. In the cortex the microglia express very few IK_{IR} . This correlates with the absence of immunoreactivity for Mac-2 and MHC class II and suggests that these cells have a "resting" phenotype. In the choroid plexus, E13.5 microglia had a larger IK_{IR} , resembling microglia that are in an alerted activation state. This correlates with the presence of microglial Mac-2 immunoreactivity in the choroid plexus at that age which is related to the occurrence of cell death in this structure. At E15.5, the accumulation of apoptotic cells and Mac-2 immunoreactivity had diminished and in accordance the IK_{IR} had decreased back to the level of resting microglia. All together our results suggest that microglia in the embryonic cortex have a rather "resting" phenotype. In an environment without developmental cell death, they express few K^+ channels. The presence of apoptotic cells transforms the embryonic microglia into an alerted activation state. Thus, like in adult and postnatal microglia, the expression of K^+ channels is linked to the microglial activation state.

4.5.2 Microglia in the embryonic brain express a small stretch-sensitive current

Application of pressure to the cell via the patch pipette resulted in the development of a stretch-sensitive current with a small amplitude, which increased somewhat over the next 5 minutes. Several studies have described the presence of a stretch-sensitive Cl^- current in microglial cells. Eder et al. have shown on primary microglia cultures that this Cl^- channel is necessary for the induction of microglial ramification [75]. A role for swelling-activated Cl^- channels in regulation of volume and morphology was also shown by Ducharme et al. [255]. Since our previous results (chapter 2) showed that microglia are very motile and that at E13.5 and E15.5 50% or more of the microglia had a morphology with one or more protrusions; it is possible that this swelling-activated current we observed is also implicated in protrusion formation and motility in these embryonic microglia. In our recordings, decreasing the extracellular Cl^- concentration significantly decreased the mean peak current density. However, the reversal potential did not change accordingly. Unlike the published studies, that all used an external solution containing HEPES, our external solution was buffered by HCO_3^- . A paper of Nilius et al. describes a volume-regulated anion channel that is permeable for bicarbonate [265]. So it is possible that the swelling-sensitive current recorded in microglial cells of the embryonic brain allows passage of other anions that are present in the extracellular solution. In order to characterize the current, the effect of specific Cl^- channels blockers, like DIDS and flufenamic acid [75, 255], should be tested. Also the effect of a HEPES-buffered extracellular solution on the current should be investigated.

4.5.3 Besides P2X receptors, embryonic microglia express few ligand-gated receptors

Recordings on microglia in primary cultures suggested that these cells express some ligand-gated ion channels. Application of 4 neurotransmitters, known to be present during embryonic development of the mouse brain, did not induce any current, suggesting that microglia in the embryonic cortex do not express functional ligand-gated ion channels for these transmitters. This however does not exclude the presence of functional metabotropic receptors.

Microglia in the developing CNS express some ionotropic purinoceptors, like P2X1, P2X4 and P2X7 [88]. Application of ATP did not induce a current at concentrations smaller than 1 mM. At a concentration of 3 mM the first ATP application induced a biphasic response and the ATP-evoked current could almost completely be blocked by a P2X7 antagonist. These results are similar to the one observed in the embryonic spinal cord (chapter 3). Our results strongly indicate that the P2X7 receptor is functionally expressed by microglia in the embryonic cortex. There was no evidence for the expression of P2X1 and P2X4 receptors. However we cannot completely rule out the possibility that functional P2X1 receptors are expressed since their fast desensitization kinetics makes their detection difficult [87, 233]. Studies suggest that microglial cells also express metabotropic purinoceptors [66, 93, 98]. Future experiments making use of qPCR combined with patch-clamp recordings should further elucidate their purinoceptor expression profile.

5 Maternal immune activation and neuropsychiatric disorders - a role for microglia? - A preliminary study

This chapter is based on:

Maternal immune activation and neuropsychiatric disorders - a role for microglia?

[Nina Swinnen](#), Sophie Smolders, Bert Brône, Pascal Legendre and Jean-Michel Rigo.

In preparation

5.1 Abstract

Several studies have indicated that inflammation during pregnancy increases the risk for the development of neuropsychiatric disorders in the offspring. Morphological brain abnormalities and deviations in immunity can be observed in patients of both autism and schizophrenia. It was suggested that the acute infection can induce changes in maternal cytokine levels which in turn can affect the fetal brain and result in the development of both neuropsychiatric disorders in the offspring. In this study the poly (I:C) model was used to mimic viral immune activation in pregnant mice in order to assess the involvement of fetal microglia in these developmental disorders. This model has been validated and used in behavioral and other studies as a model for neuropsychiatric disorders such as schizophrenia and autism.

Microglial cell density and activation level in the fetal cortex and hippocampus were determined. Despite the presence of a systemic inflammation in the pregnant mice, there was no significant difference in fetal microglial activation between the control and inflammation group.

5.2 Introduction

Maternal immune activation during pregnancy is considered a risk factor for schizophrenia and autism in the offspring [144]. In the study of the mechanisms behind this association several animal models were developed in which pregnant rodents were infected with the influenza virus, polyinosinic:polycytidylic acid (poly (I:C)) or lipopolysaccharide (LPS) [266]. These models confirmed that prenatal infection led to behavioral and neuropathological changes in the offspring after the maternal immune activation (MIA) [153, 154, 157, 159, 267, 268]. The cytokine interleukin-6 (IL-6) has been proven to be critical in the development of these deficits and changes observed in the MIA offspring [156, 269]. In addition, it has been shown that the cytokine response evoked in the mother after poly (I:C) challenge can, in some part, be transferred to the fetal environment [154, 170].

Microglial cells are known to colonize the embryonic brain early in development (embryonic day (E) 11.5) [107, 121, 270]. They are the immune cells of the CNS and are the first line of response when there is a disturbance of the brain homeostasis. An imbalance in cytokine levels caused by MIA might be able to activate them and trigger a cascade that leads eventually to the changes that are observed in the offspring of the treated pregnant mice. This hypothesis is supported by several observations. Some studies found indications of an active neuroinflammatory process, with microglial cell activation, in the brain of autistic patients [148, 163]. Others have observed changes in microglial activation in the brain of schizophrenic patients [164, 165]. Recent studies also indicated that there is an augmented microglial density in different brain regions of adult MIA offspring (poly (I:C) model) [166, 167]. Finally, treatment with anti-inflammatory cytokines has been shown to prevent the development of the characteristic behavior in the offspring after maternal poly (I:C) injection [170]. These results all indicate that MIA has an effect on the microglia in the offspring. More recently, the effect of LPS-induced MIA was shown to shift embryonic microglia in a classical cytotoxic activation state and to enhance phagocytosis of neural precursors by microglia [127]. Yet it remains unclear whether poly (I:C) exerts an effect on the microglial cells of the offspring during fetal development. In our study, MIA was induced at two different gestational days, E11.5 and E15.5. Our previous results (see chapter 2) have shown that at those stages the

microglial cell density peaks in the embryonic cortex and are thus important time points in microglial development. We wanted to determine if MIA can activate embryonic microglial cells and thus determine whether they are involved in triggering the development of psychiatric disorders by the activation of the maternal immune system by a viral mimic.

We show that poly (I:C)-induced MIA has no effect on microglial density and on the expression of activation markers during embryonic development. Results of slice cultures indicate that fetal microglia can get activated by LPS but not by IL-6 and poly (I:C).

5.3 Materials & Methods

5.3.1 Animals

All experiments were conducted in accordance with the European Community guiding principles on the care and use of animals and with the approval of the Ethical Committee on Animal Research of the Hasselt University. Mice were maintained in the animal facility of the Hasselt University in accordance with the guidelines of the Belgian Law and the European Council Directive. To visualize microglia in the embryonic cortex the transgenic CX3CR1-eGFP knock-in mice [41] were used. In these animals, eGFP is expressed under the promoter of CX3CR1, known as the fractalkine receptor, resulting in green fluorescent microglial cells [41]. The heterozygous CX3CR1-eGFP +/- embryos used in this study were obtained by crossing wild type C57BL/6 females with homozygous CX3CR1-eGFP +/+ male mice (obtained from the European Mouse Mutant Archive – EMMA with the approval of Stephen Jung [41]). Females were checked for vaginal plugs each morning, the day of conception was designated as embryonic day 0.5 (E0.5).

5.3.2 Maternal immune activation and IL-6 determination

At day E11.5 or E15.5 mice received i.p. a single dose of poly (I:C) (20mg/kg) (Sigma-Aldrich, Bornem, Belgium) or vehicle (saline). Five hours after injection maternal blood was collected, the maternal serum was aliquoted and stored at -80°C until the IL-6 ELISA assays were performed [153, 156]. To determine the IL-6 levels in embryonic brains after injection, embryos were isolated five hours after poly (I:C) or saline injection. Embryonic brains were isolated and homogenized. The supernatants was aliquoted and stored at -80°C until the IL-6 ELISA assays were performed. IL-6 concentrations in maternal serum and embryonic brain samples were determined using the Mouse IL-6 ELISA Kit from Thermo Scientific (Rockford, Illinois, USA), following the manufacturer's instructions. The analysis was conducted using a FLUOstar OPTIMA plate reader (BMG Labtech, Ortenberg, Germany).

5.3.3 Immunohistochemistry

Pregnant mice were sacrificed by means of cervical dislocation at the desired embryonic day and the embryos were removed. The heads of E11.5, E12.5 and

E15.5 embryos were fixed in 4% paraformaldehyde for 3h at 4°C, 5h for E17.5 embryos. After fixation, the embryonic heads were cryoprotected overnight in PBS + 30% sucrose, frozen in optimal cutting temperature compound (Tissue-Tek) and stored at -80°C until sectioned. Ten-micrometer-thick coronal tissue sections were cut on a Leica CM1900 uv cryostat, mounted on Superfrost Plus glasses and stored at -20°C until staining.

To check whether embryonic microglia could be activated, 300- μ m thick coronal brain slices (E15.5) were cultured for 24 hours in control medium, with 10 ng/ml IL-6 (Invitrogen, PMC0065), 50 μ g/ml poly (I:C) or 1 μ g/ml LPS (Calbiochem, cat#437625, lot # D00120458). Afterwards slices were fixed for 1h in 4% paraformaldehyde and overnight cryoprotected in PBS + 30% sucrose, frozen in optimal cutting temperature compound (Tissue-Tek) and stored at -80°C until sectioned into 20- μ m thick coronal coupes.

To determine if the CX3CR1-eGFP cells observed were effectively microglial cells we used an antibody directed against ionized calcium binding adaptor molecule 1 (Iba-1), a marker for microglial cells. In order to determine the activation state of the microglia, we used an antibody against Mac-2, inducible nitric oxide synthase (iNOS) and IL-1 β . An antibody against the toll-like receptor (TLR) 3 was used to check for the presence of the respective receptor in the embryonic CNS and microglial cells. All primary antibodies and working solutions are listed in Table 5.1.

Table 5.1. Overview of the primary antibodies.

Primary Antibody	Company	Reference	Dilution
Anti-Iba-1	WAKO	019-19741	1:500
Anti-Mac-2	American Type Culture Collection	TIB-166	1:250
Ant-iNOS	Abcam	ab15323	1:250
Anti-IL-1 β	Abcam	Ab9722	1:100
Anti-TLR3	AbD Serotec	AHP1019G	1:200

Quantitative analysis of microglial cells was performed on images of 10 or 20- μ m-thick coronal embryonic brain sections (Fig. 5.1). Images were taken with a Nikon Eclipse 80i microscope and a Nikon digital sight camera DS-2MBWc (10x Nikon plan objective (numerical aperture (NA) of 0.25) and a 20x Plan Fluor objective (NA of 0.5)).

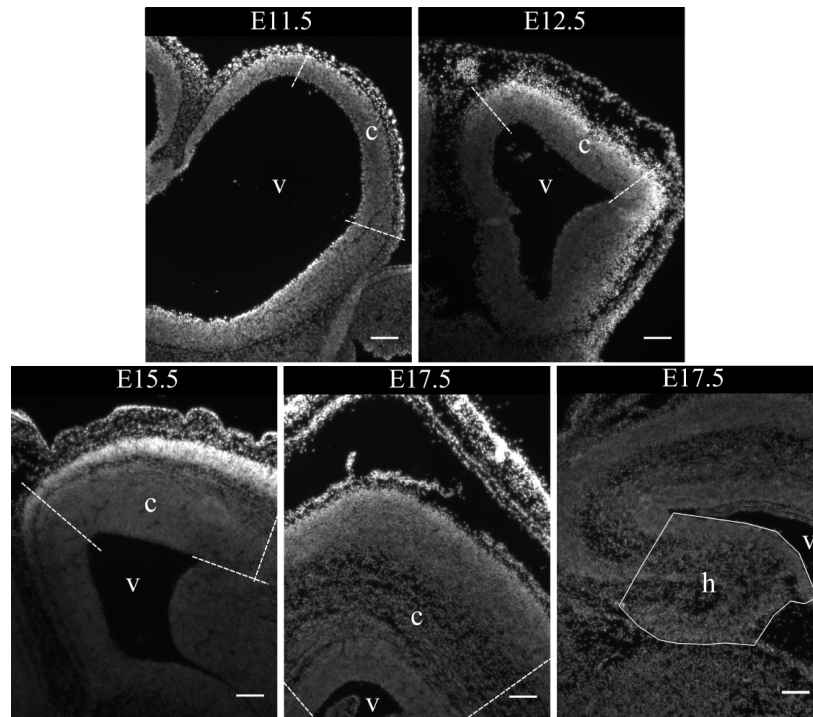


Figure 5.1. Indication of the analyzed areas in the embryonic cortex and hippocampus. Coronal sections of the embryonic ages that were analyzed. The DAPI channel is shown in grey. The dotted lines mark out the investigated cortical areas. c; cortex; h, hippocampal area; v, ventricle. Scale bar = 100 μ m.

5.3.4 Statistics

Images (1600 x 1200) were analyzed with ImageJ 1.45e software (NIH, USA; <http://rsb.info.nih.gov/ij/>). Only eGFP-positive cell bodies were taken into account for the measurements. Quantifications were made per cortical slice. (number of slices = n). All values are expressed as mean \pm S.E.M. Statistical significance was assessed by Mann Whitney test, Kruskal Wallis test or two-way-anova with post test, p-values smaller than 0.05 were considered significant.

5.4 Results

Studies showed that IL-6 plays an important role in the development of MIA-induced deficits and changes observed in the offspring [156]. Therefore, 5 hours after injection of either saline or poly (I:C), the IL-6 level in the maternal serum samples was determined in order to estimate the induced immune response in the pregnant mouse. There was a significant increase in the level of IL-6 in the sera of female mice belonging to the poly (I:C) group on both gestation days (E11.5: 2361 ± 479 pg/ml and E15.5: 1023 ± 190 pg/ml) when compared to their respective controls (E11.5: 17 ± 3 pg/ml and E15.5: 33 ± 15 pg/ml) (Fig. 5.2).

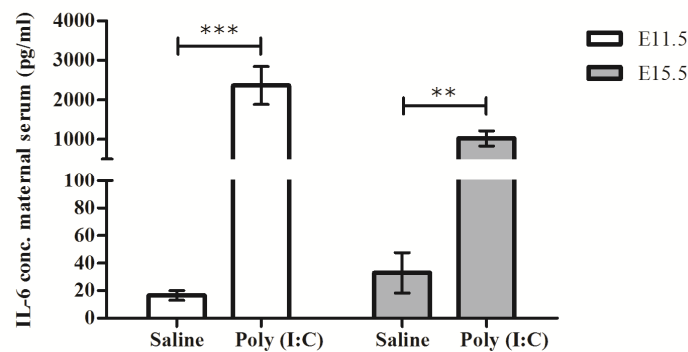


Figure 5.2. IL-6 concentration in the maternal serum 5 hours after injection at E11.5 and E15.5 with saline or poly (I:C). Values are mean \pm SEM of the IL-6 concentration (pg/ml), Mann Whitney test was used for statistical analysis. Number of dams in the control and inflammation group respectively at E11.5 = 20/16 and at E15.5 = 6/6. (** $p < 0.01$; *** $p < 0.001$).

It has been demonstrated that the evoked cytokine response after poly (I:C) challenge can, in some part, be transferred from the maternal to the fetal environment [154, 170]. The IL-6 concentration in the embryonic brains was determined. We observed a trend to an increase in the IL-6 concentration when comparing the poly (I:C) group (E11.5: 241 ± 94 % and E15.5: 160 ± 47 pg/ml) with the control (set at 100%) (Fig. 5.3), similar as Patterson et al. [271].

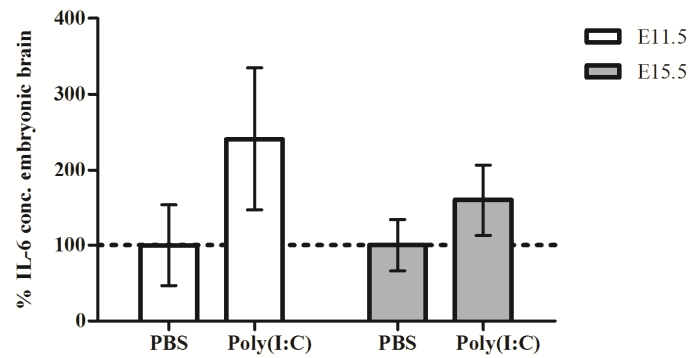


Figure 5.3. IL-6 concentration in the embryonic brain 5 hours after injection at E11.5 and E15.5 with saline or poly (I:C). Values are mean \pm SEM of the percentage of the IL-6 concentration. The average IL-6 level obtained per offspring in the poly (I:C) group are expressed as the percentage of deviation from the mean levels of the saline group of the corresponding gestation day. Mann Whitney test was used for statistical analysis. Number of experiments in the control and inflammation group respectively at E11.5 = 5/9 and at E15.5 = 7/6.

Microglial activation has been observed in the brain of autistic [148, 163] and schizophrenic patients [164, 165]. Recent studies also indicated that there is an augmented microglial density in different brain regions of adult MIA offspring (poly (I:C) model) [166, 167]. Quantification of the fetal microglial cell density in the cortex (at E11.5, E12.5, E15.5 and E17.5) and hippocampal area (at E17.5) after treatment of the pregnant mice showed no significant differences (Table 5.2).

Table 5.2. Microglial cell density in the cortex and hippocampal area of embryos derived from the control group and the group that was subjected to maternal inflammation at E11.5 and E15.5.

Injection at E11.5				
Brain structure	<i>Cortex</i>			<i>Hippocampus</i>
Embryonic age	<i>E11.5</i>	<i>E12.5</i>	<i>E17.5</i>	<i>E17.5</i>
Saline	48.3 ± 8.2	39.9 ± 3.2	85.9 ± 6.5	156.5 ± 6.1
Poly (I:C)	38.5 ± 5.9	43.1 ± 2.5	86.8 ± 4.8	170.1 ± 5.9
P value	0.23	0.32	0.78	0.09
Injection at E15.5				
Brain structure	<i>Cortex</i>		<i>Hippocampus</i>	
Embryonic age	<i>E15.5</i>	<i>E17.5</i>	<i>E17.5</i>	
Saline	106.1 ± 7.7	85.1 ± 10.5	152.2 ± 4.4	
Poly (I:C)	104.6 ± 4.9	92.4 ± 9.4	132.7 ± 7.2	
P value	0.84	0.79	0.13	

Values are mean ± SEM of the number of microglial cells per mm², Mann Whitney test was used for statistical analysis. When injected at E11.5 numbers of embryonic brains in the saline and poly (I:C) group were respectively: E11.5 = 7/6; E12.5 = 10/9; E17.5 cortex = 6/9; E17.5 hippocampus = 7/8. When injected at E15.5 numbers of embryonic brains in the saline and poly (I:C) group were respectively: E15.5 = 5/5; E17.5 cortex = 5/6; E17.5 hippocampus = 5/6.

To determine if MIA induced a change in microglial activation level, we performed an immunostaining for Mac-2/Galectin-3, iNOS and IL-1 β . Increased expression of Mac-2/Galectin-3 is related to the phagocytic phenotype in immune cells [50-52]. iNOS is upregulated after microglial cells get activated, leading to increased nitric oxide production, which is harmful for neurons [59, 272]. The pro-inflammatory cytokine IL-1 β is produced by activated microglia and involved in causing cell death [53, 59]. There was no significant expression of the markers in the control group (Mac-2 < 5%, iNOS < 10% and IL-1 β < 5% of the microglial cells were positive). Induction of MIA did not result in an increase of the percentage of microglia expressing these markers after treatment on both gestation days (Mac-2 < 5%, iNOS < 10% and IL-1 β 10% of the microglial cells were positive) (data not shown).

The absence of expression of specific activation markers raised the question whether fetal microglia can be activated. Acute embryonic brain slices (E15.5) were treated with IL-6, poly (I:C) or LPS and again stained for Mac-2/Galectin-3, iNOS and IL-1 β (see Fig. 5.4 for an example of the staining). Since the

experiments of Cunningham [127] and Smith [156] have shown that these substances can affect microglial cells.

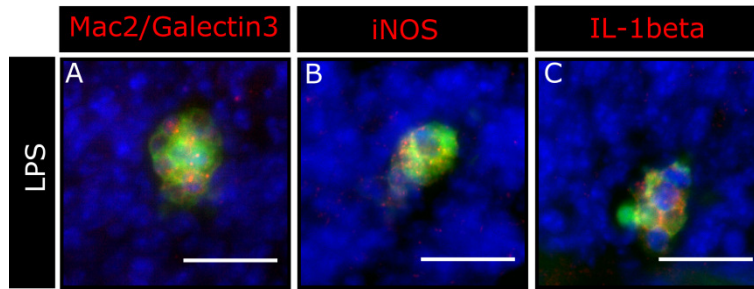


Figure 5.4. Examples of the activation marker stainings on the acute slices treated with LPS. **A)** Microglia (green) positive for Mac-2/Galectin-3 (red), **B)** positive for iNOS (red) and **C)** for IL-1 β (red). Examples of the different immunostainings were taken from slices treated for 24 hours with 1 μ g/ml LPS. Scale bar = 20 μ m.

There was no significant difference in the percentage of microglia being immunoreactive for Mac-2/Galectin-3 between the four different groups (Fig. 5.5). There was a significant difference in the percentage of microglial positive for iNOS ($p < 0.05$; Kruskal-Wallis test). The slices treated with LPS had a significant higher percentage of microglia expressing iNOS when compared to the control ($p < 0.05$; Kruskal-Wallis test) (Fig. 5.5). There was a significant difference in the percentage of microglial positive for IL-1 β ($p < 0.05$; Kruskal-Wallis test) (Fig. 5.5).

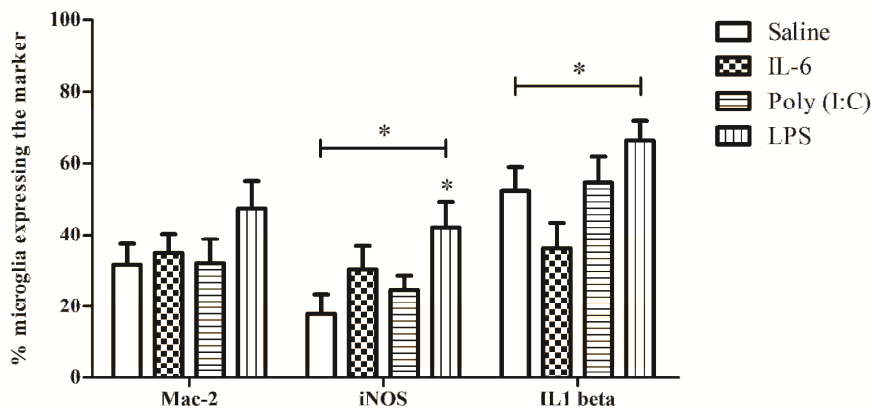


Figure 5.5 (Previous page). Microglial activation in acute brain slices. Quantification of the expression of three activation markers (Mac-2, iNOS and IL-1 β) by microglia in E15.5 brain slices cultured with IL-6 10 ng/ml, poly (I:C) 50 μ g/ml or LPS 1 μ g/ml. Kruskal Wallis test was used for statistical analysis. Number of coupes for Mac-2/iNOS/IL-1 β in: saline group = 23/23/27; IL-6 group = 22/19/16; poly (I:C) group = 18/25/19; LPS group = 21/21/22.

5.5 Discussion

Several studies have indicated that maternal inflammation during pregnancy induces behavioral and neurological changes in the offspring that indicate the development of a neuropsychiatric disorder like autism or schizophrenia. Recently, a few papers have shown that in adult offspring subjected to poly (I:C)-induced MIA the microglial cells are altered, leading to an increased microglial cell number and a reduced arborization [166, 268, 273]. However they did not check the embryonic microglia. Our results showed that induction of MIA at E11.5 or E15.5 did not increase the microglial cell density. Suggesting that the maternal inflammation did not influence the embryonic microglial migration or proliferation processes. Nor did we find a difference in microglial activation level in the embryonic cortex and hippocampal area, suggesting that MIA did not lead to activation of the embryonic microglia.

A recent study of early postnatal (P) effects of poly (I:C) induced MIA showed that the detected microglial changes were only observed at P30 and not earlier (P10) [273]. Together with our results this suggests that embryonic microglia are not immediately activated when MIA occurs. MIA induced not only a cytokine response in the maternal unit but also alters several cytokine levels in the placenta and the fetus [271]. This complicates elucidating the site where the cytokines act upon to potentially alter brain development since cytokines can act directly on neural progenitors and neurons [274, 275]. For example, IL-6 and LIF can influence the differentiation of neural progenitor cells [137]. These data, in combination with the lack of microglial activation in our MIA study suggests that the acute maternal inflammation affects other systems/cell types during embryonic stages. These MIA-induced early abnormalities might result in an altered CNS environment in the offspring that in turn affects the microglial cells at later developmental stages. This hypothesis is supported by the observations made in recent studies. Manitz et al., have shown that poly (I:C)-induced MIA changes in microglial density were only observed at P30 and not at P10 [273]. Garay et al. on the other hand found no effect on microglial cell density [160]. The changes observed in several neurotransmitter systems after poly (I:C)-induced MIA became only apparent in the adult and not earlier in the prepubertal period. A study of Richetto et al. found that GABAergic gene expression, like GABA receptor subunits and vesicular transporters, is altered in

the adult prefrontal cortex after MIA. [276]. Holloway et al. found changes in the serotonin and glutamate signaling in the adult frontal cortex after poly (I:C) injection into pregnant mice [277]. Both groups reported that these changes were not present at pre-pubertal ages.

A study of Cunningham et al. showed that two LPS injections resulted in microglial activation in the rat embryo, presented as an increased percentage of microglia expressing iNOS and IL-1 β [127]. Our results on the brain slices indicate that LPS can indeed activate embryonic microglia however poly (I:C) and IL-6 failed to do the same. In addition, experiments with LPS injections on the same age as we have injected poly (I:C) could be useful to determine if there is a different outcome depending on the infectious trigger. In our experiments we only checked the expression level of 3 activation markers, in the future it will be interesting to determine the expression level of a larger group of cytokines and factors that are formed when microglia get activated. Additionally, the expression of IK_{IR} and IK_{DR} can be determined after MIA induction, since their expression is also an indication of the activation level. This will give a more complete view about the effects of poly (I:C)-induced MIA on the fetus and will allow making a distinction between different microglial activation states (inflammatory versus anti-inflammatory) that could occur in the fetal brain.

6 Summary and general discussion

Microglial cells are the resident macrophages of the adult CNS. They are responsible for the protection of the nervous system, they maintain the tissue homeostasis and are able to modulate different processes like neurogenesis and angiogenesis [18, 20, 138]. Recent studies have identified yolk sac myeloid progenitors as the source of microglial cells [107]. Microglial (progenitor) cells invade the CNS early in embryonic development, at a moment that just precedes the beginning of neurogenesis in the cortex of mouse embryos [174, 175, 177]. Their early presence suggests that they play a role in CNS development. Several studies have shown that microglia can already influence the development and differentiation of several cell types in the immature CNS [19, 22, 23, 25].

In this thesis, we aimed at characterizing the invasion pattern and phenotype of microglia in the embryonic brain. We focused on the developing cortex and choroid plexus to study the microglial characteristics by means of the expression of different immunohistochemical markers (Mac-2, Ki-67) and patch-clamp recordings (K^+ channels, ATP-induced currents). Additionally, we investigated the microglial involvement in the developing cortex and hippocampal area in a poly (I:C)-induced maternal immune activation model for neurodevelopmental disorders. To these ends, we used a mouse model in which eGFP is expressed under the promoter of the fractalkine receptor, rendering microglia (progenitors) green fluorescent. The inflammation model used (i.p. single dose of poly (I:C) (20mg/kg)) is a well established model to induce maternal immune activation (MIA) and results in well documented neurodevelopmental deficits and behavioral changes in the offspring [153, 156, 271, 278, 279].

This chapter discusses the most important results and findings of this thesis. A schematic overview of the data is represented in Fig. 6.1.

Characteristics of microglial cells in the embryonic brain

In the embryonic spinal cord, the first microglial invasion wave occurs as early as E11.5. Microglial cells begin to invade the parenchyma at the end of neuronal migration during which local neuronal networks become functional, some microglial cells interact with dying motoneurons at the onset of their developmental cell death [121]. Accordingly, embryonic microglia could have an active role during the development of the spinal cord neuronal networks.

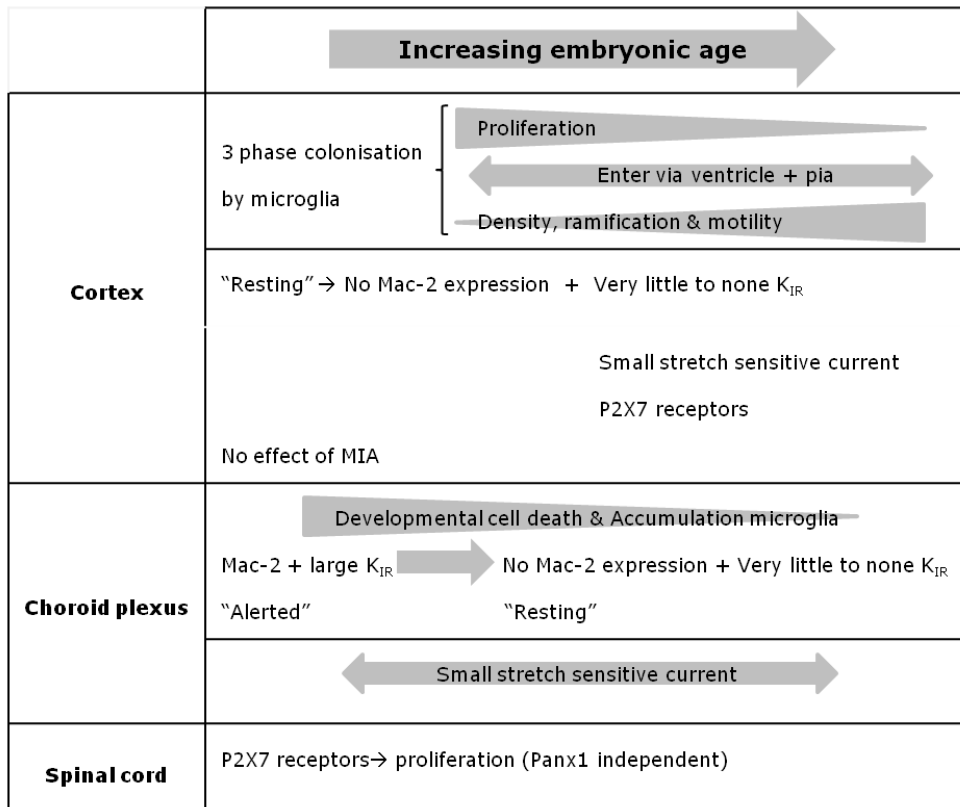


Figure 6.1. Schematic representation of the microglial characteristics in the developing CNS.

Microglia invade the developing cortex and spinal cord at similar ages in mouse embryos [107, 121]. However the cortical development occurs at later stages than that of the spinal cord. It is unclear if the embryonic microglia, although of similar origin, have similar functions in both embryonic structures according to their developmental stages. This remained an open question, as the invasion pattern of the cortex by embryonic microglia with respect to the developmental stages of this structure was poorly documented and information about their characteristics is scarce. Consequently, we investigated the colonization processes of the embryonic cortex by microglia *in vivo* and *ex vivo*, with respect to the well-known developmental pattern of the embryonic brain. Our results show that the colonization of the cortex by microglial cell occurs in three phases; the microglial cell number increases slowly in the first one (E10.5 tot E14.5), massively in the second phase (E14.5 to E15.5) and again slowly in the last

phase (E15.5 to E17.5). Based on our results, proliferation only plays an important role in the first invasion phase. Invasion of the cortical parenchyma by microglia from peripheral sources occurs via the pial membrane and the ventricles. With increasing embryonic age the morphology transformed from a predominant amoeboid form to a ramified one, but this did not imply that the cells were static. We observed that, like in the adult CNS, the embryonic microglia are highly motile. Sending out and retracting processes during their migration (**chapter 2**). The activation state of a microglial cell can be linked to the expression of certain immunological markers [50, 52] and K^+ rectifier channels [61, 62, 66]. In the cortex, the microglia did not express Mac-2 (**chapter 2**), iNOS or IL-1 β (**chapter 5**) and had little to none IK_{IR} (**chapter 4**), suggesting they have a "resting" phenotype.

We also characterized the microglia in the developing choroid plexus. In this structure major morphological changes take place during development. We observed an accumulation of amoeboid microglia positive for Mac-2, which coincided with the occurrence of developmental cell death in this structure (**chapter 2**). The morphological/immunological phenotype correlated with the expression of a clear IK_{IR} , but no IK_{DR} (**chapter 4**). Together, these results suggest that these microglia are in an "alerted" activation level. This is most probably induced by the presence of dead cells in order to clear them from the tissue. Experiments on embryos lacking microglia, such as PU.1 KO animals, should give us a better understanding whether the microglia are responsible for induction of the developmental cell death that is present in the developing choroid plexus. Results of other groups indicate that in other regions of the developing CNS microglia are important to induce apoptosis via the production of superoxide and TNF α [32, 49, 132].

Our results demonstrate that even though embryonic microglia originate from the same source, being the yolk sac, their behavior and properties differ depending on the CNS structure they invade. This suggests that their developmental functions are not pre-programmed but depend on the cues they receive from their micro-environment.

Embryonic microglial cells express P2X receptors

Previous results of the collaborating laboratory in Paris on the embryonic spinal cord have shown that microglial cells begin to invade the parenchyma at E11.5. The colonization process of the spinal cord by microglia involves proliferation and invasion from the periphery. Some microglial cells interact with dying motoneurons at the onset of their developmental cell death (E13.5), a time at which they reach an activated state, proliferate and phagocytose dying motoneurons [121]. In **chapter 3** we investigated the molecular mechanisms underlying microglia proliferation during spinal cord invasion in the embryo since this remained largely unknown. In the adult, *in vitro* studies have shown that a number of factors can evoke both microglia activation and proliferation [3]. Examples of these factors are agonists for the purinergic receptors, such as the P2X7 receptor [200]. Embryonic microglia can express P2X1, P2X4 and P2X7 receptors [88]. However their functions remain unknown at these developmental stages. In the adult, P2X7 is involved, in addition to microglia activation and proliferation, in a variety of important effector functions of microglia [3, 201-204]. Our qPCR results indicate that spinal cord microglia express P2X4, P2X7, Panx-1 and P2X1 transcripts. Based on the pharmacological profile of the ATP-induced current, we showed that this current was induced via P2X7 receptors. Application of ATP induced a biphasic response; this pore dilatation gets in literature often attributed to the functional coupling of P2X7 to Panx1 [206]. However our results on Panx1 knock-out mice suggest this biphasic response reflects an integral pore dilatation of the P2X7 receptor. When using P2X7 receptor knock-out mice, we observed a reduction in microglial proliferation but no effect on microglial activation or migration. Indicating that the P2X7 receptor is only important in controlling the proliferation of embryonic spinal cord microglia. We performed some similar experiments on cortical microglia (**chapter 4**). Again, ATP induced a biphasic response which could almost completely be blocked by a P2X7 receptor specific antagonist.

In the future, more experiments on the cortical microglia are necessary in order to determine whether the P2X7 receptor plays the same role in these cells as in the spinal cord and whether the effect of P2X7 receptor activation is also Panx1 independent. However, in the spinal cord at the time the experiments were

performed approximately 25% of the microglia were proliferating. At the ages we have performed our patch-clamp experiments 28% (E13.5) and 10% (E15.5) of the microglia were positive for Ki-67, so there could be a role for the P2X7 receptor in microglia proliferation at E13.5. Remarkably, ATP induced a larger current at E15.5 than at E13.5. The P2X7 receptor is known to promote microglial activation besides proliferation [200]. Since less microglial cells are proliferating at later stages (E15.5) in embryonic development it could be possible that, in the cortex, this receptor is involved at activation. The P2X7 receptor requires high amounts of ATP ($> 100 \mu\text{M}$) to be activated, which could be released in the local CNS environment upon leakage from injured or dead cells. However, at the ages we performed our experiments (E12.5 to E17.5) we did not observe many apoptotic cells in the developing cortex. Suggesting the microglial cells are slowly upregulating their expression level of P2X7 to the point when neuronal loss occurs, which peaks at P5-P7 in the rodent neocortex [280, 281], in order to get quickly activated when they sense locally a high concentration of ATP.

In addition, the presence of ATP induced currents should be measured on choroid plexus microglia. Especially at the time point when developmental cell death occurs in this structure. P2X7 KO embryos could reveal if the P2X7 receptor is involved in the activation of the microglial cells at that moment of development.

Further experiments on the embryonic microglia are necessary in order to determine their expression profile of different types of P1 and P2 receptors. Purinergic receptors are important for motility and migration. In the adult brain, multiple purinoceptors are being expressed on resting microglia, like P2X4, P2Y12, A1 and A3, which are thought to be important in regulating their dynamic motility. Upon activation, the P1 and P2 receptor expression profile will change which will result in morphological changes and migration [66, 92, 98]. The P2Y12 and A3 receptors are important for process extension towards the injury. Upregulation of A_{2A} and P2X4 receptors leads to process retraction and migration [98]. Our results have indicated that embryonic microglial cells are very dynamic. A better understanding of their purinoceptor expression will help elucidating the mechanisms behind their dynamics and how they populate the developing nervous system. It is plausible to hypothesize that during

development the expression of purinoceptor subtypes will change as they finish migrating, take up their final position and transform into a more ramified morphology.

Embryonic microglia in an inflammation model of neuropsychiatric diseases

Maternal inflammation during pregnancy is considered as a risk factor for the development of neuropsychiatric disorders, like autism and schizophrenia, in the offspring [144, 146, 147]. We decided to use the poly (I:C) model as inflammation model in our experiments (**chapter 5**) since this is an established model [156, 166, 278, 279]. As resident immune cells of the brain it seems logical that the embryonic microglia would be affected by MIA, however, their involvement in the etiology of neuropsychiatric disorders has never been studied. Therefore, we induced MIA on two different embryonic days (E11.5 or E15.5) since previous results (chapter 2) have shown that at those stages the microglial cell density peaks in the embryonic cortex. The MIA had no effect on microglial cell density, suggesting that maternal inflammation did not influence the embryonic microglial migration or proliferation process. We did not find a difference in the expression of Mac-2, iNOS or IL-1 β , three activation markers, suggesting that MIA did not affect the activation level of the embryonic microglial cells. Direct stimulation of embryonic brain slices with IL-6 (reported to be an important factor in the MIA induced changes), poly (I:C) and LPS showed that embryonic microglia could be activated by LPS, however there was no effect of the first two stimuli. It will be of use to check the expression of other cytokines and factors that can be produced by microglia as well as the channels responsible for the IK_{IR} and IK_{DR} , to allow a quick comparison between our control and inflammation model. This will allow getting a more detailed view on the phenotype of embryonic microglia and how they can be affected by maternal immune activation.

A study of Manitz et al. showed that poly (I:C) treatment during pregnancy led to an increased microglial cell number at P30, however at an earlier stage (P10) no effect was observed and at a later age (P100) this difference could no longer be observed [273]. This suggests that the effect of MIA on the microglial cells of

the offspring is probably a secondary effect. Maternal inflammation might exert an initial effect on the neural precursor development which could result in a changed environment. As we have shown in chapter 2 that the micro-environment has an effect on microglial activation/behavior, which could in turn then influence the microglia at later stages.

The study of Cunningham et al., that used two injections of LPS to induce maternal inflammation, found an increased percentage of microglial cells expressing iNOS and IL1 β but they saw no effect on the morphology of the microglial cells. In our study we used a single injection of poly (I:C). It is possible that the first injection only leads to a "primed" microglial state. In the case of Cunningham et al. the microglia could become fully activated after the second inflammatory challenge, which is absent in our study. There is evidence that microglia are able to become primed by a prior pathology or genetic predisposition which results in a more vigorously response to a subsequent inflammatory stimulation. In some neurodegenerative disease models (for example Alzheimer's, Parkinson's and prion disease) in rodents leads injection of LPS or poly (I:C) to a more severe pathology. The hallmark of the primed microglial cell is acute induction of IL-1 β [282], one of the cytokines that was increased after the LPS injections in the study of Cunningham [127].

A recent study by Giovanoli et al., investigated the effect of the combined exposure to a prenatal immune challenge (poly (I:C) at E9) and peripubertal stress (from P30 to 40), two known developmental stressors, in mice [268]. The combination of the prenatal and peripubertal exposure resulted in the development of sensorimotor gating deficiencies and led to increased dopamine levels in the adult hippocampus. At peripubertal age, the combination of both stressors resulted in altered neuroimmune responses, presented as increased microglial cell number and elevated levels of IL-1 β and TNF α in the hippocampus and prefrontal cortex. These latter changes were transient, as they were not longer present in the adult [268]. Another group recently investigated the interaction between maternal inflammation and susceptible genotypes for schizophrenia in mice. They found that low doses of poly (I:C) worsened the deficits in pre-pulse inhibition and latent inhibition in 16 week old mice with mutations in the schizophrenia susceptibility gene but had no effect in wild-type animals. Also the IL-6 levels were more increased in the fetal brains of the

susceptible genotype group when compared to the control. This indicates that genetic and environmental factors can interact to worsen the schizophrenia-related behavior [283].

These results suggest that prenatal insults or genetics could act as “primer” which increases the vulnerability of the offspring to subsequent pre/postnatal environmental challenges. This could in part explain why not all children that are born after the mother suffered from influenza infection during pregnancy develop a neuropsychiatric disease.

It would be fruitful for us to perform experiments with LPS injection on the same age as we have injected poly (I:C) in order to determine if the outcome depends on the infectious prenatal trigger that was used and to check whether a repeated poly (I:C) challenge does activate the embryonic microglial cells.

In conclusion, our results demonstrate that even though embryonic microglia originate from the same source, being the yolk sac, their behavior and properties differ depending on the CNS structure they invade. This suggests that their developmental functions depend on the cues they receive from their micro-environment. The expression of the same functional P2X receptor type suggests that to some extent there is a pre-programming or “standard microglia model” present that is conserved throughout the CNS but can be further elaborated or optimized depending on their micro-environment.

7 Nederlandse samenvatting

Microglia zijn de residente immuuncellen van het centraal zenuwstelsel (CZS). In het adulte CZS zijn ze belangrijk voor de bescherming tegen pathogenen en schade, de weefselhomeostase en kunnen ze verschillende processen, zoals neurogenese, beïnvloeden. Microglia kunnen reeds vroeg in de embryonale ontwikkeling gedetecteerd worden. Verschillende onderzoeksgroepen hebben aangetoond dat ze dan al een belangrijke rol spelen. In dit onderzoeksproject werd het invasiepatroon en de fenotypische karakteristieken van microglia in de embryonale hersenen onderzocht aangezien de informatie hieromtrent beperkt is. Onze resultaten tonen aan dat microglia in de embryonale cortex een "rustend" fenotype hebben; ze brengen weinig activatiemerkers tot expressie (**hoofdstuk 2**) en hebben zo goed als geen inwaarts rectificerende K^+ kanalen (**hoofdstuk 4**). Toch zijn ze net als in de adulte hersenen erg dynamisch. Tijdens de ontwikkeling van de plexus choroideus treedt er geprogrammeerde celdood op. Gedurende deze periode accumuleren geactiveerde microglia in deze structuur, waarschijnlijk om de dode cellen te fagocyteren (**hoofdstuk 2**). Proliferatie van microglia in het embryonale ruggenmerg is afhankelijk van P2X7 receptoren (**hoofdstuk 3**). Dezelfde receptoren vonden we terug op microglia van de cortex (**hoofdstuk 4**). Bijkomende experimenten zijn nodig om te bepalen of deze receptoren ook in de cortex belangrijk zijn voor microgliale proliferatie.

Uit de literatuur is gebleken dat infecties en immuunactivatie tijdens de zwangerschap een verhoogd risico geven op de ontwikkeling van neuropsychiatrische aandoeningen, zoals autisme en schizofrenie, bij de nakomelingen. Aangezien microglia de immuuncellen van het CZS zijn en deze reeds tijdens embryonale ontwikkeling aanwezig zijn hebben wij onderzocht of ze geactiveerd worden na immuunactivatie tijdens de zwangerschap. Hiervoor hebben we gebruik gemaakt van een gevalideerd model waarbij poly (I:C) geïnjecteerd wordt in zwangere muizen. Onze resultaten geven aan dat, ondanks het optreden van een systemische inflammatie in de moedermuis, er geen verhoogde microgliale densiteit of activatie aanwezig is in de hersenen van de embryo's (**hoofdstuk 5**). Dit was echter een preliminaire studie en meer activatiemerkers moeten worden onderzocht om een conclusie te trekken omtrent wat het effect is van inflammatie tijdens de zwangerschap op de embryo's.

8 Résumé français

Les cellules microgliales sont les cellules immunitaires résidentes du système nerveux central (SNC). Dans le SNC adulte, elles sont importantes pour la protection contre les agents pathogènes et les lésions, l'homéostasie tissulaire et elles peuvent affecter différents processus, comme la neurogenèse.

Les cellules microgliales peuvent déjà être détectées au début du développement embryonnaire du SNC. Plusieurs groupes de recherche ont montré qu'elles jouent déjà un rôle important dans le développement normal. Dans ce projet de recherche nous avons étudié l'invasion et les caractéristiques phénotypiques des cellules microgliales du cerveau embryonnaire. Nos résultats démontrent que les microglies dans le cortex embryonnaire ont un phénotype de « repos »; elles expriment peu de marqueurs d'activation (**chapitre 2**) et n'ont presque aucun canaux K^+ à rectification entrante (**chapitre 4**). Pourtant, elles sont très dynamiques comme dans le cerveau adulte. Au cours du développement du plexus choroïde, des microglies activées au phénotype phagocytaire s'accumulent à un moment coïncidant avec un pic d'apoptose dans cette structure (**chapitre 2**). La prolifération des microglies dans la moelle épinière embryonnaire dépend de récepteurs P2X7 (**chapitre 3**). Nous avons retrouvé les mêmes récepteurs sur les cellules microgliales du cortex (**chapitre 4**). D'autres expériences sont nécessaires pour déterminer si ces récepteurs jouent également un rôle dans la prolifération des microglies corticales. Diverses études ont démontré que les infections et l'activation immunitaire pendant la grossesse donnent un risque accru de développement de maladies neuropsychiatriques, comme l'autisme et la schizophrénie, chez les enfants. Puisque les microglies sont les cellules immunitaires du SNC et qu'elles sont présentes au cours du développement embryonnaire, nous avons examiné si elles sont activées après une réaction immunitaire maternelle pendant la grossesse. Pour cela, nous avons utilisé un modèle validé où du poly (I: C) est injecté dans les souris gestantes. Nos résultats indiquent que, malgré la présence d'une inflammation systémique maternelle, il n'y a aucune augmentation de densité ou d'activation des cellules microgliales dans le cerveau embryonnaire après induction d'une réaction immunitaire maternelle (**chapitre 5**).

Reference list

1. Del Rio-Hortega, P., *El tercer elemento de los centros nerviosos I La microglia en estado normal II Intervención de la microglia en los procesos patológicos III Naturaleza probable de la microglia*. Bol Soc Esp Biol, 1919. **9**: p. 69-120.
2. Del Rio-Hortega, P., *Microglia*, in *Cytology and Cellular Pathology of the Nervous System*, P. W., Editor. 1932, Paul B. Hoeber: New York. p. 481-534.
3. Kettenmann, H., et al., *Physiology of microglia*. Physiol Rev, 2011. **91**(2): p. 461-553.
4. Rezaie, P. and D. Male, *Mesoglia & microglia--a historical review of the concept of mononuclear phagocytes within the central nervous system*. J Hist Neurosci, 2002. **11**(4): p. 325-74.
5. Nimmerjahn, A., F. Kirchhoff, and F. Helmchen, *Resting microglial cells are highly dynamic surveillants of brain parenchyma in vivo*. Science, 2005. **308**(5726): p. 1314-8.
6. Davalos, D., et al., *ATP mediates rapid microglial response to local brain injury in vivo*. Nat Neurosci, 2005. **8**(6): p. 752-8.
7. Lawson, L.J., et al., *Heterogeneity in the distribution and morphology of microglia in the normal adult mouse brain*. Neuroscience, 1990. **39**(1): p. 151-70.
8. de Haas, A.H., H.W. Boddeke, and K. Biber, *Region-specific expression of immunoregulatory proteins on microglia in the healthy CNS*. Glia, 2008. **56**(8): p. 888-94.
9. Elkabes, S., E.M. DiCicco-Bloom, and I.B. Black, *Brain microglia/macrophages express neurotrophins that selectively regulate microglial proliferation and function*. J Neurosci, 1996. **16**(8): p. 2508-21.
10. Ren, L., et al., *Differential expression of inflammatory mediators in rat microglia cultured from different brain regions*. Brain Res Mol Brain Res, 1999. **65**(2): p. 198-205.
11. Wirenfeldt, M., et al., *Reactive microgliosis engages distinct responses by microglial subpopulations after minor central nervous system injury*. J Neurosci Res, 2005. **82**(4): p. 507-14.
12. Stence, N., M. Waite, and M.E. Dailey, *Dynamics of microglial activation: a confocal time-lapse analysis in hippocampal slices*. Glia, 2001. **33**(3): p. 256-66.
13. Kurpius, D., et al., *Early activation, motility, and homing of neonatal microglia to injured neurons does not require protein synthesis*. Glia, 2006. **54**(1): p. 58-70.
14. Hanisch, U.K., *Microglia as a source and target of cytokines*. Glia, 2002. **40**(2): p. 140-55.
15. Block, M.L., L. Zecca, and J.S. Hong, *Microglia-mediated neurotoxicity: uncovering the molecular mechanisms*. Nat Rev Neurosci, 2007. **8**(1): p. 57-69.
16. Hanisch, U.K. and H. Kettenmann, *Microglia: active sensor and versatile effector cells in the normal and pathologic brain*. Nat Neurosci, 2007. **10**(11): p. 1387-94.
17. Frade, J.M. and Y.A. Barde, *Microglia-derived nerve growth factor causes cell death in the developing retina*. Neuron, 1998. **20**(1): p. 35-41.

18. Bessis, A., et al., *Microglial control of neuronal death and synaptic properties*. *Glia*, 2007. **55**(3): p. 233-8.
19. Walton, N.M., et al., *Microglia instruct subventricular zone neurogenesis*. *Glia*, 2006. **54**(8): p. 815-25.
20. Ekdahl, C.T., Z. Kokaia, and O. Lindvall, *Brain inflammation and adult neurogenesis: the dual role of microglia*. *Neuroscience*, 2009. **158**(3): p. 1021-9.
21. Roumier, A., et al., *Impaired synaptic function in the microglial KARAP/DAP12-deficient mouse*. *J Neurosci*, 2004. **24**(50): p. 11421-8.
22. Mazzoni, I.E. and R.L. Kenigsberg, *Microglia from the developing rat medial septal area can affect cholinergic and GABAergic neuronal differentiation in vitro*. *Neuroscience*, 1997. **76**(1): p. 147-57.
23. Jonakait, G.M., et al., *Macrophage cell-conditioned medium promotes cholinergic differentiation of undifferentiated progenitors and synergizes with nerve growth factor action in the developing basal forebrain*. *Exp Neurol*, 2000. **161**(1): p. 285-96.
24. Nicholas, R.S., M.G. Wing, and A. Compston, *Nonactivated microglia promote oligodendrocyte precursor survival and maturation through the transcription factor NF-kappa B*. *Eur J Neurosci*, 2001. **13**(5): p. 959-67.
25. Antony, J.M., et al., *Endogenous microglia regulate development of embryonic cortical precursor cells*. *J Neurosci Res*, 2011.
26. Sierra, A., et al., *Microglia shape adult hippocampal neurogenesis through apoptosis-coupled phagocytosis*. *Cell Stem Cell*, 2010. **7**(4): p. 483-95.
27. Gautier, E.L., et al., *Gene-expression profiles and transcriptional regulatory pathways that underlie the identity and diversity of mouse tissue macrophages*. *Nat Immunol*. **13**(11): p. 1118-28.
28. Boya, J., et al., *A lectin histochemistry study on the development of rat microglial cells*. *J Anat*, 1991. **175**: p. 229-36.
29. Chamak, B., A. Dobbertin, and M. Mallat, *Immunohistochemical detection of thrombospondin in microglia in the developing rat brain*. *Neuroscience*, 1995. **69**(1): p. 177-87.
30. Ignacio, A.R., et al., *Distribution of microglial cells in the cerebral hemispheres of embryonic and neonatal chicks*. *Braz J Med Biol Res*, 2005. **38**(11): p. 1615-21.
31. Rezaie, P., K. Patel, and D.K. Male, *Microglia in the human fetal spinal cord--patterns of distribution, morphology and phenotype*. *Brain Res Dev Brain Res*, 1999. **115**(1): p. 71-81.
32. Marin-Teva, J.L., et al., *Microglia promote the death of developing Purkinje cells*. *Neuron*, 2004. **41**(4): p. 535-47.
33. Biber, K., et al., *Functional expression of CXCR3 in cultured mouse and human astrocytes and microglia*. *Neuroscience*, 2002. **112**(3): p. 487-97.
34. Austyn, J.M. and S. Gordon, *F4/80, a monoclonal antibody directed specifically against the mouse macrophage*. *Eur J Immunol*, 1981. **11**(10): p. 805-15.
35. Hirsch, S., J.M. Austyn, and S. Gordon, *Expression of the macrophage-specific antigen F4/80 during differentiation of mouse bone marrow cells in culture*. *J Exp Med*, 1981. **154**(3): p. 713-25.

36. Hume, D.A., V.H. Perry, and S. Gordon, *Immunohistochemical localization of a macrophage-specific antigen in developing mouse retina: phagocytosis of dying neurons and differentiation of microglial cells to form a regular array in the plexiform layers*. J Cell Biol, 1983. **97**(1): p. 253-7.
37. Ito, D., et al., *Microglia-specific localisation of a novel calcium binding protein, Iba1*. Brain Res Mol Brain Res, 1998. **57**(1): p. 1-9.
38. Hirasawa, T., et al., *Visualization of microglia in living tissues using Iba1-EGFP transgenic mice*. J Neurosci Res, 2005. **81**(3): p. 357-62.
39. Kanazawa, H., et al., *Macrophage/microglia-specific protein Iba1 enhances membrane ruffling and Rac activation via phospholipase C-gamma -dependent pathway*. J Biol Chem, 2002. **277**(22): p. 20026-32.
40. Ahmed, Z., et al., *Actin-binding proteins coronin-1a and IBA-1 are effective microglial markers for immunohistochemistry*. J Histochem Cytochem, 2007. **55**(7): p. 687-700.
41. Jung, S., et al., *Analysis of fractalkine receptor CX3CR1 function by targeted deletion and green fluorescent protein reporter gene insertion*. Mol Cell Biol, 2000. **20**(11): p. 4106-14.
42. Harrison, J.K., et al., *Role for neuronally derived fractalkine in mediating interactions between neurons and CX3CR1-expressing microglia*. Proc Natl Acad Sci U S A, 1998. **95**(18): p. 10896-901.
43. Cardona, A.E., et al., *Control of microglial neurotoxicity by the fractalkine receptor*. Nat Neurosci, 2006. **9**(7): p. 917-24.
44. Biber, K., et al., *Neuronal 'On' and 'Off' signals control microglia*. Trends Neurosci, 2007. **30**(11): p. 596-602.
45. Rabinowitz, S.S. and S. Gordon, *Macrosialin, a macrophage-restricted membrane sialoprotein differentially glycosylated in response to inflammatory stimuli*. J Exp Med, 1991. **174**(4): p. 827-36.
46. Santos, A.M., et al., *Embryonic and postnatal development of microglial cells in the mouse retina*. J Comp Neurol, 2008. **506**(2): p. 224-39.
47. Esiri, M.M. and J.O. McGee, *Monoclonal antibody to macrophages (EMB/11) labels macrophages and microglial cells in human brain*. J Clin Pathol, 1986. **39**(6): p. 615-21.
48. Rana, I., et al., *Microglia activation in the hypothalamic PVN following myocardial infarction*. Brain Res, 2010. **1326**: p. 96-104.
49. Wakselman, S., et al., *Developmental neuronal death in hippocampus requires the microglial CD11b integrin and DAP12 immunoreceptor*. J Neurosci, 2008. **28**(32): p. 8138-43.
50. Reichert, F. and S. Rotshenker, *Galectin-3/MAC-2 in experimental allergic encephalomyelitis*. Exp Neurol, 1999. **160**(2): p. 508-14.
51. Walther, M., et al., *Galectin-3 is upregulated in microglial cells in response to ischemic brain lesions, but not to facial nerve axotomy*. J Neurosci Res, 2000. **61**(4): p. 430-5.
52. Venkatesan, C., et al., *Chronic upregulation of activated microglia immunoreactive for galectin-3/Mac-2 and nerve growth factor following diffuse axonal injury*. J Neuroinflammation, 2010. **7**: p. 32.
53. Lalancette-Hebert, M., et al., *Selective ablation of proliferating microglial cells exacerbates ischemic injury in the brain*. J Neurosci, 2007. **27**(10): p. 2596-605.

54. Dunic, J., S. Dabelic, and M. Fogel, *Galectin-3: an open-ended story*. *Biochim Biophys Acta*, 2006. **1760**(4): p. 616-35.
55. Rotshenker, S., *The role of Galectin-3/MAC-2 in the activation of the innate-immune function of phagocytosis in microglia in injury and disease*. *J Mol Neurosci*, 2009. **39**(1-2): p. 99-103.
56. Perry, V.H., *A revised view of the central nervous system microenvironment and major histocompatibility complex class II antigen presentation*. *J Neuroimmunol*, 1998. **90**(2): p. 113-21.
57. Neumann, H., *Control of glial immune function by neurons*. *Glia*, 2001. **36**(2): p. 191-9.
58. Krady, J.K., et al., *Ciliary neurotrophic factor and interleukin-6 differentially activate microglia*. *J Neurosci Res*, 2008. **86**(7): p. 1538-47.
59. Kaur, C., et al., *Microglia-derived proinflammatory cytokines tumor necrosis factor-alpha and interleukin-1beta induce Purkinje neuronal apoptosis via their receptors in hypoxic neonatal rat brain*. *Brain Struct Funct*, 2012.
60. Steelman, A.J. and J. Li, *Poly(I:C) promotes TNFalpha/TNFR1-dependent oligodendrocyte death in mixed glial cultures*. *J Neuroinflammation*. **8**: p. 89.
61. Boucsein, C., H. Kettenmann, and C. Nolte, *Electrophysiological properties of microglial cells in normal and pathologic rat brain slices*. *Eur J Neurosci*, 2000. **12**(6): p. 2049-58.
62. Boucsein, C., et al., *Purinergic receptors on microglial cells: functional expression in acute brain slices and modulation of microglial activation in vitro*. *Eur J Neurosci*, 2003. **17**(11): p. 2267-76.
63. Brockhaus, J., et al., *Membrane properties of amoeboid microglial cells in the corpus callosum slice from early postnatal mice*. *J Neurosci*, 1993. **13**(10): p. 4412-21.
64. Schilling, T. and C. Eder, *Ion channel expression in resting and activated microglia of hippocampal slices from juvenile mice*. *Brain Res*, 2007. **1186**: p. 21-8.
65. Lyons, S.A., et al., *Distinct physiologic properties of microglia and blood-borne cells in rat brain slices after permanent middle cerebral artery occlusion*. *J Cereb Blood Flow Metab*, 2000. **20**(11): p. 1537-49.
66. Avignone, E., et al., *Status epilepticus induces a particular microglial activation state characterized by enhanced purinergic signaling*. *J Neurosci*, 2008. **28**(37): p. 9133-44.
67. Franchini, L., G. Levi, and S. Visentin, *Inwardly rectifying K⁺ channels influence Ca²⁺ entry due to nucleotide receptor activation in microglia*. *Cell Calcium*, 2004. **35**(5): p. 449-59.
68. Kotecha, S.A. and L.C. Schlichter, *A Kv1.5 to Kv1.3 switch in endogenous hippocampal microglia and a role in proliferation*. *J Neurosci*, 1999. **19**(24): p. 10680-93.
69. Khanna, R., et al., *K⁺ channels and the microglial respiratory burst*. *Am J Physiol Cell Physiol*, 2001. **280**(4): p. C796-806.
70. Newell, E.W. and L.C. Schlichter, *Integration of K⁺ and Cl⁻ currents regulate steady-state and dynamic membrane potentials in cultured rat microglia*. *J Physiol*, 2005. **567**(Pt 3): p. 869-90.

71. Pannasch, U., et al., *The potassium channels Kv1.5 and Kv1.3 modulate distinct functions of microglia*. Mol Cell Neurosci, 2006. **33**(4): p. 401-11.
72. Judge, S.I., et al., *Voltage-gated potassium channels in multiple sclerosis: Overview and new implications for treatment of central nervous system inflammation and degeneration*. J Rehabil Res Dev, 2006. **43**(1): p. 111-22.
73. Moussaud, S., et al., *Characterisation of K⁺ currents in the C8-B4 microglial cell line and their regulation by microglia activating stimuli*. Cell Physiol Biochem, 2009. **24**(3-4): p. 141-52.
74. Eder, C., *Ion channels in microglia (brain macrophages)*. Am J Physiol, 1998. **275**(2 Pt 1): p. C327-42.
75. Eder, C., R. Klee, and U. Heinemann, *Involvement of stretch-activated Cl⁻ channels in ramification of murine microglia*. J Neurosci, 1998. **18**(18): p. 7127-37.
76. Eder, C. and T.E. DeCoursey, *Voltage-gated proton channels in microglia*. Prog Neurobiol, 2001. **64**(3): p. 277-305.
77. Walz, W. and L.K. Bekar, *Ion channels in cultured microglia*. Microsc Res Tech, 2001. **54**(1): p. 26-33.
78. Farber, K. and H. Kettenmann, *Physiology of microglial cells*. Brain Res Brain Res Rev, 2005. **48**(2): p. 133-43.
79. Hines, D.J., et al., *Microglia processes block the spread of damage in the brain and require functional chloride channels*. Glia, 2009. **57**(15): p. 1610-8.
80. Schlichter, L.C., et al., *The Ca²⁺ activated SK3 channel is expressed in microglia in the rat striatum and contributes to microglia-mediated neurotoxicity in vitro*. J Neuroinflammation. **7**: p. 4.
81. Tomas-Camardiel, M., et al., *In vivo expression of aquaporin-4 by reactive microglia*. J Neurochem, 2004. **91**(4): p. 891-9.
82. Eugenin, E.A., et al., *Microglia at brain stab wounds express connexin 43 and in vitro form functional gap junctions after treatment with interferon-gamma and tumor necrosis factor-alpha*. Proc Natl Acad Sci U S A, 2001. **98**(7): p. 4190-5.
83. Bordey, A. and D.D. Spencer, *Chemokine modulation of high-conductance Ca(2+)-sensitive K(+) currents in microglia from human hippocampi*. Eur J Neurosci, 2003. **18**(10): p. 2893-8.
84. Kuhn, S.A., et al., *Microglia express GABA(B) receptors to modulate interleukin release*. Mol Cell Neurosci, 2004. **25**(2): p. 312-22.
85. Farber, K., U. Pannasch, and H. Kettenmann, *Dopamine and noradrenaline control distinct functions in rodent microglial cells*. Mol Cell Neurosci, 2005. **29**(1): p. 128-38.
86. Liu, G.J., et al., *Glutamate induces directed chemotaxis of microglia*. Eur J Neurosci, 2009. **29**(6): p. 1108-18.
87. North, R.A., *Molecular physiology of P2X receptors*. Physiol Rev, 2002. **82**(4): p. 1013-67.
88. Xiang, Z. and G. Burnstock, *Expression of P2X receptors on rat microglial cells during early development*. Glia, 2005. **52**(2): p. 119-26.
89. Ulmann, L., et al., *Up-regulation of P2X4 receptors in spinal microglia after peripheral nerve injury mediates BDNF release and neuropathic pain*. J Neurosci, 2008. **28**(44): p. 11263-8.

90. Tsuda, M., et al., *P2X4 receptors induced in spinal microglia gate tactile allodynia after nerve injury*. *Nature*, 2003. **424**(6950): p. 778-83.
91. Haynes, S.E., et al., *The P2Y12 receptor regulates microglial activation by extracellular nucleotides*. *Nat Neurosci*, 2006. **9**(12): p. 1512-9.
92. Ohsawa, K., et al., *P2Y12 receptor-mediated integrin-beta1 activation regulates microglial process extension induced by ATP*. *Glia*. **58**(7): p. 790-801.
93. Koizumi, S., et al., *UDP acting at P2Y6 receptors is a mediator of microglial phagocytosis*. *Nature*, 2007. **446**(7139): p. 1091-5.
94. Farber, K. and H. Kettenmann, *Purinergic signaling and microglia*. *Pflugers Arch*, 2006. **452**(5): p. 615-21.
95. Inoue, K., *The function of microglia through purinergic receptors: neuropathic pain and cytokine release*. *Pharmacol Ther*, 2006. **109**(1-2): p. 210-26.
96. Synowitz, M., et al., *A1 adenosine receptors in microglia control glioblastoma-host interaction*. *Cancer Res*, 2006. **66**(17): p. 8550-7.
97. Haselkorn, M.L., et al., *Adenosine A1 receptor activation as a brake on the microglial response after experimental traumatic brain injury in mice*. *J Neurotrauma*, 2010. **27**(5): p. 901-10.
98. Koizumi, S., et al., *Purinergic receptors in microglia: Functional modal shifts of microglia mediated by P2 and P1 receptors*. *Glia*. **61**(1): p. 47-54.
99. Orr, A.G., et al., *Adenosine A(2A) receptor mediates microglial process retraction*. *Nat Neurosci*, 2009. **12**(7): p. 872-8.
100. Khakh, B.S., et al., *International union of pharmacology. XXIV. Current status of the nomenclature and properties of P2X receptors and their subunits*. *Pharmacol Rev*, 2001. **53**(1): p. 107-18.
101. Gever, J.R., et al., *Pharmacology of P2X channels*. *Pflugers Arch*, 2006. **452**(5): p. 513-37.
102. von Kugelgen, I., *Pharmacological profiles of cloned mammalian P2Y-receptor subtypes*. *Pharmacol Ther*, 2006. **110**(3): p. 415-32.
103. Fredholm, B.B., et al., *International Union of Pharmacology. XXV. Nomenclature and classification of adenosine receptors*. *Pharmacol Rev*, 2001. **53**(4): p. 527-52.
104. Roberts, J.A., et al., *Molecular properties of P2X receptors*. *Pflugers Arch*, 2006. **452**(5): p. 486-500.
105. Chan, W.Y., S. Kohsaka, and P. Rezaie, *The origin and cell lineage of microglia: new concepts*. *Brain Res Rev*, 2007. **53**(2): p. 344-54.
106. Rezaie, P., *Microglia in the Human Nervous System during Development*. *Neuroembryology* 2003. **2003**;2: p. 18-31.
107. Ginhoux, F., et al., *Fate mapping analysis reveals that adult microglia derive from primitive macrophages*. *Science*, 2010. **330**(6005): p. 841-5.
108. Dalmau, I., et al., *Dynamics of microglia in the developing rat brain*. *J Comp Neurol*, 2003. **458**(2): p. 144-57.
109. Ashwell, K., *Development of microglia in the albino rabbit retina*. *J Comp Neurol*, 1989. **287**(3): p. 286-301.
110. Ashwell, K.W., et al., *The appearance and distribution of microglia in the developing retina of the rat*. *Vis Neurosci*, 1989. **2**(5): p. 437-48.

111. Billiards, S.S., et al., *Development of microglia in the cerebral white matter of the human fetus and infant*. J Comp Neurol, 2006. **497**(2): p. 199-208.
112. Marin-Teva, J.L., et al., *Tangential migration of ameboid microglia in the developing quail retina: mechanism of migration and migratory behavior*. Glia, 1998. **22**(1): p. 31-52.
113. Sanchez-Lopez, A., et al., *Radial migration of developing microglial cells in quail retina: a confocal microscopy study*. Glia, 2004. **46**(3): p. 261-73.
114. Mizutani, M., et al., *The fractalkine receptor but not CCR2 is present on microglia from embryonic development throughout adulthood*. J Immunol, 2012. **188**(1): p. 29-36.
115. Herbomel, P., B. Thisse, and C. Thisse, *Zebrafish early macrophages colonize cephalic mesenchyme and developing brain, retina, and epidermis through a M-CSF receptor-dependent invasive process*. Dev Biol, 2001. **238**(2): p. 274-88.
116. Chitu, V. and E.R. Stanley, *Colony-stimulating factor-1 in immunity and inflammation*. Curr Opin Immunol, 2006. **18**(1): p. 39-48.
117. Erblich, B., et al., *Absence of colony stimulation factor-1 receptor results in loss of microglia, disrupted brain development and olfactory deficits*. PLoS One, 2011. **6**(10): p. e26317.
118. Walton, M.R., et al., *PU.1 expression in microglia*. J Neuroimmunol, 2000. **104**(2): p. 109-15.
119. Schulz, C., et al., *A lineage of myeloid cells independent of Myb and hematopoietic stem cells*. Science, 2012. **336**(6077): p. 86-90.
120. Kierdorf, K., et al., *Microglia emerge from erythromyeloid precursors via Pu.1- and Irf8-dependent pathways*. Nat Neurosci. **16**(3): p. 273-80.
121. Rigato, C., et al., *Pattern of invasion of the embryonic mouse spinal cord by microglial cells at the time of the onset of functional neuronal networks*. Glia, 2011. **59**(4): p. 675-95.
122. Navascues, J., et al., *Entry, dispersion and differentiation of microglia in the developing central nervous system*. An Acad Bras Cienc, 2000. **72**(1): p. 91-102.
123. Cuadros, M.A. and J. Navascues, *The origin and differentiation of microglial cells during development*. Prog Neurobiol, 1998. **56**(2): p. 173-89.
124. Monier, A., et al., *Entry and distribution of microglial cells in human embryonic and fetal cerebral cortex*. J Neuropathol Exp Neurol, 2007. **66**(5): p. 372-82.
125. Monier, A., et al., *Distribution and differentiation of microglia in the human encephalon during the first two trimesters of gestation*. J Comp Neurol, 2006. **499**(4): p. 565-82.
126. Cuadros, M.A., et al., *Microglia development in the quail cerebellum*. J Comp Neurol, 1997. **389**(3): p. 390-401.
127. Cunningham, C.L., V. Martinez-Cerdeno, and S.C. Noctor, *Microglia regulate the number of neural precursor cells in the developing cerebral cortex*. J Neurosci. **33**(10): p. 4216-33.
128. Cuadros, M.A., et al., *Development of microglia in the quail optic tectum*. J Comp Neurol, 1994. **348**(2): p. 207-24.

129. Ashwell, K., *The distribution of microglia and cell death in the fetal rat forebrain*. Brain Res Dev Brain Res, 1991. **58**(1): p. 1-12.
130. Cuadros, M.A., et al., *First appearance, distribution, and origin of macrophages in the early development of the avian central nervous system*. J Comp Neurol, 1993. **330**(1): p. 113-29.
131. Wang, C.C., et al., *Immunohistochemical study of amoeboid microglial cells in fetal rat brain*. J Anat, 1996. **189 (Pt 3)**: p. 567-74.
132. Sedel, F., et al., *Macrophage-derived tumor necrosis factor alpha, an early developmental signal for motoneuron death*. J Neurosci, 2004. **24**(9): p. 2236-46.
133. Paolicelli, R.C., et al., *Synaptic pruning by microglia is necessary for normal brain development*. Science, 2011. **333**(6048): p. 1456-8.
134. Schafer, D.P., et al., *Microglia sculpt postnatal neural circuits in an activity and complement-dependent manner*. Neuron, 2012. **74**(4): p. 691-705.
135. Aarum, J., et al., *Migration and differentiation of neural precursor cells can be directed by microglia*. Proc Natl Acad Sci U S A, 2003. **100**(26): p. 15983-8.
136. Jonakait, G.M., et al., *Microglial regulation of cholinergic differentiation in the basal forebrain*. Dev Neurobiol, 2011. **72**(6): p. 857-64.
137. Nakanishi, M., et al., *Microglia-derived interleukin-6 and leukaemia inhibitory factor promote astrocytic differentiation of neural stem/progenitor cells*. Eur J Neurosci, 2007. **25**(3): p. 649-58.
138. Rymo, S.F., et al., *A two-way communication between microglial cells and angiogenic sprouts regulates angiogenesis in aortic ring cultures*. PLoS One, 2011. **6**(1): p. e15846.
139. Fantin, A., et al., *Tissue macrophages act as cellular chaperones for vascular anastomosis downstream of VEGF-mediated endothelial tip cell induction*. Blood, 2010. **116**(5): p. 829-40.
140. Hagberg, H., P. Gressens, and C. Mallard, *Inflammation during fetal and neonatal life: implications for neurologic and neuropsychiatric disease in children and adults*. Ann Neurol, 2011. **71**(4): p. 444-57.
141. Brown, A.S., *The environment and susceptibility to schizophrenia*. Prog Neurobiol, 2010.
142. Fombonne, E., *Epidemiology of pervasive developmental disorders*. Pediatr Res, 2009. **65**(6): p. 591-8.
143. Ross, C.A., et al., *Neurobiology of schizophrenia*. Neuron, 2006. **52**(1): p. 139-53.
144. Brown, A.S., *Epidemiologic studies of exposure to prenatal infection and risk of schizophrenia and autism*. Dev Neurobiol. **72**(10): p. 1272-6.
145. Buehler, M.R., *A proposed mechanism for autism: an aberrant neuroimmune response manifested as a psychiatric disorder*. Med Hypotheses, 2011. **76**(6): p. 863-70.
146. Atladottir, H.O., et al., *Maternal infection requiring hospitalization during pregnancy and autism spectrum disorders*. J Autism Dev Disord. **40**(12): p. 1423-30.
147. Atladottir, H.O., et al., *Association of hospitalization for infection in childhood with diagnosis of autism spectrum disorders: a Danish cohort study*. Arch Pediatr Adolesc Med. **164**(5): p. 470-7.

148. Vargas, D.L., et al., *Neuroglial activation and neuroinflammation in the brain of patients with autism*. *Ann Neurol*, 2005. **57**(1): p. 67-81.
149. Arion, D., et al., *Molecular evidence for increased expression of genes related to immune and chaperone function in the prefrontal cortex in schizophrenia*. *Biol Psychiatry*, 2007. **62**(7): p. 711-21.
150. Hashimoto, T., et al., *Alterations in GABA-related transcriptome in the dorsolateral prefrontal cortex of subjects with schizophrenia*. *Mol Psychiatry*, 2008. **13**(2): p. 147-61.
151. Hallmayer, J., et al., *Genetic heritability and shared environmental factors among twin pairs with autism*. *Arch Gen Psychiatry*. **68**(11): p. 1095-102.
152. Riley, B. and K.S. Kendler, *Molecular genetic studies of schizophrenia*. *Eur J Hum Genet*, 2006. **14**(6): p. 669-80.
153. Shi, L., et al., *Maternal influenza infection causes marked behavioral and pharmacological changes in the offspring*. *J Neurosci*, 2003. **23**(1): p. 297-302.
154. Meyer, U., et al., *The time of prenatal immune challenge determines the specificity of inflammation-mediated brain and behavioral pathology*. *J Neurosci*, 2006. **26**(18): p. 4752-62.
155. Meyer, U., et al., *Adult brain and behavioral pathological markers of prenatal immune challenge during early/middle and late fetal development in mice*. *Brain Behav Immun*, 2008. **22**(4): p. 469-86.
156. Smith, S.E., et al., *Maternal immune activation alters fetal brain development through interleukin-6*. *J Neurosci*, 2007. **27**(40): p. 10695-702.
157. Fortier, M.E., G.N. Luheshi, and P. Boksa, *Effects of prenatal infection on prepulse inhibition in the rat depend on the nature of the infectious agent and the stage of pregnancy*. *Behav Brain Res*, 2007. **181**(2): p. 270-7.
158. Fatemi, S.H., et al., *Prenatal viral infection leads to pyramidal cell atrophy and macrocephaly in adulthood: implications for genesis of autism and schizophrenia*. *Cell Mol Neurobiol*, 2002. **22**(1): p. 25-33.
159. Lowe, G.C., G.N. Luheshi, and S. Williams, *Maternal infection and fever during late gestation are associated with altered synaptic transmission in the hippocampus of juvenile offspring rats*. *Am J Physiol Regul Integr Comp Physiol*, 2008. **295**(5): p. R1563-71.
160. Garay, P.A., et al., *Maternal immune activation causes age- and region-specific changes in brain cytokines in offspring throughout development*. *Brain Behav Immun*.
161. Dougherty, K.D., C.F. Dreyfus, and I.B. Black, *Brain-derived neurotrophic factor in astrocytes, oligodendrocytes, and microglia/macrophages after spinal cord injury*. *Neurobiol Dis*, 2000. **7**(6 Pt B): p. 574-85.
162. Zhu, P., et al., *Ramified microglial cells promote astroglialogenesis and maintenance of neural stem cells through activation of Stat3 function*. *FASEB J*, 2008. **22**(11): p. 3866-77.
163. Morgan, J.T., et al., *Microglial activation and increased microglial density observed in the dorsolateral prefrontal cortex in autism*. *Biol Psychiatry*, 2010. **68**(4): p. 368-76.

-
164. Radewicz, K., et al., *Increase in HLA-DR immunoreactive microglia in frontal and temporal cortex of chronic schizophrenics*. J Neuropathol Exp Neurol, 2000. **59**(2): p. 137-50.
 165. Wierzba-Bobrowicz, T., et al., *Quantitative analysis of activated microglia, ramified and damage of processes in the frontal and temporal lobes of chronic schizophrenics*. Folia Neuropathol, 2005. **43**(2): p. 81-9.
 166. Juckel, G., et al., *Microglial activation in a neuroinflammatory animal model of schizophrenia--a pilot study*. Schizophr Res, 2011. **131**(1-3): p. 96-100.
 167. Ratnayake, U., et al., *Behaviour and hippocampus-specific changes in spiny mouse neonates after treatment of the mother with the viral-mimetic Poly I:C at mid-pregnancy*. Brain Behav Immun. **26**(8): p. 1288-99.
 168. Pont-Lezica, L., et al., *Physiological roles of microglia during development*. J Neurochem, 2011.
 169. Kettenmann, H., F. Kirchhoff, and A. Verkhratsky, *Microglia: new roles for the synaptic stripper*. Neuron. **77**(1): p. 10-8.
 170. Meyer, U., et al., *Adult behavioral and pharmacological dysfunctions following disruption of the fetal brain balance between pro-inflammatory and IL-10-mediated anti-inflammatory signaling*. Mol Psychiatry, 2008. **13**(2): p. 208-21.
 171. Rezaie, P. and D. Male, *Colonisation of the developing human brain and spinal cord by microglia: a review*. Microsc Res Tech, 1999. **45**(6): p. 359-82.
 172. Streit, W.J., *Microglia and macrophages in the developing CNS*. Neurotoxicology, 2001. **22**(5): p. 619-24.
 173. Vilhardt, F., *Microglia: phagocyte and glia cell*. Int J Biochem Cell Biol, 2005. **37**(1): p. 17-21.
 174. Caviness, V.S., Jr., T. Takahashi, and R.S. Nowakowski, *Numbers, time and neocortical neuronogenesis: a general developmental and evolutionary model*. Trends Neurosci, 1995. **18**(9): p. 379-83.
 175. Qian, X., et al., *Timing of CNS cell generation: a programmed sequence of neuron and glial cell production from isolated murine cortical stem cells*. Neuron, 2000. **28**(1): p. 69-80.
 176. Rezaie, P., *Microglia in the Human Nervous System during Development*. Neuroembryology, 2003. **2003**;2: p. 18-31.
 177. Gotz, M. and W.B. Huttner, *The cell biology of neurogenesis*. Nat Rev Mol Cell Biol, 2005. **6**(10): p. 777-88.
 178. Andjelkovic, A.V., et al., *Macrophages/microglial cells in human central nervous system during development: an immunohistochemical study*. Brain Res, 1998. **814**(1-2): p. 13-25.
 179. Scholzen, T. and J. Gerdes, *The Ki-67 protein: from the known and the unknown*. J Cell Physiol, 2000. **182**(3): p. 311-22.
 180. Cheong, J.W., et al., *Induction of apoptosis by apicidin, a histone deacetylase inhibitor, via the activation of mitochondria-dependent caspase cascades in human Bcr-Abl-positive leukemia cells*. Clin Cancer Res, 2003. **9**(13): p. 5018-27.
 181. Meijering, E., O. Dzyubachyk, and I. Smal, *Methods for cell and particle tracking*. Methods Enzymol, 2012. **504**: p. 183-200.
-

182. Tan, S.S., et al., *Separate progenitors for radial and tangential cell dispersion during development of the cerebral neocortex*. *Neuron*, 1998. **21**(2): p. 295-304.
183. Anderson, S.A., et al., *Interneuron migration from basal forebrain to neocortex: dependence on Dlx genes*. *Science*, 1997. **278**(5337): p. 474-6.
184. Anderson, S.A., et al., *Distinct cortical migrations from the medial and lateral ganglionic eminences*. *Development*, 2001. **128**(3): p. 353-63.
185. Ransohoff, R.M. and A.E. Cardona, *The myeloid cells of the central nervous system parenchyma*. *Nature*, 2010. **468**(7321): p. 253-62.
186. Bystron, I., C. Blakemore, and P. Rakic, *Development of the human cerebral cortex: Boulder Committee revisited*. *Nat Rev Neurosci*, 2008. **9**(2): p. 110-22.
187. Cina, C., et al., *Expression of connexins in embryonic mouse neocortical development*. *J Comp Neurol*, 2007. **504**(3): p. 298-313.
188. Rakic, P., *A small step for the cell, a giant leap for mankind: a hypothesis of neocortical expansion during evolution*. *Trends Neurosci*, 1995. **18**(9): p. 383-8.
189. Haydar, T.F., et al., *Differential modulation of proliferation in the neocortical ventricular and subventricular zones*. *J Neurosci*, 2000. **20**(15): p. 5764-74.
190. Kurz, H., *Physiology of angiogenesis*. *J Neurooncol*, 2000. **50**(1-2): p. 17-35.
191. Kamiryo, T., et al., *Development of the rat meninx: experimental study using bromodeoxyuridine*. *Anat Rec*, 1990. **227**(2): p. 207-10.
192. Sturrock, R.R., *A morphological study of the development of the mouse choroid plexus*. *J Anat*, 1979. **129**(Pt 4): p. 777-93.
193. Johansson, P.A., et al., *Blood-CSF barrier function in the rat embryo*. *Eur J Neurosci*, 2006. **24**(1): p. 65-76.
194. Furuta, Y., D.W. Piston, and B.L. Hogan, *Bone morphogenetic proteins (BMPs) as regulators of dorsal forebrain development*. *Development*, 1997. **124**(11): p. 2203-12.
195. Currle, D.S., et al., *Direct and indirect roles of CNS dorsal midline cells in choroid plexus epithelia formation*. *Development*, 2005. **132**(15): p. 3549-59.
196. von Frowein, J., A. Wizenmann, and M. Gotz, *The transcription factors Emx1 and Emx2 suppress choroid plexus development and promote neuroepithelial cell fate*. *Dev Biol*, 2006. **296**(1): p. 239-52.
197. Peri, F. and C. Nusslein-Volhard, *Live imaging of neuronal degradation by microglia reveals a role for v0-ATPase a1 in phagosomal fusion in vivo*. *Cell*, 2008. **133**(5): p. 916-27.
198. Svahn, A.J., et al., *Development of ramified microglia from early macrophages in the zebrafish optic tectum*. *Dev Neurobiol*, 2012.
199. Raivich, G., *Like cops on the beat: the active role of resting microglia*. *Trends Neurosci*, 2005. **28**(11): p. 571-3.
200. Monif, M., et al., *The P2X7 receptor drives microglial activation and proliferation: a trophic role for P2X7R pore*. *J Neurosci*, 2009. **29**(12): p. 3781-91.

201. Brough, D., et al., *Purinergic (P2X7) receptor activation of microglia induces cell death via an interleukin-1-independent mechanism*. Mol Cell Neurosci, 2002. **19**(2): p. 272-80.
202. Ferrari, D., et al., *Purinergic modulation of interleukin-1 beta release from microglial cells stimulated with bacterial endotoxin*. J Exp Med, 1997. **185**(3): p. 579-82.
203. Mingam, R., et al., *In vitro and in vivo evidence for a role of the P2X7 receptor in the release of IL-1 beta in the murine brain*. Brain Behav Immun, 2008. **22**(2): p. 234-44.
204. Hide, I., et al., *Extracellular ATP triggers tumor necrosis factor-alpha release from rat microglia*. J Neurochem, 2000. **75**(3): p. 965-72.
205. Surprenant, A., et al., *The cytolytic P2Z receptor for extracellular ATP identified as a P2X receptor (P2X7)*. Science, 1996. **272**(5262): p. 735-8.
206. Pelegrin, P. and A. Surprenant, *Pannexin-1 mediates large pore formation and interleukin-1beta release by the ATP-gated P2X7 receptor*. Embo J, 2006. **25**(21): p. 5071-82.
207. Di Virgilio, F., et al., *Cytolytic P2X purinoceptors*. Cell Death Differ, 1998. **5**(3): p. 191-9.
208. Le Feuvre, R., D. Brough, and N. Rothwell, *Extracellular ATP and P2X7 receptors in neurodegeneration*. Eur J Pharmacol, 2002. **447**(2-3): p. 261-9.
209. Jiang, L.H., et al., *N-methyl-D-glucamine and propidium dyes utilize different permeation pathways at rat P2X(7) receptors*. Am J Physiol Cell Physiol, 2005. **289**(5): p. C1295-302.
210. Sim, J.A., et al., *Reanalysis of P2X7 receptor expression in rodent brain*. J Neurosci, 2004. **24**(28): p. 6307-14.
211. Nicke, A., et al., *A functional P2X7 splice variant with an alternative transmembrane domain 1 escapes gene inactivation in P2X7 knock-out mice*. J Biol Chem, 2009. **284**(38): p. 25813-22.
212. Guan, C., et al., *A review of current large-scale mouse knockout efforts*. Genesis, 2010. **48**(2): p. 73-85.
213. Seminario-Vidal, L., et al., *Rho Signaling Regulates Pannexin 1-mediated ATP Release from Airway Epithelia*. J Biol Chem, 2011. **286**(30): p. 26277-86.
214. Scain, A.L., et al., *Glycine release from radial cells modulates the spontaneous activity and its propagation during early spinal cord development*. J Neurosci, 2010. **30**(1): p. 390-403.
215. Gomes, P., et al., *ATP release through connexin hemichannels in corneal endothelial cells*. Invest Ophthalmol Vis Sci, 2005. **46**(4): p. 1208-18.
216. Ma, W., et al., *Pharmacological characterization of pannexin-1 currents expressed in mammalian cells*. J Pharmacol Exp Ther, 2009. **328**(2): p. 409-18.
217. Sim, J.A., et al., *Altered hippocampal synaptic potentiation in P2X4 knock-out mice*. J Neurosci, 2006. **26**(35): p. 9006-9.
218. Charrier, C., et al., *Characterization of neural stem cells in the dorsal vagal complex of adult rat by in vivo proliferation labeling and in vitro neurosphere assay*. Neuroscience, 2006. **138**(1): p. 5-16.

219. Ho, M.K. and T.A. Springer, *Mac-2, a novel 32,000 Mr mouse macrophage subpopulation-specific antigen defined by monoclonal antibodies*. J Immunol, 1982. **128**(3): p. 1221-8.
220. Huang, Y.J., et al., *The role of pannexin 1 hemichannels in ATP release and cell-cell communication in mouse taste buds*. Proc Natl Acad Sci U S A, 2007. **104**(15): p. 6436-41.
221. Pelegrin, P. and A. Surprenant, *The P2X(7) receptor-pannexin connection to dye uptake and IL-1beta release*. Purinergic Signal, 2009. **5**(2): p. 129-37.
222. Qureshi, O.S., et al., *Regulation of P2X4 receptors by lysosomal targeting, glycan protection and exocytosis*. J Cell Sci, 2007. **120**(Pt 21): p. 3838-49.
223. Shinozaki, Y., et al., *Direct Observation of ATP-Induced Conformational Changes in Single P2X4 Receptors*. PLoS Biol, 2009. **7**(5): p. e103.
224. Gudipaty, L., et al., *Regulation of P2X(7) nucleotide receptor function in human monocytes by extracellular ions and receptor density*. Am J Physiol Cell Physiol, 2001. **280**(4): p. C943-53.
225. Khakh, B.S., et al., *Neuronal P2X transmitter-gated cation channels change their ion selectivity in seconds*. Nat Neurosci, 1999. **2**(4): p. 322-30.
226. Coddou, C., et al., *Formation of carnosine-Cu(II) complexes prevents and reverts the inhibitory action of copper in P2X4 and P2X7 receptors*. J Neurochem, 2002. **80**(4): p. 626-33.
227. North, R.A. and A. Surprenant, *Pharmacology of cloned P2X receptors*. Annu Rev Pharmacol Toxicol, 2000. **40**: p. 563-80.
228. Guo, C., et al., *Evidence for functional P2X4/P2X7 heteromeric receptors*. Mol Pharmacol, 2007. **72**(6): p. 1447-56.
229. Hibell, A.D., et al., *Complexities of measuring antagonist potency at P2X(7) receptor orthologs*. J Pharmacol Exp Ther, 2001. **296**(3): p. 947-57.
230. Liu, X., et al., *Identification of key residues coordinating functional inhibition of P2X7 receptors by zinc and copper*. Mol Pharmacol, 2008. **73**(1): p. 252-9.
231. Jiang, L.H., et al., *Brilliant blue G selectively blocks ATP-gated rat P2X(7) receptors*. Mol Pharmacol, 2000. **58**(1): p. 82-8.
232. Donnelly-Roberts, D.L., et al., *Mammalian P2X7 receptor pharmacology: comparison of recombinant mouse, rat and human P2X7 receptors*. Br J Pharmacol, 2009. **157**(7): p. 1203-14.
233. Parker, K.E., *Modulation of ATP-gated non-selective cation channel (P2X1 receptor) activation and desensitization by the actin cytoskeleton*. J Physiol, 1998. **510 (Pt 1)**: p. 19-25.
234. Royle, S.J., et al., *Non-canonical YXXGPhi endocytic motifs: recognition by AP2 and preferential utilization in P2X4 receptors*. J Cell Sci, 2005. **118**(Pt 14): p. 3073-80.
235. Bernier, L.P., et al., *P2X4 receptor channels form large noncytolytic pores in resting and activated microglia*. Glia, 2012. **60**(5): p. 728-37.
236. Raouf, R., et al., *Differential regulation of microglial P2X4 and P2X7 ATP receptors following LPS-induced activation*. Neuropharmacology, 2007. **53**(4): p. 496-504.

-
237. Boumechache, M., et al., *Analysis of assembly and trafficking of native P2X4 and P2X7 receptor complexes in rodent immune cells.* J Biol Chem, 2009. **284**(20): p. 13446-54.
238. Acuna-Castillo, C., et al., *Differential role of extracellular histidines in copper, zinc, magnesium and proton modulation of the P2X7 purinergic receptor.* J Neurochem, 2007. **101**(1): p. 17-26.
239. Yan, Z., et al., *The P2X7 receptor channel pore dilates under physiological ion conditions.* J Gen Physiol, 2008. **132**(5): p. 563-73.
240. Locovei, S., et al., *Pannexin1 is part of the pore forming unit of the P2X(7) receptor death complex.* FEBS Lett, 2007. **581**(3): p. 483-8.
241. Tsukimoto, M., et al., *P2X7 receptor-dependent cell death is modulated during murine T cell maturation and mediated by dual signaling pathways.* J Immunol, 2006. **177**(5): p. 2842-50.
242. Qu, Y., et al., *Pannexin-1 is required for ATP release during apoptosis but not for inflammasome activation.* J Immunol, 2011. **186**(11): p. 6553-61.
243. Chekeni, F.B., et al., *Pannexin 1 channels mediate 'find-me' signal release and membrane permeability during apoptosis.* Nature, 2010. **467**(7317): p. 863-7.
244. Bianco, F., et al., *A role for P2X7 in microglial proliferation.* J Neurochem, 2006. **99**(3): p. 745-58.
245. Sano, H., et al., *Critical role of galectin-3 in phagocytosis by macrophages.* J Clin Invest, 2003. **112**(3): p. 389-97.
246. Schwab, J.M., et al., *AIF-1 expression defines a proliferating and alert microglial/macrophage phenotype following spinal cord injury in rats.* J Neuroimmunol, 2001. **119**(2): p. 214-22.
247. Egan, T.M. and B.S. Khakh, *Contribution of calcium ions to P2X channel responses.* J Neurosci, 2004. **24**(13): p. 3413-20.
248. Pocock, J.M. and H. Kettenmann, *Neurotransmitter receptors on microglia.* Trends Neurosci, 2007. **30**(10): p. 527-35.
249. Morihata, H., et al., *Potentiation of a voltage-gated proton current in acidosis-induced swelling of rat microglia.* J Neurosci, 2000. **20**(19): p. 7220-7.
250. Menteyne, A., et al., *Predominant functional expression of Kv1.3 by activated microglia of the hippocampus after Status epilepticus.* PLoS One, 2009. **4**(8): p. e6770.
251. Noda, M., et al., *AMPA-kainate subtypes of glutamate receptor in rat cerebral microglia.* J Neurosci, 2000. **20**(1): p. 251-8.
252. Hoshiko, M., et al., *Deficiency of the microglial receptor CX3CR1 impairs postnatal functional development of thalamocortical synapses in the barrel cortex.* J Neurosci. **32**(43): p. 15106-11.
253. Norenberg, W., P.J. Gebicke-Haerter, and P. Illes, *Voltage-dependent potassium channels in activated rat microglia.* J Physiol, 1994. **475**(1): p. 15-32.
254. Eder, C., et al., *Properties of voltage-gated currents of microglia developed using macrophage colony-stimulating factor.* Pflugers Arch, 1995. **430**(4): p. 526-33.
255. Ducharme, G., et al., *Small-conductance Cl⁻ channels contribute to volume regulation and phagocytosis in microglia.* Eur J Neurosci, 2007. **26**(8): p. 2119-30.
-

256. Rappert, A., et al., *Secondary lymphoid tissue chemokine (CCL21) activates CXCR3 to trigger a Cl⁻ current and chemotaxis in murine microglia*. *J Immunol*, 2002. **168**(7): p. 3221-6.
257. Schlichter, L.C., T. Mertens, and B. Liu, *Swelling activated Cl⁻ channels in microglia: Biophysics, pharmacology and role in glutamate release*. *Channels (Austin)*. **5**(2): p. 128-37.
258. Martin, D.K., et al., *Human macrophages contain a stretch-sensitive potassium channel that is activated by adherence and cytokines*. *J Membr Biol*, 1995. **147**(3): p. 305-15.
259. Gaspar, P., O. Cases, and L. Maroteaux, *The developmental role of serotonin: news from mouse molecular genetics*. *Nat Rev Neurosci*, 2003. **4**(12): p. 1002-12.
260. Benitez-Diaz, P., et al., *Prenatal and postnatal contents of amino acid neurotransmitters in mouse parietal cortex*. *Dev Neurosci*, 2003. **25**(5): p. 366-74.
261. Herlenius, E. and H. Lagercrantz, *Development of neurotransmitter systems during critical periods*. *Exp Neurol*, 2004. **190 Suppl 1**: p. S8-21.
262. Ben-Ari, Y., et al., *GABAA, NMDA and AMPA receptors: a developmentally regulated 'menage a trois'*. *Trends Neurosci*, 1997. **20**(11): p. 523-9.
263. Heng, J.I., G. Moonen, and L. Nguyen, *Neurotransmitters regulate cell migration in the telencephalon*. *Eur J Neurosci*, 2007. **26**(3): p. 537-46.
264. Zimmermann, H., *Nucleotide signaling in nervous system development*. *Pflugers Arch*, 2006. **452**(5): p. 573-88.
265. Nilius, B., J. Prenen, and G. Droogmans, *Modulation of volume-regulated anion channels by extra- and intracellular pH*. *Pflugers Arch*, 1998. **436**(5): p. 742-8.
266. Patterson, P.H., *Immune involvement in schizophrenia and autism: etiology, pathology and animal models*. *Behav Brain Res*, 2009. **204**(2): p. 313-21.
267. Harvey, L. and P. Boksa, *A stereological comparison of GAD67 and reelin expression in the hippocampal stratum oriens of offspring from two mouse models of maternal inflammation during pregnancy*. *Neuropharmacology*. **62**(4): p. 1767-76.
268. Giovanoli, S., et al., *Stress in puberty unmasks latent neuropathological consequences of prenatal immune activation in mice*. *Science*, 2013. **339**(6123): p. 1095-9.
269. Samuelsson, A.M., et al., *Prenatal exposure to interleukin-6 results in inflammatory neurodegeneration in hippocampus with NMDA/GABA(A) dysregulation and impaired spatial learning*. *Am J Physiol Regul Integr Comp Physiol*, 2006. **290**(5): p. R1345-56.
270. Swinnen, N., et al., *Complex invasion pattern of the cerebral cortex by microglial cells during development of the mouse embryo*. *Glia*, 2013. **61**(2): p. 150-63.
271. Patterson, P., Xu, W., Smith, S., Devarman, B., *Maternal Immune Activation, Cytokines and Autism*, in *Autism*, A.W. Zimmerman, Editor. 2008, Humana Press: Totowa, NJ.

-
272. Verney, C., et al., *Early microglial colonization of the human forebrain and possible involvement in periventricular white-matter injury of preterm infants*. *J Anat.* **217**(4): p. 436-48.
273. Manitz, M.P., et al., *The role of microglia during life span in neuropsychiatric disease - an animal study*. *Schizophr Res.*
274. Bauer, S., B.J. Kerr, and P.H. Patterson, *The neuropoietic cytokine family in development, plasticity, disease and injury*. *Nat Rev Neurosci*, 2007. **8**(3): p. 221-32.
275. Deverman, B.E. and P.H. Patterson, *Cytokines and CNS development*. *Neuron*, 2009. **64**(1): p. 61-78.
276. Richetto, J., et al., *Prenatal Immune Activation Induces Maturation-Dependent Alterations in the Prefrontal GABAergic Transcriptome*. *Schizophr Bull.*
277. Holloway, T., et al., *Prenatal stress induces schizophrenia-like alterations of serotonin 2A and metabotropic glutamate 2 receptors in the adult offspring: role of maternal immune system*. *J Neurosci.* **33**(3): p. 1088-98.
278. Shi, L., et al., *Activation of the maternal immune system alters cerebellar development in the offspring*. *Brain Behav Immun*, 2009. **23**(1): p. 116-23.
279. Ito, H.T., et al., *Maternal immune activation alters nonspatial information processing in the hippocampus of the adult offspring*. *Brain Behav Immun.* **24**(6): p. 930-41.
280. de la Rosa, E.J. and F. de Pablo, *Cell death in early neural development: beyond the neurotrophic theory*. *Trends Neurosci*, 2000. **23**(10): p. 454-8.
281. Sanno, H., et al., *Control of postnatal apoptosis in the neocortex by RhoA-subfamily GTPases determines neuronal density*. *J Neurosci.* **30**(12): p. 4221-31.
282. Cunningham, C., *Microglia and neurodegeneration: The role of systemic inflammation*. *Glia.* **61**(1): p. 71-90.
283. Lipina, T.V., et al., *Maternal immune activation during gestation interacts with *Disc1* point mutation to exacerbate schizophrenia-related behaviors in mice*. *J Neurosci.* **33**(18): p. 7654-66.

Curriculum Vitae

Nina Swinnen werd geboren op 4 augustus 1986 te Leuven. In 2004 behaalde ze haar diploma Algemeen Secundair Onderwijs (ASO) in de studierichting sportwetenschappen aan het Koninklijk Atheneum van Diest. In hetzelfde jaar begon ze haar studies aan de Universiteit Hasselt/transnationale universiteit Limburg (tUL) waar ze in 2009 met grote onderscheiding afstudeerde als master in de Biomedische Wetenschappen. Haar eindwerk getiteld 'Functional characterization of glycine effects on oligodendroglial cell lines' voerde ze uit in het labo van Prof. dr. Jean-Michel Rigo. Vervolgens startte ze in september 2009 met haar doctoraat aan het Biomedisch Onderzoeksinstituut van de Universiteit Hasselt. Tijdens deze periode volgde ze verschillende cursussen, o.a. project management en wetenschappelijk schrijven en presenteren, en hielp ze mee aan de organisatie van het tweede μ FIBR symposium. De resultaten die werden bekomen tijdens dit doctoraat werden deels gepubliceerd in internationale tijdschriften en werden gepresenteerd op verschillende (inter)nationale meetings.

Bibliography

Publications

- Microglia Proliferation Is Controlled by P2X7 Receptors in a Pannexin-1-Independent Manner during Early Embryonic Spinal Cord Invasion.
Rigato C*, **Swinnen N***, Buckinx R, Couillin I, Mangin JM, Rigo JM, Legendre P*, Le Corronc H*. (* contributed equally)
Journal of Neuroscience. 2012 Aug 22;32(34):11559-11573. (IF = 7.115)
- Complex invasion pattern of the cerebral cortex by microglial cells during development of the mouse embryo.
Swinnen N, Smolders S, Avila A, Notelaers K, Paesen R, Ameloot M, Brône B, Legendre P*, Rigo JM*. (* contributed equally)
Glia. 2013 Feb;61(2):150-63. doi: 10.1002/glia.22421. (IF = 5.066)

Oral presentations

- Microglia in the embryonic neocortex - Maternal Inflammation affects embryonic microglia.
N Swinnen , C Rigato , B Brône , P Legendre and JM Rigo.
Autumn Meeting of the Belgian Society of Cell and Developmental Biology (22-10-2010).
- Microglia in the embryonic cortex.
N Swinnen , B Brône , P Legendre and JM Rigo.
Belgian society of fundamental and clinical physiology and pharmacology – Spring meeting (16-03-2012).

Selected Poster presentations

- Microglia In The Embryonic Neocortex – Maternal Inflammation deregulates embryonic microglia.
N. Swinnen, C. Rigato, B. Brône, P. Legendre, JM. Rigo.
18th Biennial Meeting of the International Society for Developmental Neuroscience (06 to 09-06-2010).
- Maternal Inflammation deregulates microglia in the embryonic cortex.
N. Swinnen, S. Smolders, C. Rigato, B. Brône, P. Legendre, JM. Rigo
Belgian society of fundamental and clinical physiology and pharmacology – Autumn meeting (16-10-2010).
- Maternal inflammation affects the microglia in the embryonic cortex.
N Swinnen , B Brône , P Legendre and JM Rigo.
Summer meeting Belgian Society of Cell and Developmental Biology (01 and 02-07-2011).
- Microglia in the embryonic cortex.
N Swinnen , B Brône , P Legendre and JM Rigo.
The 10th European meeting of Glial Cells in Health and Disease (13 to 17-09-2011).

- Microglia invasion and migration in the embryonic neocortex
JM Rigo, **N Swinnen**, S Smolders, A Avila Macaya, B Brône, P Legendre.
Society for Neuroscience meeting: Neuroscience 2011 (12 to 16-11-2011)
- Microglia in the embryonic cortex.
N Swinnen , B Brône , P Legendre and JM Rigo.
IUAP meeting P6/31 program: molecular and cellular mechanisms of electrical excitability (16-12-2011).
- Microglia in the embryonic cortex - mature team players or young bench sitters?
N Swinnen, S Smolders, B Brône, P Legendre, JM Rigo.
The 11th European Meeting on Glial Cell Function in Health and Disease (3 to 6-07-2013).

Bursaries

- Student bursary to attend the 18th Biennial Meeting of the International Society for Developmental Neuroscience in Estoril.
- Boehringer Ingelheim Fonds travel grants (in 2011 and 2013) to stay and work in Paris in the lab of Pascal Legendre at UPMC 06.
- GLIA stipend to attend the XI European Meeting on Glial Cell Function in Health and Disease in Berlin.

Dankwoord

O my..het is gedaan. Ik moet bekennen dat het me nooit gelukt zou zijn zonder de steun van een aantal mensen. Daarom zou ik in dit laatste deeltje graag iedereen bedanken.

Allereerst een woord van dank aan mijn twee promotoren: prof. Jean-Michel Rigo en dr. Pascal Legendre. Jean-Michel, na een stage op de oligo's bij Sheen wist ik dat ik in deze groep graag aan een doctoraat begon. Er was een plaats op een nieuw project rond microglia..een heel nieuw onderwerp voor mij. Met uw hulp is het me toch aardig gelukt experimenten te bedenken..die natuurlijk niet altijd van de eerste keer lukten, want dat is nu eenmaal onderzoek ☺. De afgelopen 4 jaar kon ik steeds bij u terecht met al mijn vragen, bezorgdheden of voor gewoon een bemoedigend woordje. Maar ook voor het bespreken van de resultaten en het nalezen en doornemen van posters en artikels, bedankt hiervoor.

Dear Pascal, when I applied for this PhD position I knew it was in collaboration with a university in Paris. I was a bit scared and uncertain in the beginning but when I arrived for the first time at Jussieu you were immediately very helpful. You showed me how to work with the set-up and explained me everything about the microglia in the spinal cord. Going to another country also allowed me to work on my "social skills". So thank you for giving me the opportunity to work in your lab, I learned a lot. When I was in Paris I worked together with Chiara and Herve. They were very nice colleagues and I would also give some special thanks to them.

Ook mijn co-promotor, prof. Brône, mag ik niet vergeten. Bert, jij hebt mij leren patchen tijdens mijn stage. Merci voor al het geduld want het was toch niet altijd even simpel ☺. Menig maal heb ik aan uw deur gestaan met vragen, bezorgdheden of om iets na te lezen en dan kon ik altijd bij u terecht, danku daarvoor.

Dear members of the jury, I would also like to thank you for critically evaluating my thesis and for the constructive comments which contributed to the improvement of my thesis.

Natuurlijk wil ik ook al mijn BIOMED collega's bedanken voor de leuke momenten op de BBQ, de BIOMED dag en de verschillende congressen.

Quirine, mijn bureaugenootje en Klaagmuur, ontelbare keren heb je mijn gezaag moeten aanhoren. Ik kon bij u altijd terecht met vragen, de een had al wat meer met het werk te maken dan de andere. We hebben veel afgelachen en als het eens wat minder ging was je er steeds om me een hart onder de riem te steken en Riverside op te zetten. Mede daardoor ben ik niet aan "de 3x" geraakt ;-)
Nen dikke merci daarvoor!

Sophie, de eerste studente die ik moest begeleiden (scary! ☺) blijkbaar heb ik en de fysiologie toen een goeie indruk gemaakt want je bent mij komen vervoegen in de microglia-club. Samen hebben we het leed van "de-irritante-muizen-willen-niet-kweken" gedeeld maar natuurlijk ook veel gelachen. Nu ben jij de "leidster" van de microglia's ;-)) en met Silke heb je een goed teamlid bij.

De rest van de fysiologie groep: Valérie, Ann, Marjolein, Elke, Ambily, Ariel, Giovanni, Dorien en Virginie..jullie hebben allemaal bijgedragen aan de leuke werksfeer die er in onze groep altijd was.

Tussen fysiologie en biofysica is er altijd een "vruchtbare samenwerking" geweest. Meermaals ben ik in de kelder langsgelopen om hulp te vragen met mijn analyse of gewoon om eventjes mijn hoofd leeg te maken. Rik, Ben, Kathleen en Nick bedankt om me telkens te helpen en te luisteren. Kathleen, na de karaoke en het optreden van jouw koor had ik de zangmicrobe ook te pakken en naast collega's zijn jij en Quirine nu ook mijn zangbuddies. Merci om altijd een luisterend oor te bieden als ik mijn hart moest luchten.

De oude collega's, Inge en Katherine, onze kook- en baklessen samen waren een leuke ontspanning. En ook de dames van morfologie mag ik niet vergeten; Sofie, Annelies, Petra en Wendy, de babbels met jullie aan de senseo of op de bureau waren altijd een aangename afleiding.

Rosette, Jo, Petra, Wilfried, Joke, Eline, Regine en Paul; al jullie hulp, het maken van oplossingen, verzorgen van de dieren..was allemaal onmisbaar de afgelopen 4 jaar. Aangezien het onmogelijk is om alle collega's afzonderlijk op te noemen een welgemeende merci aan alle BIOMED collega's.

Mijn vrienden en vriendinnen die er de afgelopen jaren voor me waren mag ik zeker ook niet vergeten. Andreas, Helmi, Karen, Stefanie en Anja (baby-sis ☺) merci voor al die gezellige momenten en leuke avondjes uit ;-p als de experimenten weer niet waren gelopen zoals het zou moeten waren de shopnamiddagen of cocktails en bubbels een welkome afleiding, thanks babies! Arno, little situation ☺, we zijn misschien niet zo vaak samen op stap geweest (maar goed ook) maar uw babbels en onnozelteiten hebben mij toch ook altijd de nodige steun en afleiding gegeven.

Mama en papa, merci voor alle steun de afgelopen 9 jaar (dear lord de tijd vliegt!). Ik herinner me dat ik aan het begin van de bachelor biomedische één avond tranen met tuiten heb gehuild "ik ga het nooit kunnen..alles is in het Engels" en kijk nu ☺ al dat drama was nergens voor nodig. Merci om altijd met interesse naar mijn verhalen over het werk te luisteren. Ik vond het ook altijd super wanneer jullie me in Parijs kwamen bezoeken; die toeristische weekends waren elke keer erg leuk. En als ik dan eens een weekend naar huis kwam waren er altijd de gezellige zondagse-ententjes met de bomma's ☺. Maar ik ben jullie vooral dankbaar dat jullie mij altijd alle kansen hebben gegeven en steeds in mij hebben geloofd. Zonder jullie steun had ik dit niet gekund.

En dan, last but not least..de persoon die echt de volle lading gezaag, geklaag, tranen en craziness heeft moeten verwerken ☺ Kristof. Samen werken was niet altijd even simpel want de scheiding tussen werk en thuis werd daardoor soms erg dun. Een voordeel was wel dat je zelf maar al te goed weet hoe zwaar onderzoek soms kan zijn. Je was er steeds om me uit de dipjes te halen als ik het weer allemaal even had gehad met alles. Ik weet ook dat de afgelopen jaren niet altijd even gemakkelijk zijn geweest want elke keer als ik naar Parijs ging bleef jij alleen achter met de zorg voor ons appartementje en de poezen (and they need a lot of attention! ☺), maar je hebt dat elke keer super goed gedaan schat. En ik weet dat ik soms nogal een moeilijke ben, maar jij neemt me zoals ik ben en je bent er elke keer voor mij, thanks lou.. ik hou van je.

Just ride

